Applied and Environmental Soil Science

Integrated Approaches to Soil Contamination Monitoring

Guest Editors: Pantelis Soupios, Victor Kavvadias, Katherine Huddersman, Francesco Sdao, and Dimitrios Ntarlagiannis

Integrated Approaches to Soil Contamination Monitoring

Applied and Environmental Soil Science

Integrated Approaches to Soil Contamination Monitoring

Guest Editors: Pantelis Soupios, Victor Kavvadias, Katherine Huddersman, Francesco Sdao, and Dimitrios Ntarlagiannis

Copyright © 2016 Hindawi Publishing Corporation. All rights reserved.

This is a special issue published in "Applied and Environmental Soil Science." All articles are open access articles distributed under the Creative Commons Attribution License, which permits unrestricted use, distribution, and reproduction in any medium, provided the original work is properly cited.

Editorial Board

Lynette K. Abbott, Australia
Joselito M. Arocena, Canada
Robert L. Bradley, Canada
Artemi Cerda, Spain
Rafael Clemente, Spain
Claudio Cocozza, Italy
Hong J. Di, New Zealand
Oliver Dilly, Germany
Michael A. Fullen, UK
Ryusuke Hatano, Japan
Davey Jones, United Kingdom
Matthias Kaestner, Germany
Heike Knicker, Spain
Takashi Kosaki, Japan
Yongchao Liang, China
Teodoro M. Miano, Italy
Amaresh K. Nayak, India
Yong Sik Ok, Republic of Korea
Nikolla Qafoku, USA
Peter Shouse, USA
Balwant Singh, Australia
Keith Smettem, Australia
Marco Trevisan, Italy
Antonio Violante, Italy
Paul Voroney, Canada
Jianming Xu, China

Contents

Hindawi Publishing Corporation
Applied and Environmental Soil Science
Volume 2016, Article ID 5192691, 2 pages
http://dx.doi.org/10.1155/2016/5192691

Editorial

Integrated Approaches to Soil Contamination Monitoring

Pantelis Soupios,[1] Victor Kavvadias,[2] Katherine Huddersman,[3] Francesco Sdao,[4] and Dimitrios Ntarlagiannis[5]

[1] *Technological Educational Institute of Crete, 3 Romanou Chalepa, 73133 Chania, Greece*
[2] *Hellenic Agricultural Organization-DEMETER, Department of Soil Science of Athens, Institute of Soil and Water Resources, 1 Sofokli Venizelou Street, Lykovrisi, 141 23 Attiki, Greece*
[3] *De Montfort University, The Gateway, Leicester LE1 9BH, UK*
[4] *School of Engineering, University of Basilicata, Viale dell'Ateneo Lucano 10, Potenza, Italy*
[5] *Rutgers University, 101 Warren Street, Newark, NJ 07102, USA*

Correspondence should be addressed to Pantelis Soupios; soupios@staff.teicrete.gr

Received 9 May 2016; Accepted 9 May 2016

Copyright © 2016 Pantelis Soupios et al. This is an open access article distributed under the Creative Commons Attribution License, which permits unrestricted use, distribution, and reproduction in any medium, provided the original work is properly cited.

Top soil is a very important environmental compartment for many reasons, like it being the medium where plants grow, carbon accumulates, and so forth. But it also represents the "sink" where a wide range of waste materials, in very heterogeneous chemical forms, are disposed of and accumulate. This fact may allow contaminants to move downward the soil profile and reach subsurface and groundwater reservoirs. Agricultural activities can lead to land contamination due to the improper use of pesticides, agrochemicals, fertilizers, conditioners, and several other materials. The problem of contaminated land is exacerbated by industrial activities, including waste disposal and accidental spills that can also contribute to extensive contamination in the near surface environment. Dangerous contaminants can impact the characteristics and productivity of the surface soil as well as the subsurface and valuable natural resources conditions. Soil pollution threats human health, quality of foods, and groundwater but affects also the quality of the air.

Surface and subsurface soil monitoring and characterization can be challenging since chemical analyses at sampling points are local providing an inadequate model of the subsurface. Thus, novel, cost-effective, and multidisciplinary methods are needed to accurately describe surface/subsurface soil contamination whilst monitoring the evolution of the contamination over time producing time-lapse models. Continuous advances on characterization methods (such as automated acquisition systems of subsurface parameters), changes in regulatory standards, and the development of remediation systems further complicate this task.

With this special issue, we aim at bringing together scientists from different disciplines, with research focused on surface soil and subsurface contamination. Furthermore, we want to highlight recent research advances on characterization and monitoring methods and identify the pathways for their implementation to industry, agriculture, and society to encourage their adoption.

The manuscript entitled "Chemical and Physical Characteristics in Uncultivated Soils with Different Lithology in Semiarid Mediterranean Climate" by D. Moraetis et al. aims to identify the chemical and physical characteristics in uncultivated soils derived from different parent materials under semiarid Mediterranean climatic conditions which favored the formation of fragile soils. The authors used PCA analysis to demonstrate the soil quality stage, regarding nutrient availability showing that one of the major physicochemical characteristics such as cation exchange capacity (CEC) is controlled exclusively from mineralogy and not from organic matter. PCA also shows the unusual correlation of K^+ not only with illite content but also with the OM in fragile soils in Mediterranean climate which is evident in Crete in most of the 54 samples investigated.

The manuscript by C. Noel et al., entitled "Combining Geoelectrical Measurements and CO_2 Analyses to Monitor the Enhanced Bioremediation of Hydrocarbon-Contaminated Soils: A Field Implementation," deals with the combined application of Electrical Resistivity (ER) and Induced Polarization (IP) geophysical methods with gas analyses of CO_2 concentration and its carbon isotopic ratio,

to develop a less invasive methodology for monitoring the biodegradation of hydrocarbons. A more conductive and chargeable area which corresponds to the contaminated zone and high CO_2 emissions has been measured applying successfully geophysical and chemical methods, respectively. Combining geophysics with gas analyses is therefore a promising tool for *in situ* monitoring.

The manuscript entitled "Long-Term Dynamics of Urban Soil Pollution with Heavy Metals in Moscow," by N. E. Kosheleva and E. M. Nikiforova, deals with the spatial distributions and concentrations models of the nine heavy metals (Zn, Cd, Pb, Cu, Cr, Co, Ni, Mn, and Cs) present in top soils located in Moscow territory. Some geochemical anomalies maps, realized using the data collected in 1989, 2005, and 2010, are presented and discussed. The analysis of the geochemical anomalies maps has allowed the identification of areas characterized by different types of pollution phenomena and the evaluation of the environmental risk of the contamination. Finally, the study highlighted a significant increase of the pollution phenomena due to the increase of the heavy metals presence, which could be attributed to the growth of the total amount of industrial and motor transport emissions and change in absorption capacity of the urban soils.

The manuscript "Transport Processes in Porous Media by Self-Potential Method" by V. Giampaolo et al. describes a controlled diffusion/infiltration column experiment aiming at the monitoring of the leakage of a salty water plume by applying time-lapse self-potential (SP) measurements. The measured self-potential values were converted into salt concentration and the sand diffusion (D) and longitudinal dispersivity (αL) values were estimated by modelling the transport equations using the COMSOL Multiphysics.

The manuscript entitled "Aggregate Indices Method in Soil Quality Evaluation Using the Relative Soil Quality Index" by H. N. Pham et al. describes a new approach to assess the soil quality by aggregate indices using the Relative Soil Quality Index (RSQI). The authors applied the RSQI to assess the Soil Environmental Quality of rice intensive cultivation areas through a case study in Haiduong province in 2013. The RSQI is calculated for sampling points in 12 districts and simulated the Soil Environmental Quality on GIS map.

The manuscript entitled "Determination of Tetracycline and Fluoroquinolone Antibiotics at Trace Levels in Sludge and Soil" by M.-V. Salvia et al. describes the development of a sensitive analytical method to determine simultaneously traces of tetracycline and fluoroquinolone antibiotics in sludge and soil, based on a PLE extraction, followed by SPE purification and finally an analysis by LC-MS/MS. The method was successfully applied to the analysis of the target antibiotics in sludge as well as soil that received spreading.

Pantelis Soupios
Victor Kavvadias
Katherine Huddersman
Francesco Sdao
Dimitrios Ntarlagiannis

Hindawi Publishing Corporation
Applied and Environmental Soil Science
Volume 2016, Article ID 3590548, 13 pages
http://dx.doi.org/10.1155/2016/3590548

Research Article

Chemical and Physical Characteristics in Uncultivated Soils with Different Lithology in Semiarid Mediterranean Clima

Daniel Moraetis,[1] Nikolaos Lydakis-Simantiris,[2] Despina Pentari,[3] Emmanouil Manoutsoglou,[3] Chryssa Apostolaki,[3] and Vasilios Perdikatsis[3]

[1]*Earth Science Department, Sultan Qaboos University, College of Science, 123 Muscat, Oman*
[2]*Department of Natural Resources and the Environment, Technological and Educational Institute of Crete, 73133 Chania, Greece*
[3]*School of Mineral Resources Engineering, Technical University of Crete, 73100 Chania, Greece*

Correspondence should be addressed to Despina Pentari; pentari@mred.tuc.gr

Received 30 October 2015; Accepted 6 April 2016

Academic Editor: Francesco Sdao

Copyright © 2016 Daniel Moraetis et al. This is an open access article distributed under the Creative Commons Attribution License, which permits unrestricted use, distribution, and reproduction in any medium, provided the original work is properly cited.

The aim of this study is to identify the chemical and physical characteristics in uncultivated soils derived from different parent materials under semiarid Mediterranean climatic conditions which favoured the formation of fragile soils. The current work is of great interest in the agriculture and environmental stakeholders for providing a "benchmark" of undisturbed soil quality regarding organic content and nutrients availability. Principal Component Analysis (PCA) was used as the primary tool to demonstrate the soil quality stage, regarding nutrient availability. The statistical analysis revealed that one of the major physicochemical characteristics such as cation exchange capacity (CEC) is controlled exclusively from mineralogy and not from organic matter. Mineralogy and bulk chemical analysis is directly related to soil parent material lithology. The availability of inorganic nutrients (macro- and micronutrients) is low and relatively identical to most of the soils. PCA shows the unusual correlation of K^+ with not only illite content but also the OM in soils. The development of soils which are already of low quality in respect of organic content and nutrients is evident in Crete in most of the 54 samples investigated.

1. Introduction

Soil is the dynamic link between the biosphere and lithosphere and constitutes a practically not renewable (very low rate of formation) natural resource, with a key role for the environment and for the agriculture. It is a key component of the Earth System since it controls the hydrological, ecological, biological, and geochemical cycles [1–5]. The properties that are critical for soil quality (i.e., nutrients content, pH, and electrical conductivity) are governed by climatic, biological, and geological factors [6–9]. Mineral weathering is an important source of inorganic nutrients in soils under natural conditions [10]. Geologic gradient affects severely nutrient pools in soils [10]. Areas underlain by serpentinite or generally ultramafic rocks are rich in Mg, Fe, Ni, and Cr and depleted in K, Ca, P, and Zn [11]. On the other hand, soils developed in volcanic ash exhibit high cation exchange capacity (CEC) [12]. Hepper et al. [13] stated that CEC was controlled mainly by clay content in ash rich soils and by organic matter (OM) in ash free soils.

Apart from nutrients release through weathering processes, soil characteristics are further affected by atmospheric deposition, drainage outflow, biomass removal, and other processes such as cation exchange and organic matter decomposition, while pronounced interrelations exist between all factors mentioned above [7].

High geologic variability mainly appeared in tectonically active areas like boundaries of orogenetic belts. Crete is situated in the external plate of the Eurasian plate and exhibits a large variety of geomorphic and geologic features. So far, a number of papers have been published concerning soil taxonomy in Greece (i.e., [14, 15]). The geological framework of Crete has been studied thoroughly [16–18] and soil development appears mainly in limestones, ultramafic rocks, calcareous marls, metamorphic rocks (phyllites-quartzites), and alluvial sediments. Moreover, Crete exhibits a semiarid

Mediterranean climate (long hot-summers 20–31°C) which remained unchanged the last 20 Ma (late Miocene-early Pliocene till present) [19]. Thus, soils appear relatively fragile with low organic content, sparse vegetation, and being prone to desertification [20, 21]. The last decade a major concern has been raised regarding the preservation of our soils and that it is mentioned also in the recent accomplished European funded project Soil Transformation in European Catchments (SoilTrEC) [22]. Climate change has been reported as a severe driving force for soil deterioration in areas such as England and Wales [23–27]. Crete will also be affected by climate change and represents an area of high desertification risk. Although many studies on the soil degradation have been published for Mediterranean countries, very few are reporting the current state of uncultivated and undisturbed soils [28–30]. The reason behind it is that very few places in Europe are still intact of manmade activities. Many soil modeling studies specifically for carbon sequestration and/or erosion are missing data for undisturbed soils (initial conditions) ([31] and references therein and [32]). The lack of data is magnified when the soil lithology variability is considered. Crete still preserves several places of undisturbed soil development over different lithologies. Such areas could be used as a benchmark against which the soil manmade impact and the future climatic changes could be further quantified.

The present study aims to identify physical and chemical characteristics in undisturbed soils of different lithology of parent rock with sparse vegetation under the influence of Mediterranean climatic conditions. We aim to clearly demonstrate the fragile nature of soils from Crete for uncultivated areas with low organic content and to supply data that are important for assessing thin soils in semiarid climates. For this reason, soil samples from uncultivated areas of different bedrocks were collected and their mineralogical characteristics, physical and chemical properties, and their nutrient content were investigated. Principal Component Analysis (PCA) was applied on chemical and physical characteristics of all samples in order to identify groups of samples with common characteristics and to investigate and to rationalize the potential correlations among soil characteristics.

2. Materials and Methods

2.1. Geological Outline. The samples were collected from six areas in the island of Crete with four different bedrock lithologies. The different bedrocks are alluvial sediments (quaternary sediments) from two plateaus, ultramafic rocks, quartzite-phyllite rocks, and Neocene marly limestones. Mesozoic limestones were excluded since they are mainly situated in high altitudes with limited soil profiles. The aforementioned lithologies are present at Omalos Plateau (O) in western Crete, Lasithi Plateau in East Crete (La), Anogia in central Crete (U), Kantanos (Ka) and Kantanos-Kountoura (Kb) in western Crete, and Platanos (PL) in west Crete (Figure 1). The areas exhibit generally thin soil development.

Omalos area is situated in the west part of "Lefka Ori" mountains and its geomorphology is a typical plateau (1050 m elevation). The rock formations around the Omalos Plateau are mainly part of the Trypali limestones and less of the Plattenkalk limestones with minor outcrops of phyllites-quartzites series, whereas quaternary sediments have filled the plateau [16–18, 33]. The soil samples were collected from areas where the soil overlaid the quaternary formations (alluvial) within the plateau.

Lasithi soils were collected from Lasithi Plateau (353 m), which shows similar geological setting to Omalos Plateau. Limestones, mainly of Plattenkalk nappe and phyllites-quartzite group, are situated in the surrounding area of the plateau, whereas the soil samples were collected from the top of alluvial deposits.

Anogia area is underlain by ophiolites (mainly ultramafic rocks: peridotites). The most extended ophiolite outcrop in Crete exists in the area of Anogia village (701 m elevation). The ultramafic rocks comprise predominantly serpentinized peridotites. The overlying soil is mainly of limited thickness, whereas in land depressions and cavities the soil layer appears much thicker.

The parent rock of Kantanos area comprises metamorphic quartzite-phyllite group. Quartzite group in west Crete facies belt is characterized by an alternation of metagreywackes, meta-sandstones, and metapelites [34, 35]. Two different sets of soil samples were collected from Kantanos area (Ka) and Kantanos-Kountoura area (Kb) (both around 350 m elevation). The former soil is developed in eroded quartzite-phyllite group rich in quartz, whereas the latter is developed in phyllite-quartzite group with less quartz and higher mica content.

Platanos area comprises mainly of Neocene marls with intercalations of limestones and sandstones. The area is situated in the most western part of Crete compared to the other sampling sites (Figure 1) and elevation is 250 m.

2.2. Sample Collection and Pretreatment. Sampling was carried out using a special soil auger, designed for all soil types, and samples were collected from the top 20 cm. 54 samples were collected from sites chosen according to three strategic guidelines: (i) sites with uncultivated *in situ* soils (covered rarely by shrubs), (ii) sites where the mineralogical variation was apparent due to different parent materials, and (iii) sites with varied precipitation due to orientation (east-west). Samples were taken from six different areas, as follows (Figure 1): Omalos Plateau, nine samples (O1–O9); Kantanos, seven samples (Ka1–Ka7); Kantanos-Kountoura, eleven samples (Kb1–Kb11); Anogia, eight samples (U1–U8); Lasithi, eleven samples (La1–La11); and Platanos, eight samples (PL1–PL8). Samples were transferred to the laboratory, dried at 37°C for 48 h, and subsequently sieved through the 2 mm sieve.

2.3. Mineralogical Analysis. Mineralogical composition was determined by X-ray diffraction (XRD) technique using a Siemens D500 powder diffractometer, on two grain fractions, silt (<63 μm) and clay (<2 μm). These fractions were attained by separation with an Atterberg cylinder [36]. The data were obtained at 35 kV and 35 mA, with a graphite monochromator, using CuKa radiation. A 0.03° scanning step and 2-s scanning time per step were used for the range

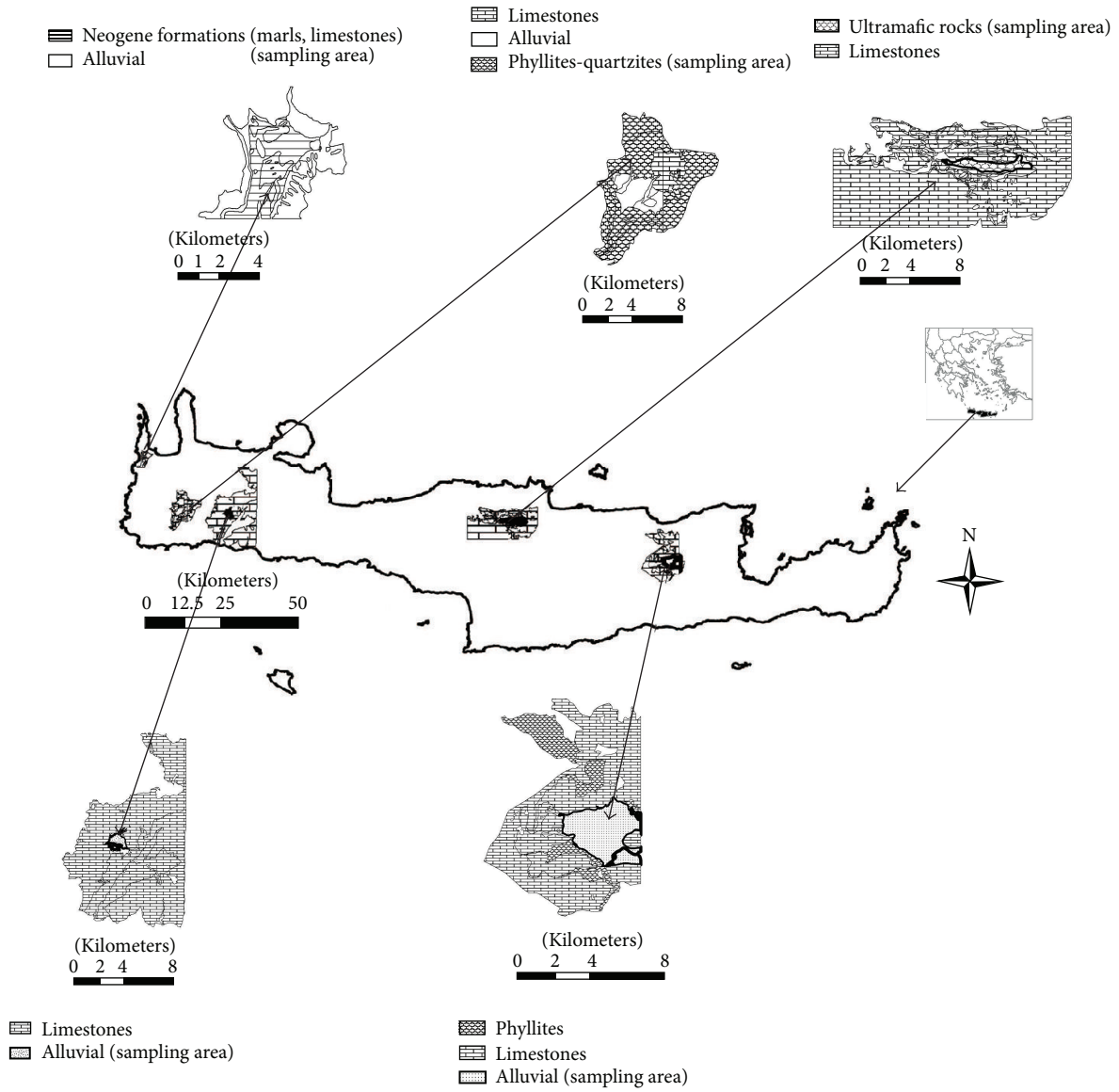

Figure 1: Geological outline in the sampling areas.

3 to 70°. The qualitative evaluation of the data was done with the Software Diffrac Plus (SOCABIM SAS France). The quantitative analysis was carried out by the Rietveld Method.

2.4. Chemical Analyses on Soils and Extraction Solutions. The bulk chemical analysis of the samples was carried out by X-ray fluorescence spectroscopy (S2 Ranger, Bruker EDS XRF), on the less than 2 mm sample fraction. Measurements were carried out at 40 kV with an Al filter (500 μm) for the heavier elements (Fe, Mn, Ti, Ca, and K) and at 20 kV for the lighter elements (P, Si, Al, Mg, and Na) without the use of filter. pH was determined in the supernatant of a soil : water mixture 1 : 2, according to Thomas [37] by a pH meter (WTW, 340i). Electrical conductivity was determined by a conductivity electrode (WTW, 340i) in the extract from saturated soil pastes. Calcium content was determined in the same extract after filtration, by flame atomic absorption spectrometry (AAS) (Perkin Elmer, AA100). Available K^+ and Mg^{2+} were extracted from soil samples by agitation in 1 M CH_3COONH_4 pH 7 solution [38, 39] and determined by AAS. Available micronutrients Fe^{2+}, Cu^{2+}, Mn^{2+}, and Zn^{2+} were extracted from the soil samples by the DTPA method, at pH 7.3 [40], and their concentrations were determined by AAS. Phosphorous extraction was carried out by a 0.5 M sodium bicarbonate solution [41] and its concentration was measured photometrically at 882 nm (HACH, DR/4000U) using a standard calibration curve. Nitrates were extracted with 1 M KCl and NO_3-N concentration was measured photometrically [42]. The concentration of organic matter was calculated according to Walkley and Black [43].

2.5. Cation Exchange Capacity-Grain Size Analysis. Cation exchange capacity (CEC) was determined by the method described by Sumner and Miller [44] modified for soils in arid regions. After the removal of $CaCO_3$ with HCl 2 N, soil

Table 1: Mineralogical quantitative analysis mean values for <63 μm and <2 μm fractions.

	<63 μm (%)						<2 μm (%)					
	O	La	U	Ka	Kb	PL	O	La	U	Ka	Kb	PL
Calcite	0.3	—	—	—	—	64.3	—	—	—	—	—	33.3
Dolomite	—	—	2.9	—	—	1.9	—	—	—	—	—	—
Quartz	67	58.2	9.7	27.4	22.7	13.2	4.5	4.4	2.2	3.1	—	5.3
Feldspars	—	13.7	—	3.7	5.8	5	—	—	—	8.6	—	—
Illite	12.1	17.6	1.3	33.3	33.2	15.5	55.8	60.8	2.8	23	71.6	43.5
Kaolinite	20.6	3.2	—	26.5	26.8	—	39.7	18.9	—	63	14.8	—
Paragonite	—	—	7.4	9.1	11.5	—	—	—	—	2.3	13.7	—
Chlorite	—	7.4	21.2	—	—	—	—	15.9	46.4	—	—	6.5
Antigorite	—	—	49.2	—	—	—	—	—	33.7	—	—	—
Talc	—	—	8.3	—	—	—	—	—	—	—	—	—
Smectite	—	—	—	—	—	—	—	—	14.8	—	—	11.4

—: not determined.

Table 2: Mean concentrations for major elements content in soils (energy dispersive-XRF); measurement relative standard error was less than 5%.

Sample	Na_2O (%)	MgO (%)	K_2O (%)	CaO (%)	TiO_2 (%)	MnO (%)	Fe_2O_3 (%)	Al_2O_3 (%)	SiO_2 (%)	P_2O_5 (%)	LOI (%)	SUM
O	0.6	0.5	1.2	1.0	0.4	0.1	3.8	8.4	83.1	<0.05	1.0	100.1
La	<0.2	3.8	1.7	0.9	0.6	0.2	6.2	23.3	61.6	0.4	1.6	100.1
U	<0.2	26.4	0.5	1.2	0.4	0.3	11.1	6.2	40.9	<0.05	13.8	100.6
Ka	1.5	0.5	1.6	0.02	0.8	0.04	4.9	14.2	72.1	0.1	4.2	99.9
Kb	1.00	<0.2	1.8	0.4	0.8	0.03	4.1	14.5	62.2	<0.05	14.9	99.7
PL	<0.2	2.5	1.7	26.4	—	0.1	2.3	4.7	24.2	—	38.4	100.2

—: not determined.

samples were saturated with $CaCl_2$ 2 N and the adsorbed Ca^{2+} was extracted using NaCl 2 N solution [45]. Determination of Ca^{2+} in extracted solutions was carried out by AAS.

The content of sand, clay, and silt of the samples (grain size analysis) was determined with the Bouyoucos method [36].

3. Results

Results for the physical and chemical parameters of soils are presented separate for each area and then PCA analysis is applied for all samples and it is presented in a separate section. Lasithi and Omalos are presented together since they are both plateau areas and Kantanos and Kantanos-Kountoura data are also presented together since both are adjacent areas with seemingly the same soil parent material.

3.1. Omalos and Lasithi Plateaus. Omalos and Lasithi soils have been developed in plateau and the parent material is alluvial deposits as has already been mentioned. The soils have contrasting characteristics in mineralogy, in bulk chemical analysis and other physical and chemical parameters. The silt fractions (<63 μm) of Omalos (O) soils exhibit higher quartz content compared to the Lasithi (La) soils and this is also reflected in the chemical analysis of the soils (Tables 1 and 2). Chlorite is present in the clay fraction (<2 μm) for La soil samples, but it is absent in O samples. Illite and kaolinite are characteristic weathering products of feldspars which are present in the bedrocks. Calcite is only a minor phase in both areas despite the widespread limestone outcrops in the plateau surrounding area attributed to the ease of calcite dissolution (karstification). O soils contain higher kaolinite and less illite content compared to La soils.

Table 2 shows the chemical composition (XRF) of the soil samples. Omalos soils have higher SiO_2 content (83.1%) compared to other areas. Lasithi samples exhibit higher MgO content (3.79%) compared to Omalos soils (0.47%).

Average, minimum, maximum values, and standard deviation (due to spatial variability) of the physicochemical parameters measured for all soils are illustrated in Table 3. Lasithi soils have statistically the same pH (7.4) compared to Omalos soils (6.4) (Table 3). This is not the case with electrical conductivity values (O: 187, La: 364 μS/cm) and this is related to different availability of nutrients in the two areas. Lasithi soils exhibit on average higher availability of nutrients compared to Omalos soils (La: 114, 228, 38 mg/kg, O: 50, 64, 5 mg/kg, for K^+, Mg^{2+}, Ca^{2+}, resp.); however, there is spatial variability for both sites which is expected in sedimentary basins such as in those plateaus.

Lasithi samples have higher CEC values (8.52 meq/100 gr), compared to Omalos soils CEC (4 meq/100 gr) (Table 3). Grain size analysis shows loam and silt loam fractions for O soils, whereas La soils are finer (mainly in clay loam fraction).

Table 3: Average values in soils from investigated areas for pH, electrical conductivity, CEC, macronutrients (Mg^{2+}, Ca^{2+}, K^{+}, NO_3^{-}, PO_4^{3-}), micronutrients (Cu^{2+}, Mn^{2+}, Fe^{2+}, Zn^{2+}), and organic matter (OM). Standard deviation, minimum, and maximum are also presented. Identical letters in the same column denote no statistical difference in average values according to *t*-test with alpha coefficient 5%.

	pH	EC (μS/cm)	CEC (meq/100 g)	K^{+} (mg/kg)	Mg^{2+} (mg/kg)	Ca^{2+} (mg/kg)	Cu^{2+} (mg/kg)	Mn^{2+} (mg/kg)	Fe^{2+} (mg/kg)	Zn^{2+} (mg/kg)	P-PO_4^{3-} (mg/kg)	N-NO_3^{-} (mg/kg)	OM%
O (9 samples)													
Average	6.4^{ba}	187^{a}	4^{a}	50^{b}	64^{a}	5^{a}	0.5^{a}	10^{a}	6^{a}	0.3^{a}	1.1^{ab}	2.6^{a}	0.64^{c}
min	5.0	75	1	23	13	0.2	0.1	1	0.1	0.1	0.4	0.8	0.19
max	8.4	487	6	80	281	15	1	26	26	0.5	2.2	5.3	2.86
stdev	1.4	133	2	8	83	6	0.2	8	9	0.2	0.7	1.5	0.87
La (11 samples)													
Average	7.4^{a}	364^{cb}	9^{b}	114^{a}	228^{b}	27^{a}	0.7^{a}	17^{a}	18^{b}	0.72^{b}	1.5^{b}	3.0^{a}	1.47^{a}
min	7.1	210	3	67	64	18	1	7	8	0.45	1.3	0.2	1.02
max	7.5	487	16	172	506	75	2	33	40	1.22	2.4	5.0	1.66
stdev	0.2	77	4	28	170	24	0.4	8	9	0.24	0.4	1.8	0.23
U (8 samples)													
Average	7.4^{a}	279^{ac}	12^{b}	66^{ab}	1611^{c}	4^{a}	0.7^{a}	7^{a}	17^{b}	0.3^{a}	0.5^{a}	7.5^{b}	0.44^{bc}
min	7.0	151	5	8	397	0.1	0.1	1	4	0.2	0.4	5.6	0.02
max	8.5	485	21	157	2572	11	2	15	31	0.7	0.7	10.3	1.00
stdev	0.5	134	6	52	845	4	0.6	6	11	0.2	0.1	1.9	0.29
Ka (7 samples)													
Average	5.6^{b}	292^{ac}	2^{a}	61^{ab}	101^{a}	10^{a}	0.3^{a}	5^{a}	7^{a}	0.4^{a}	0.7^{ab}	2.9^{a}	0.38^{bc}
min	4.9	153	1	24	24	0.6	0.2	0.2	4	0.3	0.4	2.4	0.11
max	6.5	450	3	162	209	31	0.4	20	14	0.7	1.1	3.6	1.07
stdev	0.6	99	1	47	60	12	0.1	7	3	0.1	0.2	0.5	0.32
Kb (11 samples)													
Average	6.2^{b}	603^{bc}	3^{a}	200^{c}	127^{ab}	11^{a}	0.4^{a}	19^{a}	15^{ab}	0.7^{a}	0.8^{ab}	11.6^{b}	1.09^{ab}
min	5.1	130	0.8	67	109	2	0.1	1	3	0.2	0.4	5.3	0.41
max	7.0	1697	7	374	143	33	1	90	57	3.1	1.2	34.7	1.80
stdev	0.6	477	2	24	11	10	0.3	25	16	0.8	0.3	10.3	0.60
PL (8 samples)													
Average	7.9^{a}	1496^{b}	11^{b}	90^{a}	146^{ab}	136^{a}	0.9^{a}	2^{a}	6^{a}	0.7^{b}	1.0^{ab}	17.1^{c}	0.44^{bc}
min	7.5	448	8	39	27	28	0.3	0.3	3	0.4	0.4	13.0	0.10
max	8.3	2990	21	140	197	559	2	5	7	1	3.1	24.3	1.50
stdev	0.3	1014	4	33	51	187	0.5	2	2	0.3	1.0	3.9	0.48

3.2. Anogia. Anogia soils contain abundant serpentine in both 63 μm and 2 μm soil fractions (Table 1). Serpentine is a typical constituent of ultramafic rocks (ophiolites) and outcrops in the area. The presence of talc in the silt soil fraction can also be attributed to the bedrock. Quartz content in the silt fraction is not related to the parent material. Chlorite in both silt and clay soil fractions could be either primary (from ultramafic rocks) or secondary mineral. Smectite in the clay fraction is a secondary mineral.

The chemical composition of Anogia soils resembles that of ultramafic rocks with SiO_2 content < 45% and high MgO concentration (26.4%) (Table 2).

Anogia soils exhibit an average pH value of 7.4. Electrical conductivity is rather low (279 μS/cm). Magnesium shows high availability in Anogia soils (1611 mg/kg) whereas potassium and calcium are rather low (66 and 4 mg/kg, resp.) (Table 3).

Anogia samples display the highest cation exchange capacity (12 meq/100 g) compared to the CEC of the other soils (Table 3). Anogia soils are coarse grain (sandy loam).

3.3. Kantanos and Kantanos-Kountoura. Kantanos and Kantanos-Kountoura soils contain abundant illite, kaolinite, and quartz (Table 1). Quartz is the predominant mineral in the silt fraction (<63 μm) for both Ka and Kb soils. Illite and kaolinite are present in both 63 μm and 2 μm soil fractions and both are typical products of weathered micaceous rocks such as those in phyllites-quartzites series. However, although the silt fraction of the two soils has comparable mineralogical composition, the clay fraction of Ka soil is rich in kaolinite whereas that of Kb soil has high illite content (Table 1).

Ka soils exhibit higher concentration of SiO_2 (72.1%) compared to Kb soils (62.2%) (Table 2).

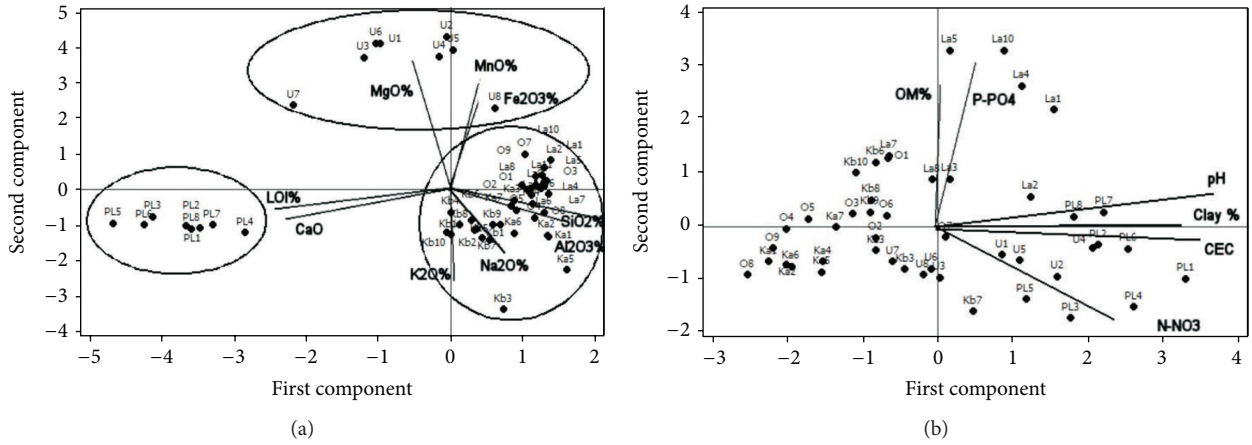

Figure 2: (a) PCA of chemical analysis (Na_2O, MgO, K_2O, Fe_2O_3, MnO, CaO, Al_2O_3, SiO_2, and LOI). (b) PCA of macronutrients availability ($N\text{-}NO_3$, $P\text{-}PO_4$) and physical parameters (clay content: clay%, organic content: OC%, and cation exchange capacity: CEC). 54 soil samples from Omalos Plateau (O), Lasithi Plateau (La), Kantanos (Ka, Kb) Anogia (U), and Platanos (PL). Variable axes are depicted in the figure.

Low pH values are observed for soil samples from Ka and Kb (5.6, 6.2), which are related to SiO_2-rich parent materials (Phyllites-Quartzites). Electrical conductivity exhibits spatial variability for both areas and the average value is higher for Kb soils (Ka: 292, Kb: 603 μS/cm). Potassium concentration in extraction solutions from the Kb soils is higher (200 mg/kg) compared to that from Ka soils (61 mg/kg) something that is in accordance with the higher illite content in the clay fraction for Kb soils (Tables 1 and 3).

Ka and Kb soils show low CEC (Ka: 2.1 meq/100 g, Kb: 3.1 meq/100 g). Moreover, soils from Ka and Kb areas are sandy loam and sandy clay loam, respectively.

3.4. Platanos. Platanos soils contain abundant calcite in both the silt and clay fractions which is related to sedimentation in shallow marine basins [46] (Table 1). Platanos soils are developed over marly limestones and sandstones (Neocene rocks). Smectite is present in the clay fraction.

On Table 2 the high CaO (26.4%) and SiO_2 (24.2%) contents are illustrated and are typical for submarine sediments with marly limestones and sandstones. MgO is noticeable (2.45%), whereas high loss on ignition (LOI) is attributed to calcite presence.

PL soils exhibit the highest pH values compared to other soils (in average 7.9, standard deviation 0.3) which can be related to the high content of basic cations (Ca^{2+}: 125 mg/kg) in extraction solution (Table 3). Moreover, PL soils have the highest electrical conductivity (1496 μS/cm).

Platanos samples exhibit the second higher cation exchange capacity (CEC) compared to other soils (11 meq/100 gr). Grain size distribution is that of clay loam for PL soils.

3.5. Principal Component Analysis. The chemical analysis (XRF) is presented in Table 2. Figure 2(a) shows the Principal Components Analysis (PCA) results for 54 samples with variables the chemical species obtained by XRF analysis. The first three principal components describe 81% of the total variability. Three groups of samples are set, that is, PL samples (high Ca content), U soils (high Mg content), and Ka, Kb, O, and La soil samples (high Si_2O content) (groups in circles in Figure 2(a)). The first component (34% variability) correlates Si_2O and Al_2O_3, the second component (32% variability) correlates MnO, Fe_2O_3, and MgO, and the third principal component strongly correlates K_2O and Al_2O_3. The categorization of Ka, Kb, O, and La in the same group shows common chemical characteristics of those soil samples. Figure 2(b) shows another PCA that is applied for physical and chemical variables such as clay content, OM, CEC, pH, $N\text{-}NO_3$, and $P\text{-}PO_4$. The first three principal components (PCs) captured 75% of the variability and there is an obvious correlation between CEC, pH, clay content, and $N\text{-}NO_3$ content. Samples from La show some increase in $P\text{-}PO_4$ that is related to organic content. The first PC (34% of variability) correlates the CEC and $N\text{-}NO_3$ content with clay content and pH. The second PC (22% of variability) strongly correlates OM% and $P\text{-}PO_4$. The third PC (19% of variability) correlates the OM% with $N\text{-}NO_3$.

Figure 3(a) shows the PCA analysis for all soil samples for variables such as macronutrients content (K^+, Mg^{2+}, and Ca^{2+}), OM%, clay content, and total illite content in both silt and clay fractions. The first three principal components described the 75% of total variability. The striking feature in this analysis is the first principal component that describes 34% of total variability and sets K^+ content, organic content, and illite content to be analogous. The illite content is referred to as corrected since the total concentration percentage includes illite in both silt and clay fractions and normalized to 100. The second PC shows (23% variability) that Ca^{2+} is related to clay content and the third PC (20% variability) correlates Mg^{2+} and K^+ with clay content. Figure 3(b) shows the PCA for all samples with variables, only the macronutrient availability. It is clear that K^+ and Mg^{2+} availability in soils is relatively the same in all samples and deviates only for Anogia soils (U-samples in circle Figures 3(a) and 3(b)) and some soil samples from Platanos area (PL-arrows in Figures 3(a) and 3(b)). Kb11 sample (arrow in Figures 3(a) and 3(b)) exhibits higher K^+ availability compared to all samples. The first two

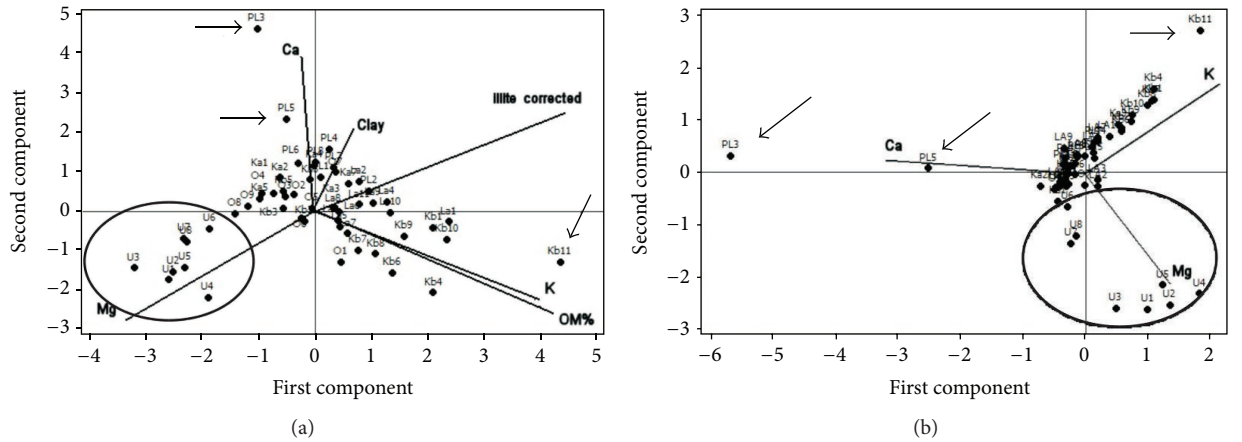

Figure 3: (a) PCA analysis of macronutrients availability (Ca^{2+}, Mg^{2+}, and K^{+}) and physical characteristics (clay content: clay%, organic content: OC%). (b) PCA analysis of macronutrients availability (Ca^{2+}, Mg^{2+}, and K^{+}). 54 soil samples included from Omalos Plateau (O), Lasithi Plateau (La), Kantanos (Ka, Kb) Anogia (U), and Platanos (PL). The variable axes are depicted in the figure.

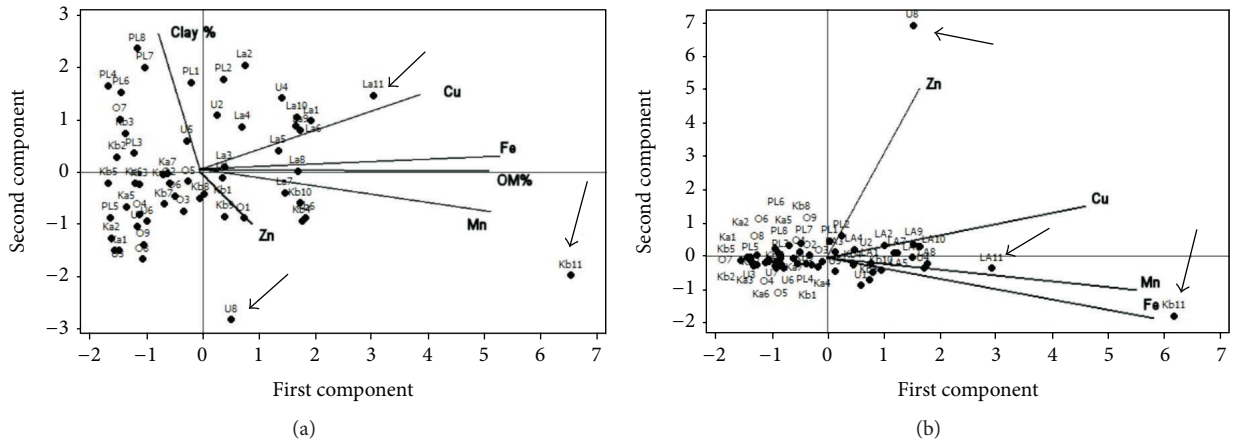

Figure 4: (a) PCA analysis of micronutrients availability (Zn^{2+}, Cu^{2+}, Fe^{2+}, and Mn^{2+}) and physical characteristics (clay content: clay%, organic content: OC%). (b) PCA analysis of micronutrients availability (Zn^{2+}, Cu^{2+}, Fe^{2+}, and Mn^{2+}). 54 soil samples from Omalos Plateau (O), Lasithi Plateau (La), Kantanos (Ka, Kb) Anogia (U), and Platanos (PL). The variable axes are depicted in the figure.

PCs capture 73% of variability and Mg^{2+} related positively to K^{+} (first PC-37% variability) whereas Ca^{2+} and Mg^{2+} are negatively correlated with K^{+} (second PC-36% variability).

Micronutrients (Zn^{2+}, Cu^{2+}, Fe^{2+}, and Mn^{2+}), clay content, and OM% are the variables for the PCA depicted in Figure 4(a). The first 3 PCs explain the 79% of the variability. The first PC (39% of variability) shows high correlation with organic content for all micronutrients apart from Zn^{2+}. The second PC (21% variability) interrelates Cu^{2+} content to clay content. The third PC (19% variability) shows low interrelation between Fe^{2+} and OM% and high correlation with Cu^{2+} and Zn^{2+}. Figure 4(b) shows PCA for the micronutrients (Zn^{2+}, Cu^{2+}, Fe^{2+}, and Mn^{2+}) and it is obvious that all samples are gathered in a cloud and only three samples are deviated (shown with black arrows in Figures 4(a) and 4(b)). The first two PCs capture 73% of total variability. The first PC (47% variability) correlates Fe^{2+} with Cu^{2+} and Mn^{2+}, and the second PC (26% variability) correlates Zn^{2+} and Cu^{2+}.

4. Discussion

4.1. Mineralogy and Chemical Analysis of Soils in relation to Different Parent Material. As it is expected, parent material influences primary mineral phases of soils. Two main reasons impose differences in the soil samples from Omalos Plateau and Lasithi Plateau and these are differences in the parent material and differences in the amount of precipitation in those areas. The presence of feldspars and chlorites and the lower quartz content in La soils compared to O soils are attributed to differences in the lithology of the weathering products (Table 1). This can be attributed to lithology differences of the surrounding rocks (phyllites and quartzites series) which they supplied with weathered products (sediments), both plateaus. In western Crete, phyllites and quartzites are dominated by quartz (Omalos Plateau-quartzites), whereas in eastern Crete they have high mica content (Lasithi Plateau-phyllites). The presence of less illite and more kaolinite in O soils compared to La soils can be attributed to higher precipitation in O plateau compared to

La plateau. Omalos Plateau is situated in higher elevation compared to Lasithi Plateau, whereas apart from the orographic gradient there is also strong directional gradient since western parts of the island gets more rain than the eastern part and that is demonstrated by recent studies (i.e., 1190–1670 mm/a in Omalos Plateau, 720–1190 mm/a in Lasithi Plateau) [47, 48]. Kourgialas et al. [49] presented the strong rainfall gradient due to elevation differences ($y = 0.7105 * x + 578.4$, y = rain, and x = elevation).

The silt fraction of Anogia soils exhibits characteristic primary mineralogy with serpentine and talc as inherited from ultramafic rocks (Table 1). Smectite (a secondary mineral) in clay fraction can be attributed to Mg abundance in soil. The detection of quartz is noteworthy; a possible explanation for the presence of quartz may be dust deposition [50, 51].

Ka and Kb soils have quartz, feldspars, and phyllosilicates (paragonite) in silt and clay fractions which are related to phyllites-quartzite parent material. Ka soils exhibit differences in secondary minerals compared to Kb soils. Ka soils contain lower illite in clay fraction compared to Kb soils, which is attributed to differences within the phyllites and quartzites series (Kb soils less acidic: low presence of quartzites) since both sampling areas are in the same elevation. This is an evident that soils from different lithology exhibit different content of secondary mineralogy like illite under the same climatic conditions (same amount of rain).

Platanos soils show mineralogy which is characteristic of the calcaric Neocene sediments (parent material) with abundant calcite in both silt and clay fractions. The presence of smectite in the PL soils is linked to MgO presence in chemical analysis. PL soils contain illite, which might be secondary and/or primary sedimentary mineral.

Smectite is present in soils with different lithological characteristics (i.e., ultramafic: U, alluvial: La, and limestone: PL). This is an indication that factors like precipitation and drainage of soils affect concentration of basic cations (i.e., Mg^{2+} and Ca^{2+}) favouring the formation of smectite. This is also evident from bulk chemical analysis where U, PL, and La exhibit significant Mg^{2+} concentrations (Table 2).

Bulk chemical analysis of soils reflects the main characteristics of the parent materials (Table 2, Figure 2). The striking feature is the relative common chemical characteristics for O, La, Ka, and Kb soils (Figure 2) which is evidence that alluvial sediments in Omalos and Lasithi Plateau are comprised of weathered products of metamorphic schists like those in Ka and Kb sites. Thus, O and La soils exhibit high SiO_2 concentration in bulk chemical analysis related to alluvial rocks lithology. O soils exhibit higher SiO_2 content compared to La soils probably due to higher precipitation in Omalos Plateau as it has been already mentioned, which promotes the increase of elements leaching and the increase of weathering resistant material like quartz. The highest MgO and FeO concentrations are found in U soils since they are inherent characteristics of its parent material (serpentine). Kb and Ka soils exhibit the highest SiO_2 concentration that is related to their parent materials (phyllites and quartzites); Kb soils show lower SiO_2 concentration compared to Ka due to less acidic parent material in the former as it has already been mentioned. PL soils show the highest CaO content compared to the other soils related to a Neocene sediment mixture of sand and marly limestones.

Soil texture shows that sedimentary parent material exhibits finer grain size soils (PL, O, and La), whereas soils with nonsedimentary parent material are coarser grained (Ka, Kb, and U). Parent material of the PL soils (soils with finer grains) is a biochemical sedimentary rock and the deposition of fine grain calcite is common [46].

4.2. Macronutrients and Micronutrients in relation to Different Soil Parent Material. PCA analysis showed strong interrelation between potassium content, organic matter, and illite content (Figure 3(a)). In addition, Ca^{2+} is related to clay content and negatively related to Mg^{2+} and K^{+}. Moreover, it is obvious from Figure 3(a) that most of the soil samples are gathered in one "cloud" without separating any group, except Anogia soils (U). The same is shown from PCA, where three macronutrients are considered as variables (K^{+}, Mg^{2+}, and Ca^{2+}) (Figure 3(b)). The previous shows soils from different lithologies (alluvial-O, La metamorphic Ka, Kb, and calcaric PL) to have identical availability of macronutrients and the samples deviating from those are Anogia samples due to high availability of Mg (samples in circles, Figures 3(a) and 3(b)) and some samples from Platanos area due to high availability of Ca (arrows in Figure 3(b)). In other words it is shown that all soils apart from Anogia samples and some from Platanos area are in a common state regarding K^{+}, Mg^{2+}, and Ca^{2+} availability. Only in Anogia soils, lithology characteristics of the parent material influence macronutrient availability such as Mg^{2+}, whereas the case is the same with some samples from Platanos area. Stutter et al. [7] showed that a strong relationship exists between basic cations (i.e., Ca^{2+}, Mg^{2+}) and basic parent material in soils. The high calcite content in PL soils is due to the origin of the Neocene parent material (sediment pool in shallow marine environment) [46] which mainly consist of unconsolidated crystals of calcite, clay minerals, and quartz. To verify the results, t-tests were applied for all samples to identify significant different average values. As it is shown in Table 3, most of the samples are not significantly different regarding K^{+} availability, apart from Kb samples, which show higher illite content. The previous is observed also in Figure 3(b) where Kb samples are along K^{+} variable axis. Omalos samples exhibit the lowest K^{+} availability and they are slightly different to La soil samples which are probably connected with increased K leaching due to higher precipitation in Omalos Plateau compared to Lasithi Plateau. In addition, potassium availability in our case is controlled by both illite content and organic matter, which is an unusual case and it is observed only when organic matter contribution in the total CEC is less than 15%, which has been shown by detailed study of Poonia and Niederbudde [52] on the K^{+} absorption in soils. The aforementioned is verified by the weak interrelation of OM% and CEC as revealed in PCA (Figure 2(b)). Visualization of the aforementioned is shown also in Figures 5(a) and 5(b) where plots of K^{+} availability versus illite content and OM content share an almost identical R^2 (0.53 to 0.59).

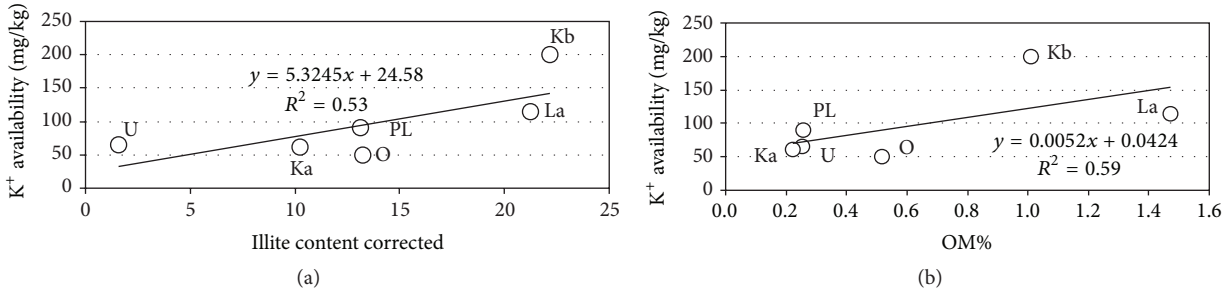

Figure 5: (a) Potassium availability versus % illite corrected content calculated from both silt and clay fractions normalized to 100%. (b) Potassium availability versus organic matter %. Fitted lines and R^2 are also shown.

Identical results can be inferred for Mg^{2+} availability; thus, all samples apart from U exhibit the same Mg^{2+} and there is again a small difference between O and La samples as it is for potassium. Calcium shows no statistical difference in average values among all soil samples and that is also the case for the soils with calcaric parent material. Someone could infer that the *in situ* uncultivated soils investigated in Crete regarding K^+, Mg^{2+}, and Ca^{2+} have reached a common stage in the availability of these nutrient elements. Differences are observed in soils like Anogia (ultramafic parent material) and in some soils in Platanos (calcaric parent material), where the lithological factor is still strong and overcomes the low organic matter availability.

Figure 4(a) shows that the micronutrients are mostly associated with organic content. Micronutrients availability in 54 soils is relatively identical as it is described in Figure 4(b). Only three samples exhibit high values of certain elements (arrows in Figures 4(a) and 4(b)), an observation that can be related to spatial lithological and/or chemical differences. Indeed, Table 3 shows on average identical statistical values for most of the micronutrients. Fe exhibits on average statistical different values only for the areas of La and U: the former is related to the high organic content (i.e., La11) whereas the latter is related to the higher content of minerals rich with Fe (i.e., chlorite) and this is also obvious in bulk chemistry of U soils (Table 2). U soils exhibit high pH, which is crucial for low leaching rate of available Mn^{2+} and Fe^{2+} into soil solution [53]. In contrast, soils with low pH (i.e., Kb11, Figures 4(a) and 4(b)) show higher availability in Mn^{2+} and Fe^{2+} and that is also observed by other researchers [54]. Thus, pH seems to influence availability of Mn^{2+} and Fe^{2+}. In addition, Cu^{2+} and Zn^{2+} concentrations are low and they do not vary significantly among the soils, probably due to the relatively low organic matter content (see Section 4.3) and/or the already low concentrations of these ions in the bedrock geology (limestones, ultra-mafic rocks, etc.).

4.3. Organic Matter, Nitrates, and Phosphates Availability in relation to Different Parent Material. OM content is similar in most of the soil samples and it is slightly lower than typical Mediterranean soils (1 to 1.5%) [55–58], except La and Kb soils due to denser vegetation in those areas (shrubs, etc.). Two observations are obvious: parent material origin does not affect the OM content of uncultivated soils in Crete and that Mediterranean climate is a crucial regulating factor of OM content in soils. López-Piñeiro et al. [59] mentioned that many soils from the Mediterranean region are poor in organic matter. The same is observed also for nitrates and phosphates in the soils studied here. Fast decomposition of OM due to climatic conditions (low rainfall, high temperatures) and low vegetation grow (low input of organic residues) lead to high rates of N mineralization and finally high leaching of nitrates through rainfall during winter time and especially by first flush events [57, 60–65]. The nitrogen-nitrate shows correlation with clay content this is related probably to positively charged sites in clays which has also been observed by others, especially in deeper soil horizons in the absence of organic matter [66]. Figure 2(b) shows P-PO_4 to be strongly correlated with organic matter. The aforementioned are also evident in Table 3 where P-PO_4 content is on average statistically different for La samples that also exhibit higher content of organic matter in some samples. The N-NO_3 abundance is different for PL soils, which are finer. Kb and U soils show also different N-NO_3 content which can be related to higher organic content and to the type of clay (i.e., smectite), respectively. More studies are needed in order to clarify these observations.

4.4. Soil Physicochemical Variations in relation to Different Soil Parent Material. Figure 2(b) shows that CEC is related to both clay content and pH and the correlation of organic content with CEC is rather weak. Only La sample exhibits high CEC which can be correlated with organic content which is different and higher compared to other soils in Crete. U, PL soils exhibit the highest CEC values and the highest smectite content compared to other soils and this is also verified by t-test. However, considering the highest theoretical CEC of smectite for U soils (70–130 meq/100 g) [67] and that only the clay fraction contributed to CEC, then 16% of the total CEC could be exchanged into extraction solution. Thus, smectite is not the only mineral contributed to CEC. Hence, Wauters et al. [68] referred to exchange sites that consist of sites in planar and/or interlayer clay minerals, humic substances, and frayed edge sites (FES) located at the edges of micaceous minerals. In addition, Fe-Mn oxide minerals can contribute to CEC [69, 70]. Thus, in our case both edges of phyllosilicates minerals (i.e., serpentine, chlorite) and oxides surfaces could contribute to CEC. pH controls CEC of such surfaces.

Table 4: Availability of nutrients in uncultivated soils in Crete and recommended values for fertilization in olive trees (recommended values obtained from TDC-OLIVE European project). Values in parentheses are standard deviation.

Sites	Available K^+ kg/ha[†]	Recommended K^+ kg/ha	Available Mg^{2+} kg/ha	Recommended Mg^{2+} kg/ha	Available Ca^{2+} kg/ha	Recommended Ca^{2+} kg/ha	Available $P\text{-}PO_4$ kg/ha	Recommended P kg/ha	Available $N\text{-}NO^3$ kg/ha	Recommended N kg/ha
O	0.13 (0.06)		0.17 (0.07)		0.01 (0.01)		0.003 (0.002)		0.007 (0.004)	
La	0.30 (0.07)		0.59 (0.13)		0.07 (0.06)		0.004 (0.002)		0.008 (0.005)	
U	0.17 (0.14)	300	4.19 (0.77)	20–34	0.01 (0.01)	360–714	0.001 (0.0002)	9–16	0.020 (0.005)	150 kg/ha
Ka	0.16 (0.12)		0.26 (0.06)		0.02 (0.03)		0.002 (0.001)		0.008 (0.001)	
Kb	0.52 (0.21)		0.13 (0.01)		0.03 (0.03)		0.002 (0.001)		0.019 (0.026)	
PL	0.24 (0.09)		0.38 (0.05)		0.33 (0.49)		0.003 (0.003)		0.045 (0.010)	

[†]Calculations considered bulk value of 1.3 g/cm^3 whereas all calculations were obtained for upper 20 cm of soil depth.

PL, U, and La soils exhibit high pH values, due to the high content of basic cations like Mg^{2+} and Ca^{2+}, whereas soils like Ka and Kb exhibit low pH, due to high content of silicon and depletion of basic cations. O and La soils exhibit different pH values despite their similar parent materials, due to differences within the alluvial deposits as already have been mentioned and/or the higher precipitation in Omalos Plateau. The dependence of CEC on pH is related to the presence of exchangeable sites on the edges of the silicate minerals and oxides and on the competitive adsorption of H^+ in exchangeable sites [71, 72]. Thus, in the absence of significant organic matter, parent material affects directly the soil pH which in turn influences CEC.

4.5. Soil Quality in Fragile Undisturbed Soils of Crete. Finally the present study shows the fragile soil development in different lithological units of Crete. To visualize the low nutrient capacity of uncultivated soils in Crete, we consider the fertilization requirements of olive trees which are a widespread cultivation in Mediterranean area [73]. Table 4 shows the availability of macronutrients per hectare in the soils investigated and the recommended values for olive trees (in average rainfall 400–700 mm). It is clearly shown that the availability of nutrients is at least 575, 6, 1647, 3300, and 3368 times lower than the recommended fertilization (TDC-Olive project) values for olive trees cultivation. The previous values are calculated by comparing the area with the higher availability for each nutrient to the nutrient recommended value for olive trees cultivation. Thus, the soil states of the undisturbed soils in semiarid Mediterranean climatic conditions have developed soils of low organic content and low nutrient availability and only in certain cases like Mg^{2+} content in Anogia.

5. Conclusions

Conclusions from the results of the chemical and mineralogical analyses in undisturbed soils in Crete can be summarized to the following.

(i) Primary mineralogical phases and bulk chemical analysis of soils reflect parent material lithology; however, PCA revealed that most of the soils showed identical macronutrient availability irrespectively of the parent rock lithology. Only the case of Mg^{2+} shows higher availability in limited samples from ultramafic parent rock.

(ii) Most of the sampling sites show that micronutrients availability has reached a common stage and is low due to low organic content. Only few samples show higher micronutrient availability related possibly to local lithological differences without significantly statistically changing the overall arguments.

(iii) PCA revealed that potassium is low and it is controlled from both the secondary minerals and the organic content in soils.

(iv) Cation exchange capacity is low and it is connected to smectite presence, edges of minerals, and pH and no relation is identified to organic matter, with the exception of one sample from Lasithi Plateau.

(v) Nutrients like nitrogen, phosphorous, Mn^{2+}, Fe^{2+}, Cu^{2+}, and Zn^{2+} are not correlated with the parent material, and all soils exhibit common behaviour while the availability in those nutrients is low.

(vi) Organic content in undisturbed soils in Mediterranean semiarid climatic conditions is low and it should be considered in future perspectives of soil modeling studies, soil management, and soil protection. Identically, macro- and micronutrients have been washed out in the undisturbed soils due to missing host sites like organic matter.

Competing Interests

The authors declare that they have no competing interests.

Acknowledgments

The project was cofunded by the European Social Fund and National Resources EPEAEK II-PYTHAGORAS. The authors are thankful for the economic support.

References

[1] P. Smith, M. F. Cotrufo, C. Rumpel et al., "Biogeochemical cycles and biodiversity as key drivers of ecosystem services provided by soils," *Soil*, vol. 1, no. 2, pp. 665–685, 2015.

[2] C. Decock, J. Lee, M. Necpalova, E. I. Pereira, D. M. Tendall, and J. Six, "Mitigating N_2O emissions from soil: from patching leaks to transformative action," *SOIL*, vol. 1, no. 2, pp. 687–694, 2015.

[3] S. D. Keesstra, V. Geissen, K. Mosse et al., "Soil as a filter for groundwater quality," *Current Opinion in Environmental Sustainability*, vol. 4, no. 5, pp. 507–516, 2012.

[4] E. C. Brevik, A. Cerdà, J. Mataix-Solera et al., "The interdisciplinary nature of *SOIL*," *SOIL*, vol. 1, no. 1, pp. 117–129, 2015.

[5] F. Berendse, J. van Ruijven, E. Jongejans, and S. Keesstra, "Loss of plant species diversity reduces soil erosion resistance," *Ecosystems*, vol. 18, no. 5, pp. 881–888, 2015.

[6] J. Pastor and J. G. Bockheim, "Distribution and cycling of nutrients in an aspen-mixed-hardwood-spodosol ecosystem in northern Wisconsin," *Ecology*, vol. 65, no. 2, pp. 339–353, 1984.

[7] M. Stutter, S. Langan, and M. Cresser, "Weathering and atmospheric deposition signatures of base cations in upland soils of NE Scotland: their application to critical load assessment," *Geoderma*, vol. 116, no. 3-4, pp. 301–324, 2003.

[8] J. L. K. Vestin, K. Nambu, P. A. W. van Hees, D. Bylund, and U. S. Lundström, "The influence of alkaline and non-alkaline parent material on soil chemistry," *Geoderma*, vol. 135, pp. 97–106, 2006.

[9] D. A. Wysocki, P. J. Schoeneberger, and H. E. Lagarry, "Soil surveys: a window to the subsurface," *Geoderma*, vol. 126, no. 1-2, pp. 167–180, 2005.

[10] R. C. Graham, W. R. Guertal, and K. R. Tice, "The pedologic nature of weathered rock," in *Whole Regolith Pedology*, D. L. Cremeens, R. B. Brown, and J. H. Huddleston, Eds., Special Publication no. 34, pp. 21–40, Soil Science Society of America (SSSA), Madison, Wis, USA, 1994.

[11] B. A. Roberts and J. Proctor, *The Ecology of Areas with Serpentinized Rocks: A World View*, Kluwer Academic Publishers, Dordrecht, The Netherlands, 1992.

[12] F. Caravaca, A. Lax, and J. Albaladejo, "Organic matter, nutrient contents and cation exchange capacity in fine fractions from semiarid calcareous soils," *Geoderma*, vol. 93, no. 3-4, pp. 161–176, 1999.

[13] E. N. Hepper, D. E. Buschiazzo, G. G. Hevia, A. Urioste, and L. Antón, "Clay mineralogy, cation exchange capacity and specific surface area of loess soils with different volcanic ash contents," *Geoderma*, vol. 135, pp. 216–223, 2006.

[14] B. R. Egli, *Ecology of the valleys in the mountains of Crete (Griechenland) [Ph.D. thesis]*, ETH, Zurich, Switzerland, 1993 (German).

[15] G. Nakos, "Relationships of bio-climatic zones and lithology with various characteristics of forest soils in Greece," *Plant and Soil*, vol. 79, no. 1, pp. 101–121, 1984.

[16] U. F. Dornsiepen and E. Manutsoglu, "Zur gliederung der phyllit-decke kretas und des peloponnes," *Zeitschrift der Deutschen Geologischen Gesellschaft*, vol. 145, pp. 286–304, 1994 (German).

[17] N. Fytrolakis, *The geological structure of Crete [Ph.D. thesis]*, National Technical University of Athens, 1980.

[18] M. Manoutsoglou, E. Spyridonos, A. Soujon, and V. Jacobshagen, "Redesign of geological map and 3D simulation of the geological structure of Samaria gorge western Crete," in *Proceedings of the 9th International Congress of the Geological Society of Greece*, P. G. Marinos, G. C. Koukis, G. C. Tsiambaos, and G. C. Stournaras, Eds., pp. 29–36, Geological Society of Greece, Athens, Greece, September 2001.

[19] J. Quade, N. Solounias, and T. E. Cerling, "Stable isotopic evidence from paleosol carbonates and fossil teeth in Greece for forest or woodlands over the past 11 Ma," *Palaeogeography, Palaeoclimatology, Palaeoecology*, vol. 108, no. 1-2, pp. 41–53, 1994.

[20] M. Tsakona and V. Gekas, "Desertification in Crete and the effect of global warming," in *Proceedings of the 5th International Conference on Environment, Ecosystems and Development (WSEAS '07)*, M. Otesteanu, S. Celikyay, N. Mastorakis, S. Lache, and F.-K. Benra, Eds., pp. 211–216, Tenerife, Spain, December 2007.

[21] N. J. Yassoglou and C. Kosmas, "Desertification in the Mediterranean Europe. A case study in Greece," RALA Report 200, Agricultural Research Institut, Reykjavik, Iceland, 1997.

[22] S. Banwart, "Save our soils," *Nature*, vol. 474, no. 7350, pp. 151–152, 2011.

[23] A. Cerdà, "Relationships between climate and soil hydrological and erosional characteristics along climatic gradients in Mediterranean limestone areas," *Geomorphology*, vol. 25, no. 1-2, pp. 123–134, 1998.

[24] A. Cerda and H. Lavee, "Runoff an erosion during the gradient climatic attitude effect caused by the pasture in the Judean Deserts," *Cuadernos Geograficos*, no. 29, pp. 27–50, 1999.

[25] A. Cerdà, "Aggregate stability against water forces under different climates on agriculture land and scrubland in southern Bolivia," *Soil and Tillage Research*, vol. 57, no. 3, pp. 159–166, 2000.

[26] A. C. Campos, J. B. Etchevers, K. L. Oleschko, and C. M. Hidalgo, "Soil microbial biomass and nitrogen mineralization rates along an altitudinal gradient on the cofre de perote volcano (Mexico): the importance of landscape position and land use," *Land Degradation and Development*, vol. 25, no. 6, pp. 581–593, 2014.

[27] B. U. Choudhury, A. R. Fiyaz, K. P. Mohapatra, and S. Ngachan, "Impact of land uses, agrophysical variables and altitudinal gradient on soil organic carbon concentration of North-Eastern Himalayan Region of India," *Land Degradation and Development*, vol. 27, no. 4, pp. 1163–1174, 2016.

[28] J. Casana, "Mediterranean valleys revisited: linking soil erosion, land use and climate variability in the Northern Levant," *Geomorphology*, vol. 101, no. 3, pp. 429–442, 2008.

[29] S. Kéfi, M. Rietkerk, C. L. Alados et al., "Spatial vegetation patterns and imminent desertification in Mediterranean arid ecosystems," *Nature*, vol. 449, no. 7159, pp. 213–217, 2007.

[30] F. E. Stamati, N. P. Nikolaidis, D. Venieri, E. Psillakis, and N. Kalogerakis, "Dissolved organic nitrogen as an indicator of livestock impacts on soil biochemical quality," *Applied Geochemistry*, vol. 26, pp. S340–S343, 2011.

[31] F. E. Stamati, N. P. Nikolaidis, and J. L. Schnoor, "Modeling topsoil carbon sequestration in two contrasting crop production to set-aside conversions with RothC—calibration issues and uncertainty analysis," *Agriculture, Ecosystems and Environment*, vol. 165, pp. 190–200, 2013.

[32] P. Panagos, K. Christos, B. Cristiano, and G. Ioannis, "Seasonal monitoring of soil erosion at regional scale: an application of the G2 model in Crete focusing on agricultural land uses," *International Journal of Applied Earth Observation and Geoinformation*, vol. 27, pp. 147–155, 2014.

[33] J. Krahl, G. Kauffmann, H. Kozur, D. Richter, O. Förster, and F. Heinritzi, "New data on the biostratigraphie of Phyllite group and the Trypali group on the island of Crete (Greece)," *Geologische Rundschau*, vol. 72, pp. 1147–1166, 1983 (German).

[34] R. Greiling and W. Skala, "The development of pre-neogenen tectonism in Phyllite-Quartzite series," *Zeitschrift der Deutschen Geologischen Gesellschaft*, vol. 127, pp. 429–433, 1976 (German).

[35] E. Seidel, *The petrology of phyllites-quartzites series crete [Ph.D. thesis]*, Habilitationsschrift TU Braunschweig, 1978 (German).

[36] G. J. Bouyoucos, "Hydrometer method improved for making particle size analyses of soils," *Agronomy Journal*, vol. 54, no. 5, pp. 464–465, 1962.

[37] G. W. Thomas, "Soil pH and soil acidity," in *Chemical Methods Methods of Soil Analysis Part 3*, D. L. Sparks, Ed., vol. 3, pp. 487–489, ASA and SSSA, Madison, Wis, USA, 1996.

[38] C. A. Bower, R. F. Reitemeier, and M. Fireman, "Exchangeable cation analysis of saline and alkali soils," *Soil Science*, vol. 73, no. 4, pp. 251–261, 1952.

[39] G. W. Thomas, "Exchangeable cations," in *Methods of Soil Analysis. Part 2*, A. L. Page, R. H. Miller, and D. R. Keeney, Eds., Agronomy Monograph 9, pp. 159–165, ASA and SSSA, Madison, Wis, USA, 1982.

[40] W. L. Lindsay and W. A. Norvell, "Development of a DTPA soil test for zinc, iron, manganese, and copper," *Soil Science Society of America Journal*, vol. 42, no. 3, pp. 421–428, 1978.

[41] S. R. Olsen, C. V. Cole, F. S. Watanabe, and L. A. Dean, *Estimation of Available Phosphorus in Soils by Extraction with Sodium Bicarbonate*, USDA Circ, 1954.

[42] D. R. Keeney, D. W. Nelson et al., "Nitrogen-inorganic forms," in *Methods of Soil Analysis. Part 2*, A. L. Page, D. R. Keeney, D. E. Baker, R. H. Miller, R. Ellis Jr., and J. D. Rhoades, Eds., Agronomy Monograph 9, pp. 643–698, ASA and SSSA, Madison, Wis, USA, 1982.

[43] A. Walkley and I. A. Black, "An examination of the degtjareff method for determining soil organic matter, and a proposed modification of the chromic acid titration method," *Soil Science*, vol. 37, no. 1, pp. 29–38, 1934.

[44] M. E. Sumner and W. P. Miller, "Cation exchange capacity and exchange coefficients," in *Methods of Soil Analysis Part 3*, D. L. Sparks, Ed., SSSA.1201-1229, pp. 1201–1229, Chemical Methods, Madison, Wis, USA, 1996.

[45] R. Dohrmann, "Problems in CEC determination of calcareous clayey sediments using the ammonium acetate method," *Journal of Plant Nutrition and Soil Science*, vol. 169, no. 3, pp. 330–334, 2006.

[46] H. G. Reading, *Sedimentary Environment: Processes, Facies and Stratigraphy*, Blackwell Science, Oxford, UK, 3rd edition, 1996.

[47] S. Naoum and I. K. Tsanis, "Orographic precipitation modeling with multiple linear regression," *Journal of Hydrologic Engineering*, vol. 9, no. 2, pp. 79–102, 2004.

[48] S. Naoum and I. K. Tsanis, "Temporal and spatial variation of annual rainfall on the island of Crete, Greece," *Hydrological Processes*, vol. 17, no. 10, pp. 1899–1922, 2003.

[49] N. N. Kourgialas, G. P. Karatzas, and N. P. Nikolaidis, "Development of a thresholds approach for real-time flash flood prediction in complex geomorphological river basins," *Hydrological Processes*, vol. 26, no. 10, pp. 1478–1494, 2012.

[50] D. H. Yaalon, "Saharan dust and desert loess: effect on surrounding soils," *Journal of African Earth Sciences*, vol. 6, no. 4, pp. 569–571, 1987.

[51] D. H. Yaalon, "Soils in the Mediterranean region: what makes them different?" *Catena*, vol. 28, no. 3-4, pp. 157–169, 1997.

[52] S. R. Poonia and E. A. Niederbudde, "Exchange equilibria of potassium in soils, V. Effect of natural organic matter on K-Ca exchange," *Geoderma*, vol. 47, no. 3-4, pp. 233–242, 1990.

[53] W. L. Lindsay and F. R. Cox, "Micronutrient soil testing for the tropics," in *Micronutrients in Tropical Food Crop Production. Fertilizer Research*, P. L. G. Vlek, Ed., pp. 169–200, Springer Netherlands, 1985.

[54] J. C. Katyal and B. D. Sharma, "DTPA-extractable and total Zn, Cu, Mn, and Fe in Indian soils and their association with some soil properties," *Geoderma*, vol. 49, no. 1-2, pp. 165–179, 1991.

[55] N. Yassoglou, C. Kosmas, and N. Moustakas, "The red soils, their origin, properties, use and management in Greece," *Catena*, vol. 28, no. 3-4, pp. 261–278, 1997.

[56] P. Dlapa, M. B. Bodí, J. Mataix-Solera, A. Cerdà, and S. H. Doerr, "Organic matter and wettability characteristics of wildfire ash from Mediterranean conifer forests," *CATENA*, vol. 135, pp. 369–376, 2015.

[57] J. L. Costa, V. Aparicio, and A. Cerdà, "Soil physical quality changes under different management systems after 10 years in the Argentine humid pampa," *Solid Earth*, vol. 6, no. 1, pp. 361–371, 2015.

[58] N. Yazdanpanah, M. Mahmoodabadi, and A. Cerdà, "The impact of organic amendments on soil hydrology, structure and microbial respiration in semiarid lands," *Geoderma*, vol. 266, pp. 58–65, 2016.

[59] A. López-Piñeiro, S. Murillo, C. Barreto et al., "Changes in organic matter and residual effect of amendment with two-phase olive-mill waste on degraded agricultural soils," *Science of the Total Environment*, vol. 378, no. 1-2, pp. 84–89, 2007.

[60] S. L. Tisdale, W. L. Nelson, J. D. Beaton, and J. L. Halvin, *Soil Fertility and Fertilizers*, Macmillan, New York, NY, USA, 5th edition, 1993.

[61] D. Moraetis, D. Efstathiou, F. Stamati et al., "High-frequency monitoring for the identification of hydrological and biogeochemical processes in a Mediterranean river basin," *Journal of Hydrology*, vol. 389, no. 1-2, pp. 127–136, 2010.

[62] B. Turgut, "Comparison of wheat and safflower cultivation areas in terms of total carbon and some soil properties under semi-arid climate conditions," *Solid Earth*, vol. 6, no. 2, pp. 719–725, 2015.

[63] A. Novara, J. Rühl, T. La Mantia, L. Gristina, S. La Bella, and T. Tuttolomondo, "Litter contribution to soil organic carbon in the processes of agriculture abandon," *Solid Earth*, vol. 6, no. 2, pp. 425–432, 2015.

[64] M. Muñoz-Rojas, A. Jordán, L. M. Zavala, D. De la Rosa, S. K. Abd-Elmabod, and M. Anaya-Romero, "Impact of land use and land cover changes on organic carbon stocks in mediterranean soils (1956–2007)," *Land Degradation and Development*, vol. 26, no. 2, pp. 168–179, 2015.

[65] L. L. Roa-Fuentes, C. Martínez-Garza, J. Etchevers, and J. Campo, "Recovery of soil C and N in a tropical pasture: passive and active restoration," *Land Degradation and Development*, vol. 26, no. 3, pp. 201–210, 2015.

[66] J.-M. Harmand, H. Ávila, R. Oliver, L. Saint-André, and E. Dambrine, "The impact of kaolinite and oxi-hydroxides on nitrate adsorption in deep layers of a Costarican Acrisol under coffee cultivation," *Geoderma*, vol. 158, no. 3-4, pp. 216–224, 2010.

[67] I. E. Odom, "Smectite clay minerals: properties and uses," *Philosophical Transactions of the Royal Society of London Series A*, vol. 311, no. 1517, pp. 391–409, 1984.

[68] J. Wauters, A. Elsen, A. Cremers, A. V. Konoplev, A. A. Bulgakov, and R. N. J. Comans, "Prediction of solid/liquid distribution coefficients of radiocaesium in soils and sediments. Part one: a simplified procedure for the solid phase characterisation," *Applied Geochemistry*, vol. 11, no. 4, pp. 589–594, 1996.

[69] G. R. C. Cooper, "Oxidation and toxicity of chromium in ultramafic soils in Zimbabwe," *Applied Geochemistry*, vol. 17, no. 8, pp. 981–986, 2002.

[70] M. E. Essington, *Soil and Water Chemistry, An Integrative Approach*, CRC Press, Washington, DC, USA, 2004.

[71] F. Bergaya, G. Lagaly, and M. Vayer, "Cation and anion exchange," in *Handbook of Clay Science, Development in Clay Science*, F. Bergaya, B. K. G. Theng, and M. Vayer, Eds., pp. 979–1001, Elsevier Science & Technology, Amsterdam, The Netherlands, 2006.

[72] M. B. McBride, *Environmental Chemistry of Soils*, Oxford University Press, New York, NY, USA, 1994.

[73] A. D'Annibale, M. Ricci, D. Quaratino, F. Federici, and M. Fenice, "Panus tigrinus efficiently removes phenols, color and organic load from olive-mill wastewater," *Research in Microbiology*, vol. 155, no. 7, pp. 596–603, 2004.

Hindawi Publishing Corporation
Applied and Environmental Soil Science
Volume 2016, Article ID 5602795, 10 pages
http://dx.doi.org/10.1155/2016/5602795

Research Article

Long-Term Dynamics of Urban Soil Pollution with Heavy Metals in Moscow

N. E. Kosheleva and E. M. Nikiforova

Faculty of Geography, Moscow State University, Leninskie Gory, Moscow 119991, Russia

Correspondence should be addressed to N. E. Kosheleva; natalk@mail.ru

Received 2 October 2015; Revised 17 December 2015; Accepted 22 December 2015

Academic Editor: Francesco Sdao

Copyright © 2016 N. E. Kosheleva and E. M. Nikiforova. This is an open access article distributed under the Creative Commons Attribution License, which permits unrestricted use, distribution, and reproduction in any medium, provided the original work is properly cited.

Results of 21-year-long (1989–2010) observations of the concentrations and the spatial distribution patterns of nine heavy metals (HMs) in topsoils of the Eastern district of Moscow are presented. The quantitative parameters of soil pollution include the annual increase rates of HM concentrations in several land-use zones. The maps of geochemical anomalies were compiled using the data collected in 1989, 2005, and 2010. The growth of the total volume of industrial and vehicles' emissions between 1989 and 2005 caused significant deposition of Pb, Zn, Cu, and Cd. The additional input of Cd to the soils is attributed to the application of sewage sludge as fertilizers. The relative increment of concentrations was the highest for Pb, Co, Cu, Ni, and Cr. In 2005–2010, the relative annual increment rate was the highest for Cr, Cd, Co, and Ni, and it increased by an order of magnitude as compared to the previous period. By contrast, Pb and Cu concentrations decreased owing to the soil reclamation, the exclusion of leaded gasoline as a fuel for vehicles and closing some hazardous enterprises. Joint analysis of snow and soil geochemical maps allows identification of the zones of actual, permanent, and relict pollution.

1. Introduction

Development of industrial cities and rapid growth of urban population aggravates ecological problems caused by air and water contamination and permanent accumulation of pollutants in soils. Heavy metals (HMs) are of special concern since they belong to very hazardous substances. The content and distribution of HMs in Moscow soils have been analyzed by many authors [1–7]. At the same time, such urgent issues of urban ecology as a long-term dynamics of soil contamination with HMs in different land-use zones have not yet been considered. The aim of this research is to study spatial-temporal trends in soil contamination with HMs in one of the most polluted districts of Moscow.

The specific purposes of the study are as follows:

(i) to investigate the main features of long-term dynamics of HM content in the soil cover in relation to land-use type and fluctuations in urban activities;

(ii) to map technogenic geochemical anomalies in urban soils for different time periods;

(iii) to determine the character and intensity of HM accumulation in urban soils by combined analysis of snow and soil geochemical maps;

(iv) to evaluate the environmental risk of the contamination on the basis of integral indices.

2. Materials and Methods

The Eastern district has been chosen as a study object; it is located on the Meshchera outwash plain. The southern, most polluted, part of the Moscow Eastern district was investigated. This territory belongs to the southern taiga Meshchera landscapes with a temperate continental climate. The snow cover appears in late October–early January and reaches the maximum height in February-March. A flat plain with altitudes of 150–160 m a.s.l. is composed of glaciofluvial sands and loams with low content of HMs [8]. Soil cover has been severely disturbed; natural sod-podzolic, podzolic-bog, and bog soils are preserved only locally in the suburbs and green areas. The major part of the area is occupied by

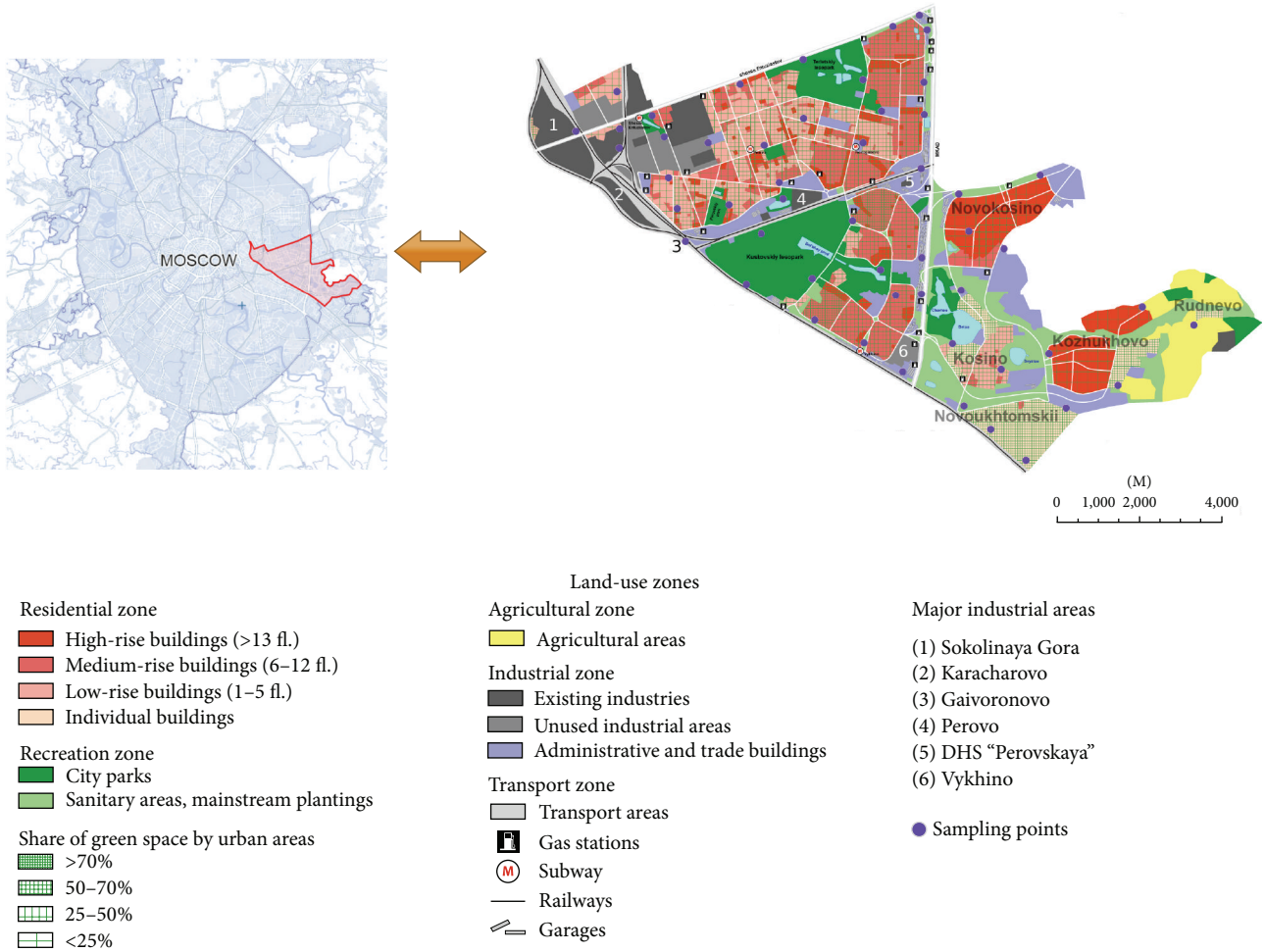

Figure 1: The map of land-use zones for the territory of the Eastern district of Moscow [12].

specific urban soils, that is, urbanozems and technozems [9], developed on filled redeposited substrates and the cultivated layer; in some parks and recreation zones, soils develop on the natural parent rocks.

The most widespread soils are urbanozems that are deeply transformed anthropogenic soils, the profiles of which change to a depth of more than 50 cm. Their main difference from natural soils is the presence of a diagnostic "urbic" horizon. This surface horizon is a filled mixed layer with an admixture (>5%) of anthropogenic inclusions (construction and industrial waste, domestic garbage); as a rule, it contains organic matter. The physical and chemical properties of this horizon change owing to the input of eolian dust [5].

The territory has multispecialized industries, including instruments and equipment producing, chemical and oil-processing factories, heating power stations, incineration plant, and a dense network of roads. Highways are the Moscow Ring Road (MKAD) and Shosse Entuziastov. Motor transport is the main source of pollution in the district [10]. The largest industrial zones are Karacharovo and Sokolinaya Gora in the north-east of the study area; Perovo in the center; Vykhino and Gaivoronovo in the south. Owing to the fall in production and decrease in the volume of wastes and emissions, the input of stationary air pollution sources decreased from 26-27% of the total mass of technogenic load, in the early 1990s to 10% at the end of the decade [11]. Nevertheless Moscow still ranks 10th–13th among Russian cities by the total pollution level from stationary sources; industry remains the most important factor responsible for the contamination of the urban environment with specific emissions.

The geochemical studies and soil sampling were performed during the summers of 1989, 2005, and 2010 at the same points (Figure 1). Samples were collected at approximately uniform grid with a sampling spacing of 700–900 m. This scheme is widely used in the world for geochemical mapping of cities [13]. Altogether 153 soil mixed samples were taken from the most humus enriched and contaminated upper (0 to 15 cm) horizons of the urban soils. Mixed samples were composed of 4 individual ones. Soddy-podzolic soils of the Meshchera Plain (45–50 km east of the city, where its influence was not displayed) were studied as background analogues. These light-textured soils develop under meadow grass-forb and forest spruce-birch communities. Ten samples

Table 1: Levels of landscape pollution with HMs and dust [14].

Levels of pollution	Dust deposition P_n, kg/km^2 per day	Total indices of HM immission Z_d	Snow pollution Z_c	Soil pollution Z_c
Low	<200	<1000	<32	<16
Medium	200–300	1000–2000	32–64	16–32
High	300–500	2000–4000	64–128	32–64
Very high	500–800	4000–8000	128–256	64–128
Maximum	>800	>8000	>256	>128

were taken from the surface horizons of the reference soils. The bulk content of Zn, Cd, Pb, Cu, Cr, Co, Ni, Mn, and Cs was determined by atomic absorption spectrometry using an Hitachi 180–70 spectrometer. To determine all the elements soil samples were transferred into the state of the solution using the mixture of acids HCl, $HClO_4$, and HNO_3, with triple evaporation and complexation of HF with boric acid. The residue was then dissolved in HCl.

The type of land use is of primary importance for the formation of technogenic geochemical anomalies; therefore land-use zoning of the territory was performed using satellite high-resolution images [12]. The following areas were specified (Figure 1): highways and industrial zones, medium-rise residential blocks within MKAD, recreation zone (parks, forest parks, and leisure areas), new high-rise buildings (Novokosino, Kozhukhovo), old residential blocks (private low-rise buildings in Novoukhtomskii, Kosino, and Rudnevo settlements), and agricultural area (arable lands of the former Mossovet sovkhoz). The zones differ in duration and intensity of anthropogenic stress. Geochemical maps were compiled using spline interpolation (Geostatistical Analyst, ArcGIS 10).

The accumulation or dispersion of dust and HMs in urban soils was evaluated using enrichment or depletion factors estimated via comparison with the data on the HM concentrations Cf in the reference soddy-podzolic soils: EF = C/Cf and DF = Cf/C, where C is the element concentration in urban soils. The results are displayed on a special plot named *geochemical spectrum*. The immission of the solid fraction of HMs to soil D equals the dust load P_n in the snow multiplied by HM concentration in it; $D = P_n \cdot C$. Exceedance of HM fallout above background values Df is characterized by a factor $K_d = D/Df$. Total multielemental pollution of snow and soil cover is defined by integral indices of immission $Z_d = \sum_{i=1}^{n} K_d - (n-1)$ and total pollution $Z_c = \sum_{i=1}^{n} \mathrm{EF} - (n-1)$, respectively, where n is number of elements with K_d or EF > 1. They summarize the excess of the HM contents in urban soils over background levels and thus display the degree of their anthropogenic geochemical transformation [14, 25, 26]. Integral indices have 5 levels which determine the degree of pollution (Table 1). Maps of these parameters reveal spatial patterns of pollution in these depositing media.

3. Results and Discussion

3.1. Accumulation of HMs in Urban Soils. The intensity of HM accumulation in the soils of the Eastern district (Figure 2) was evaluated in relation to the background soils

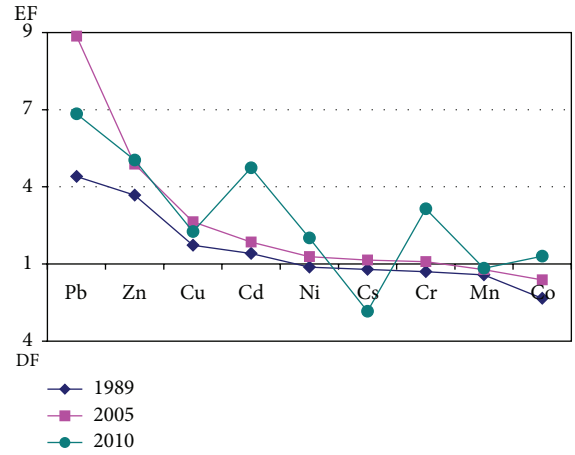

Figure 2: Geochemical spectra of urban soils in the Eastern district of Moscow showing enrichment and depletion factors (EF, DF) of metals in relation to background soils.

of Meshchera plain which have trace-level concentrations of all HMs under study, except for Cd and Cs. Low values of metal concentrations in background soils are explained by their contents in parent fluvioglacial sands [8] and the small intensity of fallout from the atmosphere [2, 9].

In 1989 the group of four elements accumulated in urban soils with the following sequence according to their enrichment factors EF (inferior indices): $Pb_{4.4}Zn_{3.7}Cu_{1.7}Cd_{1.4}$. Other metals dissipated with intensity which was defined by their depletion factors DF (top indices): $Co^{2.3}Mn^{1.4}Cr^{1.3}Cs^{1.2}Ni^{1.1}$. The content of HMs in urban soils was very variable; coefficients of variation CV of particular HMs changed from 41 to 89%, reaching 102% for Cd because of differences between the individual land-use zones.

In 2005 metals pollutants showed the increasing content while preserving the above sequence: $Pb_{9.9}Zn_{4.9}Cu_{2.6}Cd_{1.8}$. During 1989–2005 the average concentrations of two main pollutants, Pb and Zn, increased by a factor of 2.2 and 1.3, respectively. The content of Cr, Cs, and Ni came close to their background levels; only Co and Mn had concentrations below the background values (DF 1.6 and 1.2). Soil concentrations of all HMs under study were slightly less variable than in 1989 (CV 32–66% for Co, Ni, Mn, Cs, Zn, Cr, and Cu and 91-92% for Cd and Pb).

In 2010, 21 years after the beginning of investigations, further growth of soil pollution with HMs was observed, and

Table 2: Mean content of HMs (mg/kg) in topsoils of natural background and various land-use zones in the Eastern district of Moscow in 1989, 2005, and 2010.

Year (number of samples)	Pb	Zn	Cu	Cd	Co	Cr	Ni	Mn	Cs
Natural background of the Meshchera lowland									
1989 (10)	9.04	37.5	27.9	0.34	6.60	32.0	15.2	585	5.40
Highways (A) and industrial zones (P)									
1989 (12)	60.5	224	80.7	0.65	3.85	34.0	17.6	442	5.58
2005 (14)	174	305	130	0.81	5.82	51.7	26.9	518	8.08
2010 (13), A	59.5	183	67.5	1.23	8.48	89.9	32.2	412	1.90
2010 (5), P	114	286	88.0	1.37	9.3	92.2	35.4	513	1.88
Residential zone with low-rise buildings (L)									
1989 (5)	72.4	138	39.4	0.64	2.67	32.1	16.2	463	4.53
2005 (5)	159	180	65.7	0.81	3.84	47.9	22.6	549	6.34
2010 (5)	68.8	163	60.6	1.33	8.12	95.6	33.6	544	1.64
Residential zone with medium-rise buildings (M)									
1989 (16)	23.4	130	40.1	0.35	2.48	20.5	12.1	340	4.65
2005 (17)	39.9	165	58.8	0.48	3.76	29.2	17.8	414	6.47
2010 (10)	66.7	223	62.3	1.43	8.6	106	30.0	493	2.09
Residential zone with high-rise buildings (H)									
1989 (5)	16.4	76.5	24.6	0.14	1.61	16.3	9.14	260	2.43
2005 (5)	20.2	88.3	28.1	0.15	1.82	18.2	10.6	309	2.91
2010 (7)	44.1	162	54.0	1.45	8.57	104	26.1	389	1.99
Recreational zone (R)									
1989 (6)	21.1	76.7	24.3	0.17	2.44	9.24	7.58	512	4.04
2005 (6)	32.9	82.7	28.9	0.20	2.87	11.6	9.20	538	4.44
2010 (9)	49.4	147	50.4	2.05	8.8	101	29.0	482	1.87
Agricultural landscapes (AG)									
1989 (5)	45.6	96.3	57.7	1.07	3.20	34.0	18.0	535	3.74
2005 (5)	84.7	122	71.2	1.44	4.09	37.9	21.5	640	5.19
2010 (3)	34.0	173	67.0	3.70	7.7	137	27.3	492	1.47

the group of metals concentrated in topsoils was expanded up to seven elements. According to EF values, they form the following sequence: $Pb_{6.8}Zn_{5.0}Cd_{4.7}Cr_{3.1}Cu_{2.3}Ni_{2.0}$ $Co_{1.3}$. Mn and Cs have the contents below background (DF 1.2 and 2.8, resp.). Since Cs is concentrated in hydroxides of Mn, its removal (washout) from the topsoils is accompanied by a significant decrease in the content of Cs [27]. The concentration of Pb—the main pollutant—decreased by a factor of 1.4 in comparison to 2005 that could be the result of soil reclamation in combination with the exclusion of leaded gasoline as a fuel for vehicles and the closing some hazardous enterprises which produced machines and electronic equipment. The intensive growth of Cd content in urban soils is caused by its presence in the motor vehicle emissions; in agricultural and recreation zone it is related to the application of large amounts of mineral and organic fertilizers and sewage sludge which contain Cd as an admixture. Concentrations of other metals increased slightly or remained at the same level. The contents of Co, Cs, and Pb in soils became less variable, while that of Zn and Cr increased up to 68–70% and of Cd, up to 136%.

3.2. HM Content in Soils with Different Type of Land Use. Distinctions in the levels of HM concentration in soils of different land-use zones were revealed through the analysis of values in Table 2. Differences in mean HM content were evaluated by t-test. They were significant at P 90–95% for the majority of the elements and land-use zones since mixed samples which were composed of 4 individual ones were used. In 1989 Pb and Zn were accumulated in soils of all land-use zones, particularly within old low-rise residential areas (EF 8.0 and 3.7, resp.), near highways (6.7 and 6.0), and agricultural areas (5.0 and 2.6). The third priority pollutant—Cu—was mostly accumulated in the industrial and transport zones (2.9). Soils of the recreational zone and new high-rise residential areas showed low contents of HMs. Among them the greatest dispersion of Cr (DF 3.5 and 2.0) and Co (2.7 and 4.1, resp.) in comparison with background soils was observed.

In 2005 the overall picture of HMs distribution in the soils of individual zones was the same, but the concentrations of main pollutants—Pb and Zn—significantly increased (Table 2). The highest concentrations were found in the soils of highways and industrial zone (EF 19.2 and 8.1, resp.), old residential blocks (17.6 and 4.8), and agricultural areas (9.4 and 3.3). Low concentrations of the majority of HMs (Co, Cr, Cd, Ni, Mn, and Cs) in comparison with background values

Table 3: Mean surplus/decrease rate of HM contents in topsoils of the Eastern district of Moscow.

Period	Increment rate	Pb	Zn	Cu	Cd	Co	Cr	Ni	Mn	Cs
1989–2005	mg/kg per year	3.1	2.8	1.6	0.01	0.08	0.64	0.36	4.40	0.11
	%	0.08	0.03	0.04	0.03	0.04	0.03	0.03	0.02	0.03
1989–2005	mg/kg per year	−5.4	1.2	−2.1	0.20	0.90	13.0	2.2	3.8	−0.86
	%	−0.36	0.03	−0.15	0.89	0.71	0.97	0.45	0.04	−1.1

were observed in the soils of recreational zone and new high-rise residential quarters (DF 3.6–1.1).

In 2010 geochemical contrasts in the soils of individual land-use zones became less pronounced. The concentrations of Cr, Co, and Mn increased in comparison with 2005 practically in all land-use zones, and those of Pb, Cu, Zn decreased in transport and industrial zones, old residential and agricultural areas (except for Zn). The content of Pb in these zones decreased by a factor of 2.3–2.5 that is apparently related to the soil reclamation, as well as to improvement of fuel and changes of vehicle structure. The content of Cd sharply increased, especially in the soils of recreational and agricultural zones. This could be explained by the application of high doses of sewage sludge and phosphoric fertilizers.

3.3. Long-Term Dynamics of HM Anomalies in Urban Soils. The time-spatial patterns of HMs distribution in soils are presented on the maps of Z_c index compiled for several years of the 21-year-long period of observations (Figure 3). In 1989 the territory was characterized by low level of total pollution ($Z_c < 16$) as a result of rather weak industrial and transport influence on urban soils. On this background there were several small spots of low-contrast technogenic anomalies of HMs with medium level of pollution located in northwest, southeast, and central parts of the district. In the centers of these anomalies the values of Z_c indicator did not exceed 32–35.

In 2005 the existing anomalies of HMs in soil cover of the district considerably increased their size and contrast; the total pollution of soils increased by a factor of 1.7 for the 16-year period. The most contrast technogenic anomaly of HMs with Z_c about 48 in its center was formed in the northwest under the influence of emissions from the large industrial zone "Sokolinaya Gora" and Shosse Entuziastov Highway. Several anomalies along the Moscow Ring Road (MKAD at Figure 1) which were poorly expressed in 1989 became larger with maximum Z_c 32–40. Southeast anomaly of HMs in soils also became more pronounced, up to Z_c 48. Thus, the pollution level in anomalies has changed from the medium to high.

In 2010 a further increase in the areas and intensity of HM anomalies was observed. The northwest anomaly with the total index of soil pollution Z_c 48–80 expanded beyond the industrial zone "Sokolinaya Gora" and partly covered residential areas to the south of Shosse Entuziastov Highway. In the center of the district large anomaly with $Z_c >$ 100 was formed under the influence of the industrial zone "Perovo" and district heating station (DHS) "Perovskaya." In the southeast part of the district technogenic anomaly of HMs was extended to the east while the Z_c indicator increased up to 50–70. It is the result of emissions of recently constructed incineration plant near the settlement of Rudnevo.

Growing contamination of urban soils with HMs is caused not only by an increase in emissions from industry and transport in particular, but also by a change in absorption capacity of the soils. Anthropogenic transformation of the physical and chemical properties of the soils leads to the formation of complex physical and chemical barriers. They arise as a result of precipitation of carbonate construction dust enriched by fine particles, application of soil peat compost mixtures with a high content of humic substances for planting of greenery as well as flooding and soil sealing which alters its gas and redox regimes. The HM accumulation on these man-made barriers is not necessarily accompanied by a reduction in their mobility; analysis of mobile forms of HMs showed that their precipitation from the atmosphere exceeds the speed of their washout from topsoils [28].

3.4. Trends of HM Accumulation in Topsoils and Snow Cover. Tendencies of HM accumulation in the urban soils were evaluated for two periods: 1989–2005 and 2005–2010 by calculation of average annual growth of HM content in the topsoils (Table 3) which differ considerably depending on the type of land use (Figure 4).

From 1989 to 2005 the growth of HM content in soils of the Eastern district was relatively small. The maximum absolute increase was inherent of Mn (4.4 mg/kg per year) > Pb (3.1) > Zn (2.8) > Cu (1.6) > Cr (0.64). Thus, the relative rate was the greatest for Pb, Co, Cu, Ni, and Cr (0.07–0.03% per year) in the soils of industrial zones and near highways, old low-rise residential quarters, and agricultural areas (Figure 4).

In 2005–2010, the rates of HM accumulation in the soils increased and became more differentiated among the land-use zones (Figure 4). Depending on the average annual values HMs form the following sequence: Cr (13.1 mg/kg per year) > Mn (3.8) > Ni (2.2) > Zn (1.2) > Co (0.9). Cr, Cd, Co, and Ni had the maximum relative rate of growth (up to 0.5–1.0%), in comparison with the previous period it increased by tens times (Table 2). The content of Pb, Cs, and Cu significantly decreased showing negative values of the annual rate mainly owing to soil reclamation.

Uneven distribution of HM accumulation rates within the territory of the district is well seen on Figure 4. Cr and Cd show the overall growth, especially in less polluted zones (recreational, agricultural, and new residential areas), while Pb and Zn dissipate in the soils of industrial zones and highways, old low-rise residential and agricultural areas.

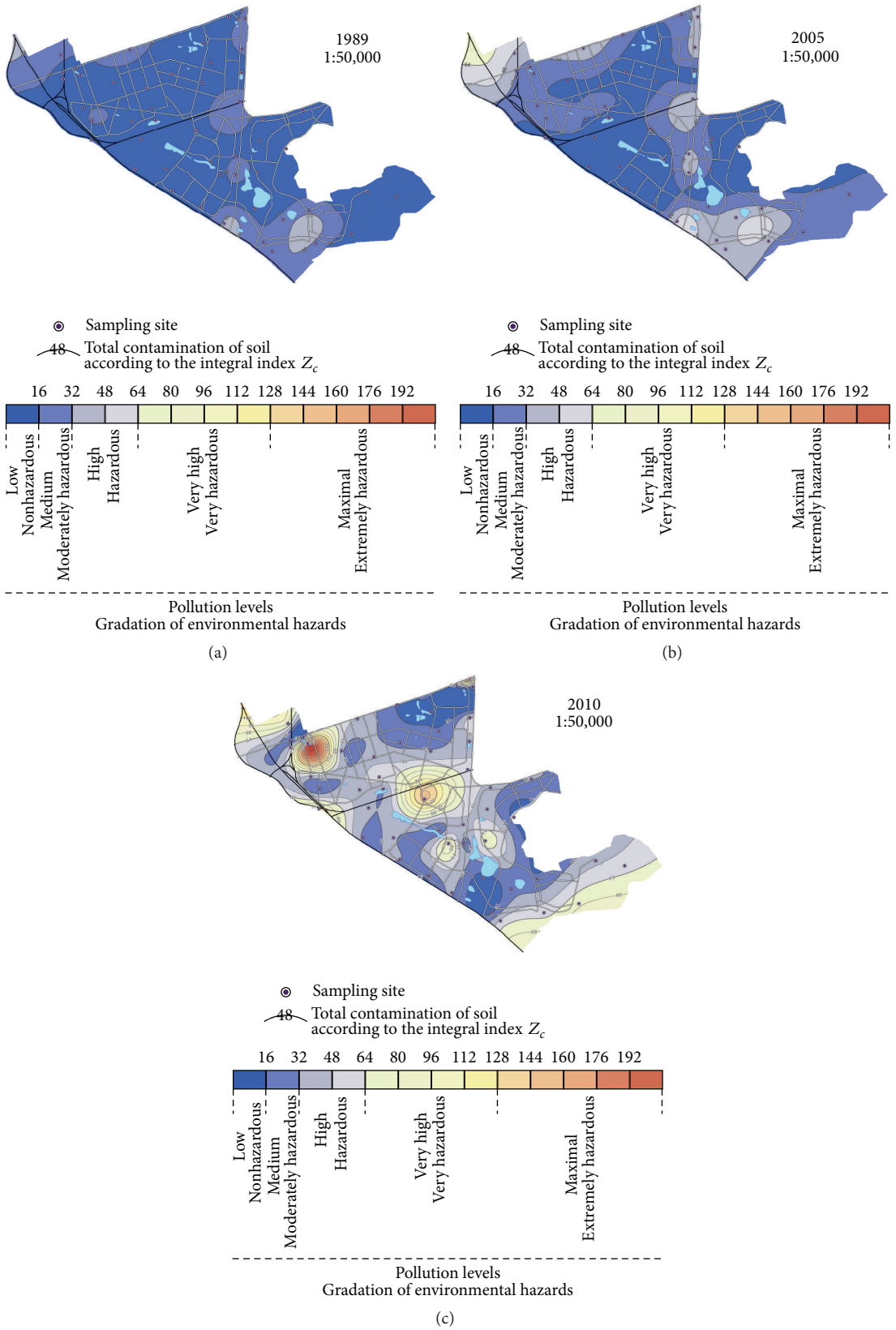

FIGURE 3: Total technogenic anomalies of HMs (according to Z_c index) in topsoils of the Eastern district of Moscow in 1989, 2005, and 2010.

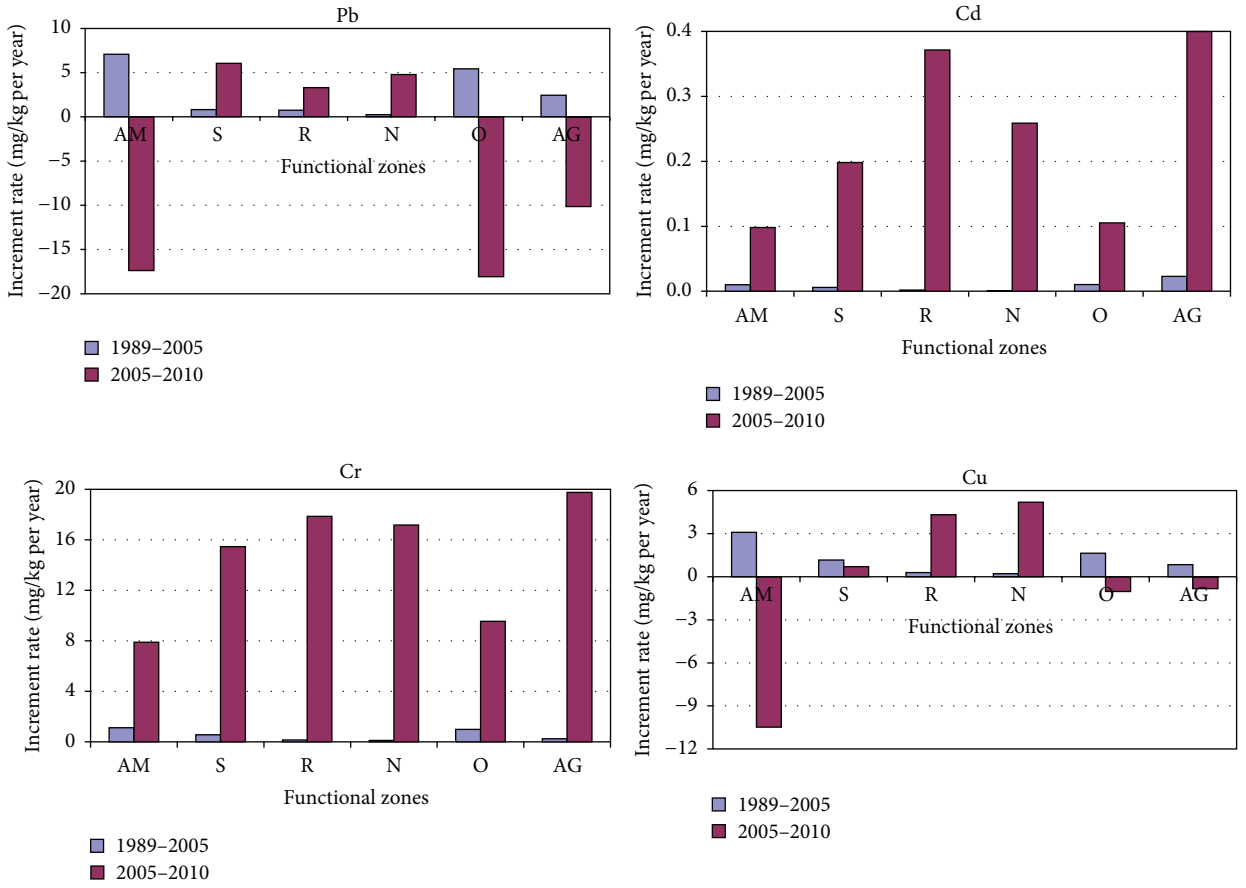

Figure 4: Average increase or reduction of the content of Pb, Cd, Zn, and Cr in the topsoils of different land-use zones in the Eastern district of Moscow for two periods of observations (1989–2005 and 2005–2010). Symbols of land-use zones are given in Table 2.

Table 4: Long-term dynamics of total HM pollution of soils in the Eastern district of Moscow depending on the type of their use.

Observation year	Average values of total index of pollution Z_c in soils of the land-use zones							
	Highways	Industrial	Medium-rise residential	High-rise residential	Recreational	Low-rise residential	Agricultural	Total for the district
1989	15.6		6.3	2.9	3.5	13.2	10.4	9.02
2005	33.4		10.3	3.7	5.0	25.5	17.2	17.3
2010	17.9	28.3	20.4	15.4	17.9	18.6	22.9	19.4

The dynamics of soil pollution was compared with the distribution of HMs in the snow. The snow cover reflects actual state of the environment while the soil represents more stable long-term pollution. Joint analysis of snow and soil geochemical maps allows identification of the areas of actual, permanent, and relict pollution. The relict technogenic anomalies occur only in soil cover, modern ones, only in snow, and permanent ones in snow and soils simultaneously [25]. The snow pollution with HMs in the Eastern district of Moscow was defined using the integral index of immission Z_d [29]. It characterizes both the composition and amount of dust which accumulates in snow. Overlay of the maps of Z_c and Z_d integral indices resulted in the identification of permanent anomalies within the major part of the district (Figure 5). In the center of the area a relict anomaly was formed as a result of elimination and reprofiling of the stationary sources of emissions. On the north, along the Shosse Entuziastov Highway a modern anomaly of HMs was discovered in the vicinity of Terletskiy park.

3.5. Assessment of Environmental State of Urban Soils. The analysis of average zonal values of the total indicator of pollution Z_c (Table 4) showed that in 1989 the most part of the territory under study was characterized by a low level of HM pollution. The average value of Z_c was only 9.0 that indicates harmless ecological condition of soils. Z_c values exceeded this level only in 10 of 49 sampling sites (i.e., 20.4%), mainly in the industrial zones and near highways.

In 2005 much less sampling points showed Z_c values < 16 (31 of 52, i.e., 59.6%). Moreover, 14 points (26.9%) shifted

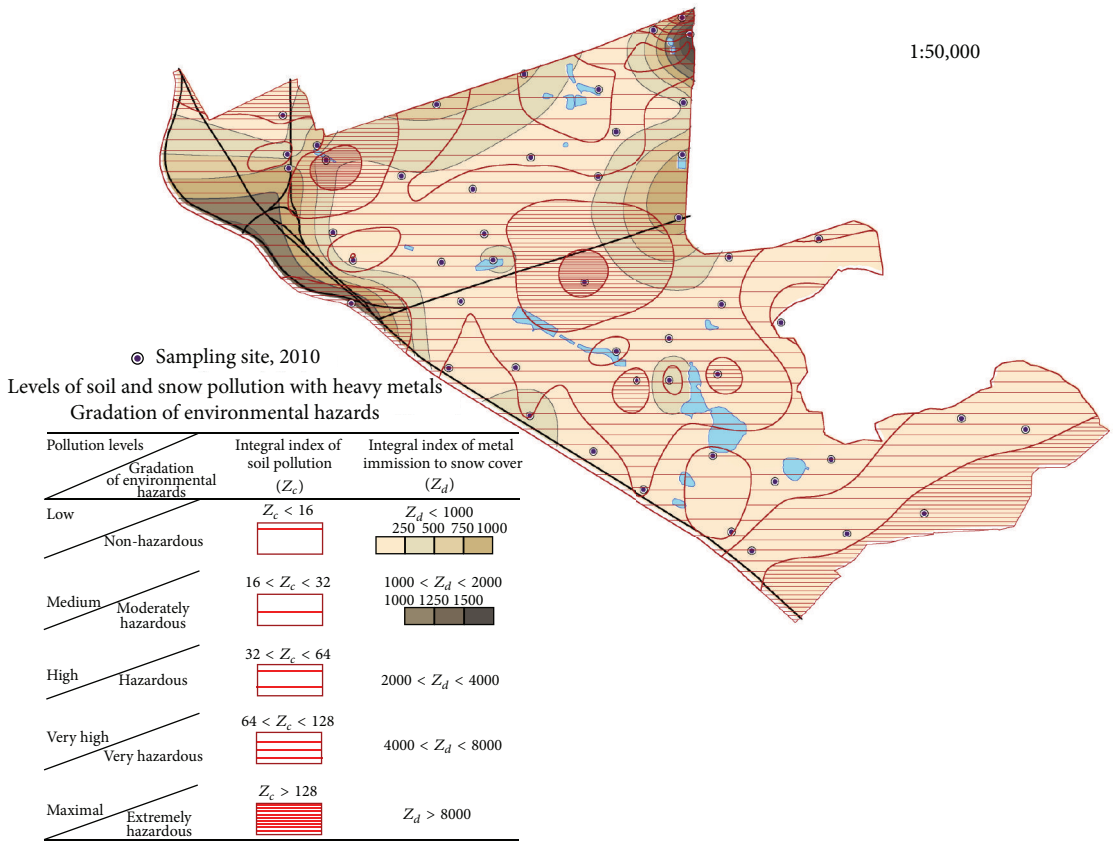

Figure 5: Location of areas of actual, permanent, and relict pollution in the Eastern district of Moscow according to anomalies in soils and snow cover.

Table 5: Clarks in the lithosphere [15] and the average contents of Pb, Zn, Cr, and Ni in soils (mg/kg) of the various cities of the world (compiled by the authors according to [16–24] and to own data for the Eastern district of Moscow, 2010).

HM	Lithosphere clark	Stockholm	Madrid	Seville	Berlin	Hamburg	London	Hong Kong	Palermo	Naples	Belgrade	Da Nang	Moscow, Eastern district
Pb	16	101	161	161	119	218	294	93.4	253	262	55.5	20.0	61.8
Zn	83	171	210	107	243	516	183	168	151	251	118	142	189
Cr	83	34.0	74.7	42.8	35.0	95.4	—	<40.0	39.0	74.0	32.1	92.2	100
Ni	58	12.8	14.1	23.5	10.7	62.5	—	<20.0	19.1	—	68.0	22.6	30.6

to medium and 7 points (13.5%) to high level of pollution. Average Z_c value for the district was 17.3 that corresponds to medium level of HM pollution of soils. There were only three land-use zones with low level of soil contamination, residential zones with medium- and high-rise buildings, and recreational zone (Table 4). In 2005 soils of the residential low-rise zone and agricultural landscapes had medium level of HM pollution, and those of highways and industrial zones had high one.

In 2010 the average Z_c value for the district increased up to 19.4. In contrast to the decrease of soil pollution level for highways, industrial and residential zones with low-rise buildings, a significant increase of HM pollution occurred in recreational, agricultural, and residential high-rise zones. Thus it is only in the latter zone where the level of soil contamination corresponds to harmless category; other zones are moderately polluted (Z_c 17.9–28.3).

To assess the ecological rank of Moscow in terms of the level of HM accumulation in soils among the cities of the world, we compared the average contents of four most common HMs (Pb Zn, Cr, and Ni) in the soils of large and capital cities of several countries with their values in the soils of the Eastern district of Moscow. Soils of the large cities of the world have rather high average HM concentrations (Table 5) comparable to Moscow quantities, especially Pb and Zn. Most intensive accumulation of Pb is typical for the soils of London, Naples, Palermo, and Hamburg, while that of Zn is typical for the soils of Hamburg, Naples, Berlin, and

Madrid. The contents of Cr and Ni are below their clarks in the lithosphere; the minimum values are observed in the soils of Madrid, Berlin, Palermo, and Stockholm. So, according to 2010 data, soils of the Eastern district of Moscow do not show particularly high levels of HM accumulation. The average content of Pb in the topsoils of the district is close to its values in the soils of Belgrade and that of Zn is close to its values in the soils of Stockholm and London. The same levels of the content of Cr, as in soils of the Eastern district, are recorded in Palermo and Hamburg, and that of Ni is recorded in Seville and Palermo.

4. Conclusions

Soils of the Eastern district of Moscow show the gradual increase of HM pollution levels. Among them Pb and Zn are the leaders with enrichment factors EF 3.7–9.9. In 2010 Cd joined them (EF 4.7); the intensive growth of its content is caused by its presence in the motor vehicle emissions as well as by application of mineral and organic fertilizers and sewage sludge containing Cd as an admixture. Over the last 5 years the contents of Pb and Cu in soils of the district decreased owing to the soil reclamation and adding uncontaminated material, the exclusion of leaded gasoline as a fuel for vehicles, and also conversion and closing a number of hazardous industrial enterprises which emit these metals.

In 1989–2005 the annual increase of HM concentrations in soils of the Eastern district was rather low. Pb and Cu demonstrated the maximum rates of increase (0.08 and 0.04% per year, resp.). In 2005–2010 rates of the annual increase of HM concentrations in soils were higher, with more pronounced differentiation in particular land-use zones. Cr, Cd, Co, and Ni had the maximum rates of increase (1.0–0.45% per year). The contents of Pb and Cu in the soils of industrial zones and highways, agricultural, and old residential areas went down. Nevertheless, these zones still have the highest contents and the widest range of elements pollutants.

At present, a medium total pollution level is common for the soils of the Eastern district, with the Z_c index reaching 28.3 in the industrial zone. The priority contaminants are Pb, Zn, and Cd. The maximum level of Pb and Zn concentrations (114 and 286 mg/kg, resp.) in topsoils has been revealed in the industrial zone, while that of Cd (3.7 mg/kg) has been revealed in the recreational zone.

To represent the stages of development of the technogenic multielemental anomalies in urban soils maps of a total index of pollution Z_c were compiled for particular years of the 21-year period of observations. Their analysis revealed a significant increase of the contrast and the area of HM anomalies in recent years, which could be attributed to the growth of the total amount of industrial and motor transport emissions and change in absorption capacity of the urban soils.

Conflict of Interests

The authors declare that there is no conflict of interests regarding the publication of this paper.

Acknowledgments

Field and chemical works were supported by the Russian Geographic Society and the Russian Foundation for Basic Research (Project no. 13-05-41191), and analysis and interpretation of geochemical data were accomplished with the financial support of the Russian Scientific Foundation (Project no. 14-27-00083). The authors thank Dr. D. V. Vlasov and Mrs. G. L. Shinkareva who took part in the field investigations. Dr. T. S. Khaybrakhmanov is much appreciated for the geochemical maps he compiled.

References

[1] E. M. Nikiforova and G. G. Lazukova, "Moscow. Perovo District. Plain landscapes," in *Ecogeochemistry of Urban Landscapes*, N. S. Kasimov, Ed., pp. 57–90, Moscow University Publishing House, Moscow, Russia, 1995 (Russian).

[2] S. B. Samaev, L. S. Sokolov, and A. S. Panteleev, "Soil pollution caused by motor traffic in Moscow," in *Automotive Complex and Ecological Safety*, pp. 266–270, Prima-Press-M, Moscow, Russia, 1999 (Russian).

[3] Yu. N. Nikolaev, T. V. Shestakova, V. V. Nefed'ev et al., *Assessment of Geochemical Contamination in the Losinyi Ostrov National Park*, Prima-Press-M, Moscow, Russia, 2000 (Russian).

[4] Kh. G. Yakubov, *Environmental Monitoring of Plantations in Moscow*, Stagirit-N, Moscow, Russia, 2005 (Russian).

[5] E. M. Nikiforova and N. E. Kosheleva, "Dynamics of contamination of urban soils with lead in the Eastern district of Moscow," *Eurasian Soil Science*, vol. 40, no. 8, pp. 880–892, 2007.

[6] E. M. Nikiforova and N. E. Kosheleva, "Fractional composition of lead compounds in soils of Moscow and Moscow region," *Eurasian Soil Science*, vol. 42, no. 8, pp. 874–884, 2009.

[7] O. V. Plyaskina and D. V. Ladonin, "Heavy metal pollution of urban soils," *Eurasian Soil Science*, vol. 42, no. 7, pp. 816–823, 2009.

[8] I. A. Avessalomova, "Landscapes of Meshchera lowplain," in *Landscape-Geochemical Principles of Background Monitoring of Natural Environment*, M. A. Glazovskaya and N. S. Kasimov, Eds., pp. 79–90, Nauka, Moscow, Russia, 1989 (Russian).

[9] T. V. Prokofyeva, I. A. Martynenko, and F. A. Ivannikov, "Classification of Moscow soils and parent materials and its possible inclusion in the classification system of Russian soils," *Eurasian Soil Science*, vol. 44, no. 5, pp. 561–571, 2011.

[10] N. I. Ivanov, Ed., *Engineering Ecology and Environmental Management*, Logos, Moscow, Russia, 2002 (Russian).

[11] V. R. Bityukova and R. Argenbrayt, "Regional peculiarities of modern ecological situation in Moscow: premises, contemporary tendencies, prospect," *Eurasian Geography and Economics*, no. 4, pp. 14–31, 2002.

[12] E. M. Nikiforova, N. E. Kosheleva, I. A. Labutina, and T. S. Khaybrakhmanov, "Geoinformation landscape-geochemical mapping of city territories (the case study of Eastern District of Moscow)," *Journal of Civil Engineering and Science*, vol. 3, no. 3, pp. 142–151, 2014.

[13] C. C. Johnston, A. Demetriades, J. Locutra, and R. T. Ottesen, *Mapping the Chemical Environment of Urban Areas*, John Wiley & Sons, Chichester, UK, 2011.

[14] N. S. Kasimov, V. R. Bityukova, A. V. Kislov et al., "Problems of urban geochemistry," *Exploration and Conservation of Mineral Resources*, no. 7, pp. 8–13, 2012 (Russian).

[15] A. P. Vinogradov, "Average content of chemical elements in the main types of igneous rocks," *Geochemistry*, no. 7, pp. 555–572, 1962 (Russian).

[16] P. Tume, J. Bech, B. Sepulveda, L. Tume, and J. Bech, "Concentrations of heavy metals in urban soils of Talcahuano (Chile): a preliminary study," *Environmental Monitoring and Assessment*, vol. 140, no. 1–3, pp. 91–98, 2008.

[17] M. Linde, H. Bengtsson, and I. Oborn, "Concentrations and pools of heavy metals in urban soils in Stockholm, Sweden," *Water, Air, & Soil Pollution: Focus*, vol. 1, pp. 83–101, 2001.

[18] H. T. T. Thuy, H. J. Tobschall, and P. V. An, "Distribution of heavy metals in urban soils—a case study of Danang-Hoian Area (Vietnam)," *Environmental Geology*, vol. 39, no. 6, pp. 603–610, 2000.

[19] X. Li, C.-S. Poon, and P. S. Liu, "Heavy metal contamination of urban soils and street dusts in Hong Kong," *Applied Geochemistry*, vol. 16, no. 11-12, pp. 1361–1368, 2001.

[20] M. Birke and U. Rauch, "Urban geochemistry: investigations in the Berlin metropolitan area," *Environmental Geochemistry and Health*, vol. 22, no. 3, pp. 233–248, 2000.

[21] M. Imperato, P. Adamo, D. Naimo, M. Arienzo, D. Stanzione, and P. Violante, "Spatial distribution of heavy metals in urban soils of Naples city (Italy)," *Environmental Pollution*, vol. 124, no. 2, pp. 247–256, 2003.

[22] L. Madrid, E. Diaz-Barrientos, E. Ruiz-Cortés et al., "Variability in concentrations of potentially toxic elements in urban parks from six European cities," *Journal of Environmental Monitoring*, vol. 8, no. 11, pp. 1158–1165, 2006.

[23] D. Crnković, M. Ristić, and D. Antonović, "Distribution of heavy metals and arsenic in soils of Belgrade (Serbia and Montenegro)," *Soil & Sediment Contamination*, vol. 15, no. 6, pp. 581–589, 2006.

[24] F. Ajmone-Marsan and M. Biasioli, "Trace elements in soils of urban areas," *Water, Air, & Soil Pollution*, vol. 213, no. 1, pp. 121–143, 2010.

[25] Yu. E. Saet, B. A. Revich, E. P. Yanin et al., *Geochemistry of the Environment*, Nedra, Moscow, Russia, 1990 (Russian).

[26] N. S. Kasimov, N. E. Kosheleva, O. I. Sorokina, S. N. Bazha, P. D. Gunin, and S. Enkh-Amgalan, "Ecological-geochemical state of soils in Ulaanbaatar (Mongolia)," *Eurasian Soil Science*, vol. 44, no. 7, pp. 709–721, 2011.

[27] A. I. Perel'man, *Geochemistry of Elements in the Hypergenesis Zone*, Nedra, Moscow, Russia, 1972 (Russian).

[28] N. E. Kosheleva, N. S. Kasimov, and D. V. Vlasov, "Factors of the accumulation of heavy metals and metalloids at geochemical barriers in urban soils," *Eurasian Soil Science*, vol. 48, no. 5, pp. 476–492, 2015.

[29] N. S. Kasimov, N. E. Kosheleva, D. V. Vlasov, and E. V. Terskaya, "Geochemistry of snow cover in the Eastern District of Moscow," *Moscow University Vestnik. Series 5. Geography*, no. 4, pp. 14–25, 2012 (Russian).

Hindawi Publishing Corporation
Applied and Environmental Soil Science
Volume 2016, Article ID 1480976, 15 pages
http://dx.doi.org/10.1155/2016/1480976

Research Article

Combining Geoelectrical Measurements and CO_2 Analyses to Monitor the Enhanced Bioremediation of Hydrocarbon-Contaminated Soils: A Field Implementation

Cécile Noel,[1,2] Jean-Christophe Gourry,[1] Jacques Deparis,[1] Michaela Blessing,[1] Ioannis Ignatiadis,[1] and Christophe Guimbaud[2]

[1]*BRGM, 3 avenue Claude Guillemin, 45060 Orléans, France*
[2]*LPC2E, CNRS, 3 avenue de la Recherche Scientifique, 45071 Orléans, France*

Correspondence should be addressed to Cécile Noel; cecile.noel@cnrs-orleans.fr

Received 2 October 2015; Accepted 12 November 2015

Academic Editor: Pantelis Soupios

Copyright © 2016 Cécile Noel et al. This is an open access article distributed under the Creative Commons Attribution License, which permits unrestricted use, distribution, and reproduction in any medium, provided the original work is properly cited.

Hydrocarbon-contaminated aquifers can be successfully remediated through enhanced biodegradation. However, *in situ* monitoring of the treatment by piezometers is expensive and invasive and might be insufficient as the information provided is restricted to vertical profiles at discrete locations. An alternative method was tested in order to improve the robustness of the monitoring. Geophysical methods, electrical resistivity (ER) and induced polarization (IP), were combined with gas analyses, CO_2 concentration, and its carbon isotopic ratio, to develop a less invasive methodology for monitoring enhanced biodegradation of hydrocarbons. The field implementation of this monitoring methodology, which lasted from February 2014 until June 2015, was carried out at a BTEX-polluted site under aerobic biotreatment. Geophysical monitoring shows a more conductive and chargeable area which corresponds to the contaminated zone. In this area, high CO_2 emissions have been measured with an isotopic signature demonstrating that the main source of CO_2 on this site is the biodegradation of hydrocarbon fuels. Besides, the evolution of geochemical and geophysical data over a year seems to show the seasonal variation of bacterial activity. Combining geophysics with gas analyses is thus promising to provide a new methodology for *in situ* monitoring.

1. Introduction

Petroleum hydrocarbon leaks and accidental spills happen commonly during the production, refining, transport, and storage of petroleum. Release of petroleum hydrocarbons into the environment causes damage to ecosystems [1] and to soil and water resources [2]. Increasing demand for drinking water and cropland with population growth requires effective remediation techniques to treat the contamination and to decrease hostile effects on health and environment. *In situ* remediation techniques such as enhanced bioremediation were shown to be effective in cleanup of the contamination [3, 4]. Enhanced bioremediation involves the addition of nutrients or electron acceptors to the subsurface environment to accelerate the natural biodegradation processes which degrade hydrocarbons [5]. Due to the potential of cost saving of *in situ* techniques compared to conventional *ex situ* techniques, there is an economical interest for commercial providers to use enhanced bioremediation [6]. However, these processes remain partially unexploited, mainly because their *in situ* monitoring, before, during, and after soil treatment operations, is often expensive and technically challenging. Indeed, where significant subsurface heterogeneity exists, conventional intrusive groundwater sampling campaigns can be insufficient to obtain relevant information as they are restricted to costly monitoring piezometers at discrete locations. New monitoring tools are needed to overcome these limitations and make the enhanced bioremediation more reliable and robust, as well as economically competitive.

Previous studies suggest that geoelectrical techniques, especially electrical resistivity (ER) and induced polarization (IP), can be used to detect the presence of LNAPLs (Light Nonaqueous Phase Liquids) [7–10] as well as monitoring the effects of their biodegradation [11–14]. Biodegradation

processes modify ground electrical properties because they change biophysicochemical conditions in the subsurface: (i) bacteria modify local redox conditions, inducing changes in self-potential (SP) [15]; (ii) microbial activity can produce organic acids and/or carbonic acid that affect the pore water conductivity, modifying both the in-phase and the quadrature conductivity [16]; (iii) during microbial growth and formation of biofilms, biomass can clog pores and potentially change the porosity and hydraulic conductivity, increasing the storage of electrical charges [17, 18]. Thus, ER and IP are expected to be effective nonintrusive tools to monitor enhanced bioremediation.

Some studies have implemented geoelectrical methods to characterize hydrocarbon-contaminated sites under biodegradation [19–22], but only few apply these methods for long-term monitoring or to prove the efficiency of enhanced bioremediation [23]. These previous field studies suggest that ER and IP are highly sensitive to the biophysicochemical processes associated with biodegradation. Nevertheless, the interpretation of geophysical data remains challenging partly because several factors may contribute to the observed electrical response (presence of metallic particles or clays, e.g.) and/or influence the electrical response in function of time (variation of water saturation and temperature). That is why geoelectrical methods are often used in conjunction with geochemical measurements (temperature, pH, redox potential, water conductivity, and dissolved oxygen content) to detect changes in the chemical and physical properties of the soil and groundwater. With the aim of minimizing the use of piezometers, microbial activity is followed by studying gas emissions at the ground surface. Indeed, aerobic degradation of hydrocarbons results in the production of CO_2 [24]. Due to its limited solubility (in alkalinity saturated groundwaters), CO_2 gas will tend to migrate toward the ground surface and surface CO_2 fluxes can be directly linked to the biodegradation intensity. Meanwhile, this CO_2 production occurs concurrently with natural root and microbial soil respiration. Thus, tools capable of quantifying CO_2 sources are also needed. Carbon stable isotopic analyses (ratio of $^{13}C/^{12}C$) use the fact that petroleum hydrocarbon isotopic signature is distinguishable (range from −18 to −34‰ versus Vienna Pee Dee Belemnite or VPDB [25]) from other aquifer components: for example, carbonate minerals have a signature between +2 and −12‰ versus VPDB [26] and the C_3 plants (plants that use the Calvin or C_3 cycle of carbon fixation) produce organic matter with isotopic signature near −25 ± 5‰ versus VPDB [25, 27, 28]. Moreover, bacteria can induce a carbon isotopic fractionation as they preferentially use the lighter isotope ^{12}C (due to the lower energy required to break intramolecular bonds) [29]. Some studies linked the CO_2 production with contaminant degradation rate in laboratory [30–32] and at contaminated field sites [33]. Some researchers have examined the isotopic signature of CO_2 and dissolved inorganic carbon from aerobic biodegradation of petroleum hydrocarbons to support their analysis [34–38]. Results reflect the difficulty in definitively attributing CO_2 produced from biodegradation of contaminants versus that from possible interferences of background CO_2 under field conditions. The other natural sources of CO_2, plant root respiration in shallow sediments and carbonate dissolution in subsurface sediments, must be taken into account in field experiments [25].

Integrating both geoelectrical methods and gas analyses could help to develop a less invasive technique with a little geochemical sampling in piezometers in order to monitor enhanced biodegradation of hydrocarbons. These tools were previously tested at laboratory scale in sand-columns with toluene as model pollutant and an exogenous bacterial strain [39]. The promising results from the column study allowed implementing a monitoring strategy at the field scale. The site was a gasoline station where gasoline and diesel fuels leaked eighteen years ago. A reactive barrier supplied the necessary oxygen to the aquifer in order to stimulate the aerobic bacterial processes since April 2014. Geoelectrical measurements and ER and IP surveys, as well as CO_2 analyses, had been performed from February 2014 until June 2015 on this site.

2. Materials and Methods

The experimentation had been implemented at a gasoline station over a 16-month period, from February 2014 to June 2015. After a preliminary characterization of the site (baseline, February 2014), and the start of the oxidative reactive barrier in April 2014, the long-term monitoring had been carried out.

The site had been equipped to monitor time-lapse changes in electrical properties of the subsurface with electrical resistivity (ER) and time domain induced polarisation (TDIP) systematic 2D tomographies. This monitoring had been combined with regular CO_2 fluxes measurements and its carbon isotopic ratio at the ground surface.

The indirect monitoring was completed with several analyses in piezometers to assess the nonintrusive survey: (i) measurements of pollutant concentration and carbon isotopic signature of selected aromatic hydrocarbons and (ii) monitoring of groundwater physicochemical properties with probes.

2.1. Site Description. The site studied was a gasoline station where gasoline and diesel fuels leaked in 1997 (Figure 1). It is still in activity but the former tank installation (source of contamination) was dismantled. Several piezometers had been drilled for previous studies on this site. These studies showed that

(i) the ground was mainly composed of silts and clays: a first layer (thickness ranging from 0.5 to 3.5 m) of backfills made of brown silts, which often contained gravels, followed by a succession of loamy strata, with varying degrees of sands, and even sandy clays with limestone or millstone blocks (until 5 to 7.5 m depth); and then argillaceous limestones are interbedded with thin layers of sandy clays;

(ii) the ground had a low permeability (between 10^{-6} and 10^{-7} m/s);

(iii) the direction of flow was northwest;

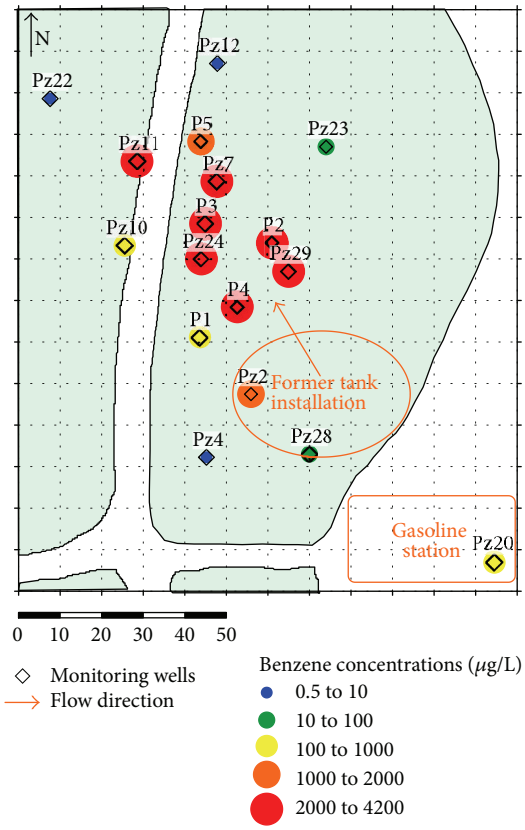

Figure 1: Map of the site showing gasoline station, former tank installation, monitoring piezometers, and the benzene concentrations measured in water in September 2013.

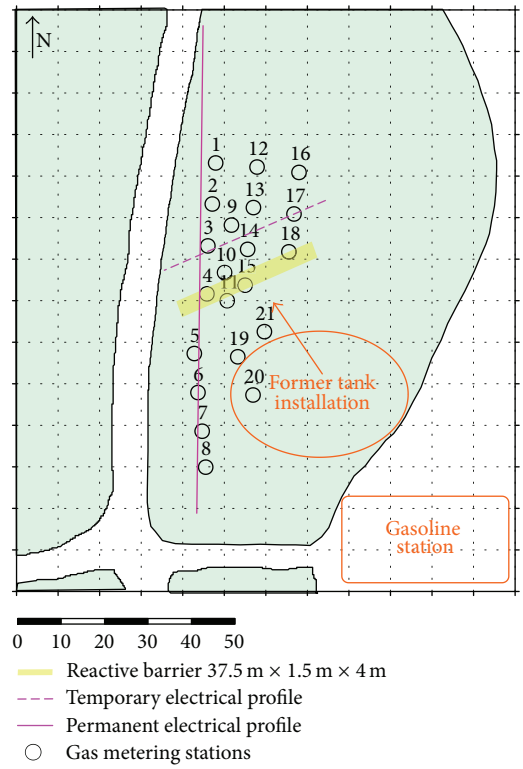

Figure 2: Map of the site showing the reactive barrier and the monitoring disposal: 2 electrical profiles and 21 gas metering stations.

(iv) the water table depth ranged between 2.5 and 4.5 m and depends on seasons (winter, summer);

(v) there was a presence of hydrocarbons in the area of the former tank installation and the fraction of benzene, toluene, ethylbenzene, and xylenes (BTEX) represented a consequent part of the pollutants (Figure 1);

(vi) there were indications of a natural attenuation (hydrocarbon degradation) which prove the presence of a bacterial flora, such as absence of dissolved oxygen, that matched the BTEX plume in water [40].

An important limiting factor in bioremediation of soils contaminated with hydrocarbons is the lack of oxygen to support microbial activities [41, 42]. Injection of aqueous H_2O_2 was the selected method to overcome this limitation and to stimulate aerobic metabolic processes.

A permeable reactive barrier of 4 m depth × 35 m long × 1.5 m wide was implemented to stop the plume migration (Figure 2). The site was equipped with 3 pumping wells just upstream the barrier, 3 injection wells in the barrier, and 2 injection wells just downstream the barrier. Pumped water was filtered through active charcoal. After filtration, diluted H_2O_2 was added to the treated water and oxygenated water was reinjected in the barrier, through the 3 injection wells, slotted from −2 to −4 m in order to deliver oxygen in the upper part of the water table. The permeability of this barrier (10^{-3} m/s) allowed an homogeneous distribution of the treating fluid. Finally, the last part of the oxygenated water was injected in 2 boreholes downstream the barrier, slotted from −6 to −8 m, to bring oxygen in the deepest part of the water table. The biostimulation was started in April 2014.

2.2. Electrical Geophysical Measurements. Geophysical methods are a standard tool for obtaining information on volumetric distributions of subsurface physical properties of rocks and fluids. Among several electrical methods which measure electrical properties of the ground, two of them were used: the electrical resistivity (ER) and the time domain induced polarization (TDIP).

In a typical ER measurement, four electrodes are used. ER instrumentation measures potential differences between pairs of electrodes, where the potentials result from a current applied by the instrumentation between two other electrodes. By making measurements with current and potential electrodes at many different locations, one can collect sufficient data which allow the construction of an electrical resistivity section (a 2D slice of the earth).

Whereas ER is sensitive to pore fluid resistivity (and consequently to total dissolved solids or ionic strength), the IP method measures the capacitive behaviour of the subsurface, which strongly depends on the properties of the mineral surface. Different studies have shown the sensitivity of IP to mineral precipitation and changes occurring at

pore-grain interfaces, where biological reactions occur [12]. TDIP measurements use the same instrumentation as ER measurements. Here, the injected current is alternately ON and OFF. The decrease of the induced voltage is measured to calculate the chargeability, which is the ground capacity to store charges. Hereafter, in this paper, the normalized chargeability (defined as the chargeability divided by the resistivity magnitude) will be calculated to free the chargeability from variation of resistivity [43].

Two time domain ER and IP profiles were carried out at the study site. Positioning of the profiles was performed according to the contaminant plume and barrier location: both profiles went across the plume, one was perpendicular to the barrier, and the other was parallel, 8 m downstream the barrier (Figure 2).

The perpendicular profile was buried permanently at 50 cm of depth. Apparent resistivity and chargeability measurements were obtained using a system with 60 stainless steel electrodes: 30 electrodes, with a constant spacing of 4 m, were dedicated to current injection, and the other 30, with a spacing of 4 m as well, were used for potential measurement to avoid electromagnetic (EM) coupling effect. The two sets of electrodes are disposed staggered, so that each electrode is laid out at a constant interval of 2 m. To achieve a good lateral resolution and to avoid EM coupling effect, the dipole-dipole array was applied to obtain the apparent resistivity and chargeability pseudosections. A Syscal R1+ (from IRIS Instruments©, Orleans, France) has been used in this study. Measurements were performed continuously every two days. The second profile, parallel to the barrier, was a temporary profile. It consists in 48 electrodes separated by 1 m. Measurements were performed every two months with an Elrec Pro (IRIS Instruments, Orleans, France).

After performing time-lapse ER and IP measurements, the electrical data were analysed in three stages:

(i) Initial anomalous data were filtered by a process of elimination:
   (a) current $I < 100$ mA;
   (b) potential $V < 0.1$ mV;
   (c) apparent chargeability $m < 0$;
   (d) error $Q > 5\%$ (resistivity measurements) and $Q > 2\%$ (chargeability measurements);

(ii) The quadrupoles in common to all the data sets were selected;

(iii) Data processing was performed with RES2DINV software [44], in time-lapse mode. The process is based on several iterations comparing the measured data with a model calculated by the software for each time series data set. This process enables obtaining a 2D distribution of resistivity and chargeability sections at every time. The following settings were used to define the type of constrains applied during the time-lapse inversion process:
   (a) The relative importance given to minimize the difference between models at different times is controlled by the time-lapse damping factor. A value of 0 to 5 can be generally used: if a value of 0 is used, the inversion of the different time series data sets would be carried out independently; if a value of 1 is used, equal weight would be given to reducing the difference between the models at different times; a larger value of the damping factor forces the different time models to be more similar. After some previous tests, a value of 3 was selected.
   (b) Time-difference roughness filter was set for "smooth changes" between time models.
   (c) The maximum number of iterations was 5.

2.3. CO_2 Analyses: Emissions Fluxes and Carbon Isotopic Ratio. The geoelectrical measurements were combined with CO_2 analyses. The measurements of CO_2 effluxes at the ground surface demonstrate the occurrence and rate of aerobic hydrocarbon biodegradation [33]. However, to determine the accuracy of the method, contaminated-derived soil respiration must be distinguished from chemistry of mineral-carbonates and from the natural soil respiration, resulting from biodegradation of dead organic matter and plant root respiration.

CO_2 produced by fossil hydrocarbon degradation may be distinguished from that produced by other processes based on the carbon isotopic compositions, characteristic of the source material, and/or fractionation accompanying microbial metabolism. Indeed, carbon isotopic signature of CO_2 reaches those of contaminant and it can be accompanied by significant carbon isotope fractionation [37].

Stable isotopic ratio represents the abundance of the rare isotope with respect to the abundant isotope ($^{13}C/^{12}C$). Due to slight analytical variations, it is common to compare isotopic ratios measured in an unknown sample to those in a standard material; this results in the delta notation:

$$\delta^{13}\mathrm{C}\,(‰) = \left[\frac{\left(^{13}\mathrm{C}/^{12}\mathrm{C}\right)_{\mathrm{sample}}}{\left(^{13}\mathrm{C}/^{12}\mathrm{C}\right)_{\mathrm{VPDB}}} - 1\right] * 1000 \qquad (1)$$

with $(^{13}C/^{12}C)_{VPDB} = 0.011237$ [45].

CO_2 concentration and $\delta^{13}C$ isotopic ratio in produced CO_2 are measured by a high-resolution laser infrared spectrometer, called SPIRIT (Spectrometer Infrared *In Situ* Tropospheric) and developed by the LPC2E (CNRS, Orleans, France). This spectrometer is an adaptation of the original SPIRIT, described in Guimbaud et al. (2011) [46] and used for greenhouse gas emissions at the air-land interface [47, 48], by the implementation of a quantum cascade laser using the $^{12}CO_2$ and $^{13}CO_2$ ro-vibrational lines. The uncertainty for $\delta^{13}C$ determination on field deployment is on the order of 0.4‰. A complete description of the adapted SPIRIT for $^{13}C/^{12}C$ isotopic ratio quantification is available in Guimbaud et al. [49]. The spectrometer is directly connected with a closed accumulation chamber set on a permanent PVC cylinder collar (diameter = 30 cm) sunk into the soil to measure CO_2 emission fluxes and $\delta^{13}(CO_2)$. The ground

Table 1: List of probes in the monitoring piezometers (function and depth).

Monitoring piezometer	Probes	Depth (m)
Pz4	O_2	6.15
	Water level	4.15
	Conductivity	4
Pz7	O_2	3.68
	Conductivity	4.13
Pz2	Temperature A	5.29
	Temperature B	7.36
	Temperature C	9.3
	Water level	6.3
P2	Temperature	5.09
Pz24	O_2	4.98
	Conductivity	5.14
P4	O_2	5.09
	Conductivity	4.98
	Water level	5.06

surface inside the PVC collar was cleared of vegetation (grass, roots) over 15 cm depth. We had 21 measuring points on the site, upstream, above, and downstream the reactive barrier (Figure 2). Measurements were performed every two months since February 2014.

2.4. Geochemical Monitoring in Piezometers. To assess the indirect monitoring of the enhanced bioremediation, chemical analyses were performed every two months in water samples from monitoring piezometers. BTEX concentration and carbon isotopic ratios of these BTEX were measured. Moreover, some piezometer probes had measured continuously the water table level, temperature, conductivity, and oxygen rate in monitoring piezometers (Table 1).

3. Results

3.1. Baseline Characterization. Baseline characterization consisted of collecting datasets prior to the oxygen injection (February-March 2014).

3.1.1. Geophysical Data. Figure 3 shows the results for the permanent profile in March 2014. This profile went through the barrier (metric point 51 m) and was within close proximity to several piezometers (from north to south: Pz12, P5, Pz7, P3, Pz24, P1, and Pz4) whose positions are plotted on Figure 3. The temporary profile was located around 8 m downstream the barrier and it overlapped with two piezometers (from west to east: Pz24 and P2, Figure 4).

The electrical resistivity tomography from the permanent profile showed resistivities between 40 and 80 Ω·m, over the 6 first meters, which correspond to the sandy-loamy layer of the aquifer. From 6-meter depth, resistivity was much smaller (<20 Ω·m) and this may be associated with a sandy clay level. The tomography from the temporary profile displayed the same resistivity range since the pilot site is quite homogeneous. Nevertheless, areas less resistant (<30 Ω·m)

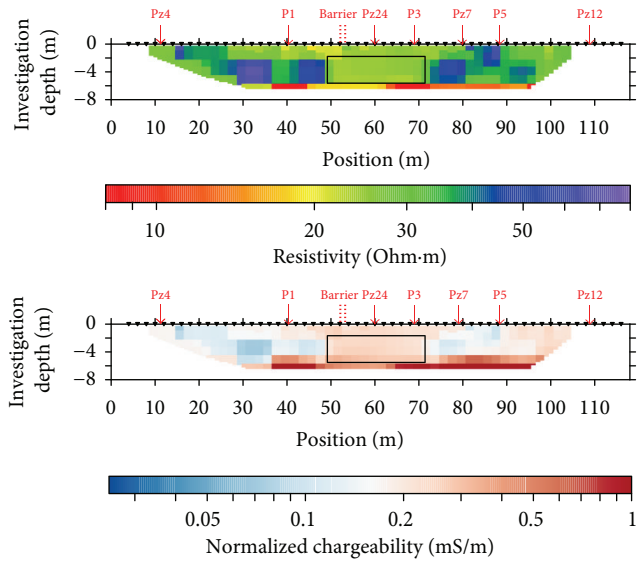

Figure 3: Resistivity and normalized chargeability sections across the plume for the permanent electrical profile, on 6th March 2014. The black rectangle highlights a zone of lower resistivity and higher normalized chargeability.

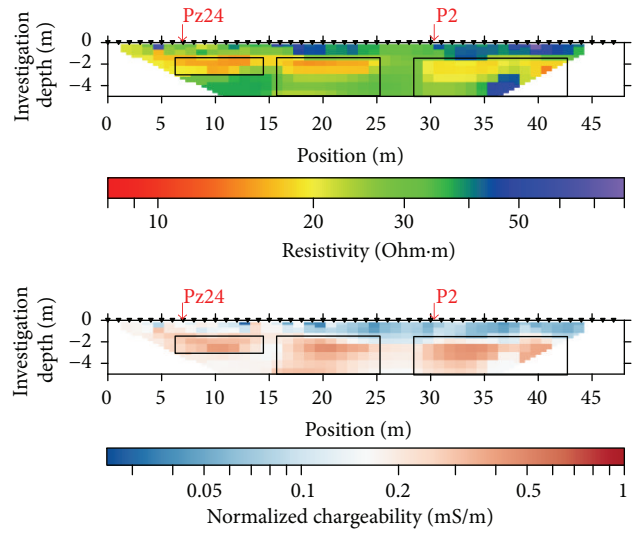

Figure 4: Resistivity and normalized chargeability sections across the plume for the temporary electrical profile, on 6th March 2014. The black rectangles highlight zones of lower resistivity and higher normalized chargeability.

could be identified between 1.5 and 6 m depth, on both profiles:

(i) Between the metric points 50 and 72 m for the permanent profile.

(ii) Between the metric points 7 and 14 m; 16 and 25 m; and 29 and 42 m, for the temporary profile.

Regarding the normalized chargeability tomographies (chargeability divided by resistivity), the values were in the range of 0.025 to 1 mS/m, and the zones of higher normalized

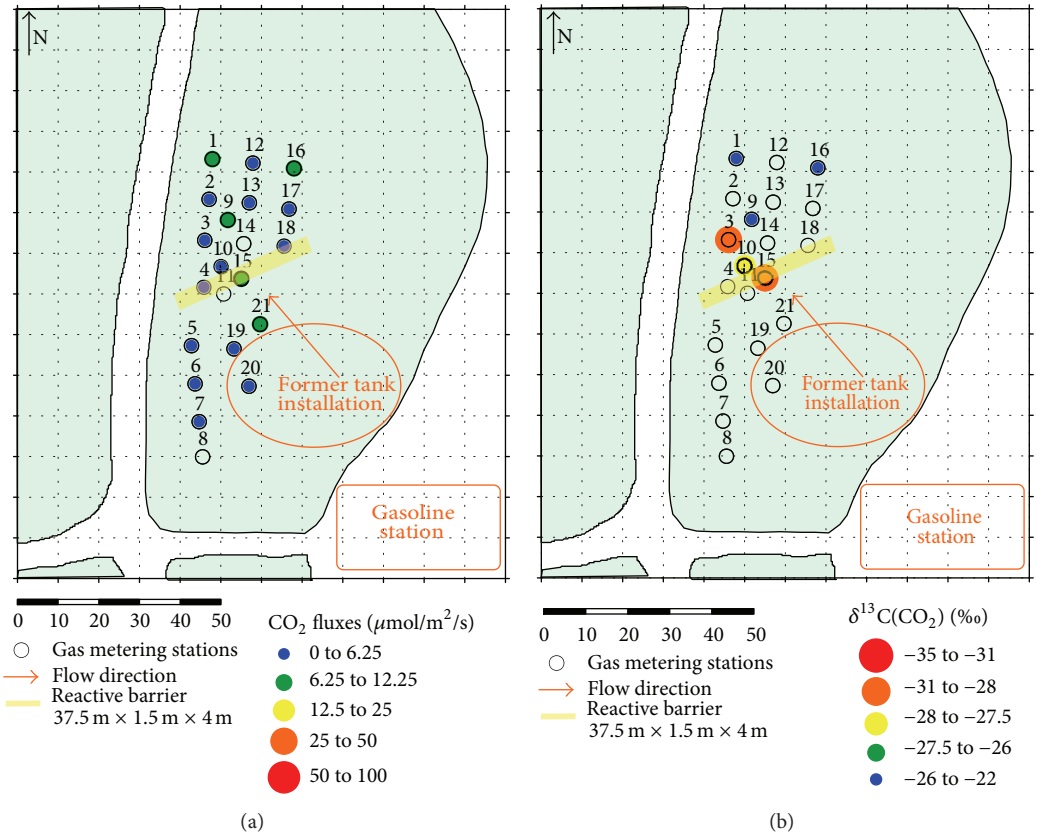

Figure 5: Maps of measured CO_2 emissions (a) and its carbon isotopic ratio versus VPDB (b), in February 2014.

chargeability (>0.2 mS/m) matched the lower resistivity zones. These normalized chargeability anomalies correspond to a polarization effect. On the permanent profile, the normalized chargeability was quite high beyond 6 m depth. This confirms the presence of clays, very chargeable, at these depths.

According to the geochemical data (Figure 1), the localization of these anomalies (higher normalized chargeability and lower resistivity) matched the hydrocarbon polluted area, downstream the former tank installation, at the top of the water table, where natural biodegradation produces conductive byproducts and where chargeable bacteria are numerous (proximity of an organic carbon source).

3.1.2. SPIRIT Data. Figure 5 displays the maps of measured CO_2 emissions and its carbon isotopic ratio in February 2014. There were quite high CO_2 emissions on this site, around 3.8 μmol·m^{-2}·s^{-1}, despite the fact that, during cold periods (December–March), gas fluxes are presumably very low [50, 51]. These results were consistent with those found by Sihota et al. (2011) [33] where the average CO_2 efflux associated with contaminant degradation in the hydrocarbon-contaminated zone was estimated at 2.6 μmol·m^{-2}·s^{-1}. Moreover, the measured $\delta^{13}C(CO_2)$, ranging between −22.2 ± 0.4‰ and −28.8 ± 0.4‰ versus VPDB (averaging −25.3 ± 3‰), were very negative compared to $\delta^{13}C$ of atmospheric CO_2 (around −11‰ versus VPDB, one meter above the ground) and distinguishable from $\delta^{13}C$ of CO_2 from vegetation respiration (around −28‰ versus VPDB [25, 27, 28]). This was an indication of natural biodegradation of hydrocarbons. Indeed, during biodegradation, CO_2 has an isotopic signature near those of the carbon source, which is quite negative in the case of fossil organic carbon (range from −23 to −29‰ versus VPDB for the BTEX of the site [40]).

3.2. Cleanup Progress after One Year of Biostimulation. Figure 6 presents the BTEX (benzene, toluene, ethylbenzene, and xylenes) concentrations over time for 4 piezometers, between February 2014 (two months before barrier activation) and April 2015 (one year after barrier activation). There was an increase in the pollutant concentrations due to the remobilization of contaminants during the barrier construction. The discharge of BTEX may have had significantly slowed down the oxygen diffusion downstream the barrier: it had been quickly consumed and the amount of H_2O_2 could not be increased for avoiding bacteria stress. And, one year after the beginning of biostimulation, there was just a little decrease in benzene and toluene concentrations.

3.3. One Year of Electrical Monitoring. Before barrier activation, it was possible to localize a zone of natural biodegradation on the permanent and the temporary profile (Figures 3 and 4). Figure 7 shows the evolution of the electrical data over a year of enhanced biodegradation, for the permanent profile.

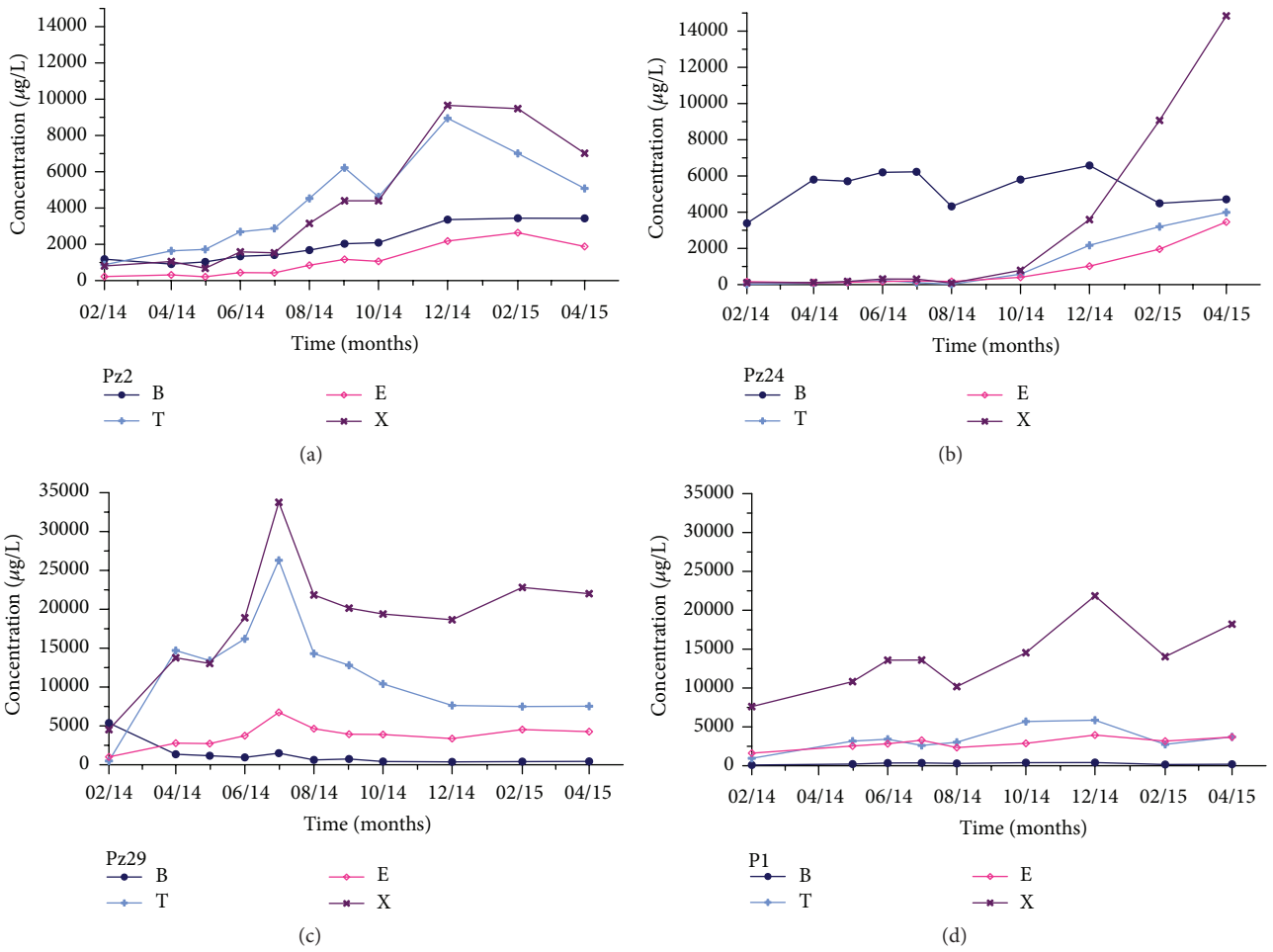

FIGURE 6: Evolution of BTEX (benzene, toluene, ethylbenzene, and xylenes) concentrations in water over time, measured in four monitoring piezometers: Pz2 (a), Pz24 (b), Pz29 (c), and P1 (d), between February 2014 and April 2015.

The resistivity model sections were obtained after time-lapse inversion of 12 datasets, spaced about a month, acquired between March 2014 and April 2015. The convergence of iterative inversion is excellent (<1% for resistivity and <2 for normalized chargeability) and it is comparable with the noise level of the resistivity meter (1%, according to Iris Instruments).

In order to compare the electrical data taking into account the impact of temperature and water saturation on electrical resistivity and chargeability, the inversed data were considered only in the saturated zone and adjusted at 25°C thanks to a linear law [52, 53]:

$$\frac{\rho_{25}}{\rho_T} = \alpha * (T - 25) + 1, \quad (2)$$

where ρ_T is resistivity at temperature T (°C), ρ_{25} is resistivity at 25°C, and α (°C^{-1}) is a temperature compensation factor. The temperature compensation factor α was calculated based on Pz4 (located in a nonpolluted area) temperature data and found to be equal to 0.014, which means that resistivity decreases by 1.4% when temperature increases by 1°C.

Figure 7 shows the anomaly of lower resistivity and higher normalized chargeability on all the tomographies, from March 2014 to April 2015. It was possible to identify two periods of decreasing resistivity and increasing normalized chargeability: a first period from March 2014 to October 2014, and a second period from March 2015 to April 2015. In order to quantify the evolution of the differences, the percentage difference of resistivity and normalized chargeability from March 2014 were calculated (Figure 8). A decrease in resistivity up to 15% is noticed in the area of interest (between metric points 50 and 70 m) at the end of the summer of 2014. However, such a seasonal variation cannot be seen on water conductivity (Figure 9(a)). Regarding normalized chargeability, the tendency is less clear and there are increases outside the area of interest as well.

3.4. One Year of CO_2 (Fluxes and Carbon Isotope Ratio) Monitoring. Gas monitoring was carried out every one-two months, between February 2014 and June 2015. The time allowed for measurements was very short (2 days per campaign). As a consequence, priority was given to flux measurements and then to isotopic ratio measurements of metering points with the highest emissions (more accurate).

CO_2 fluxes ranged between 2.5 and 100 μmol·m^{-2}·s^{-1} (Figure 10(a)). As there was no vegetation inside the PVC

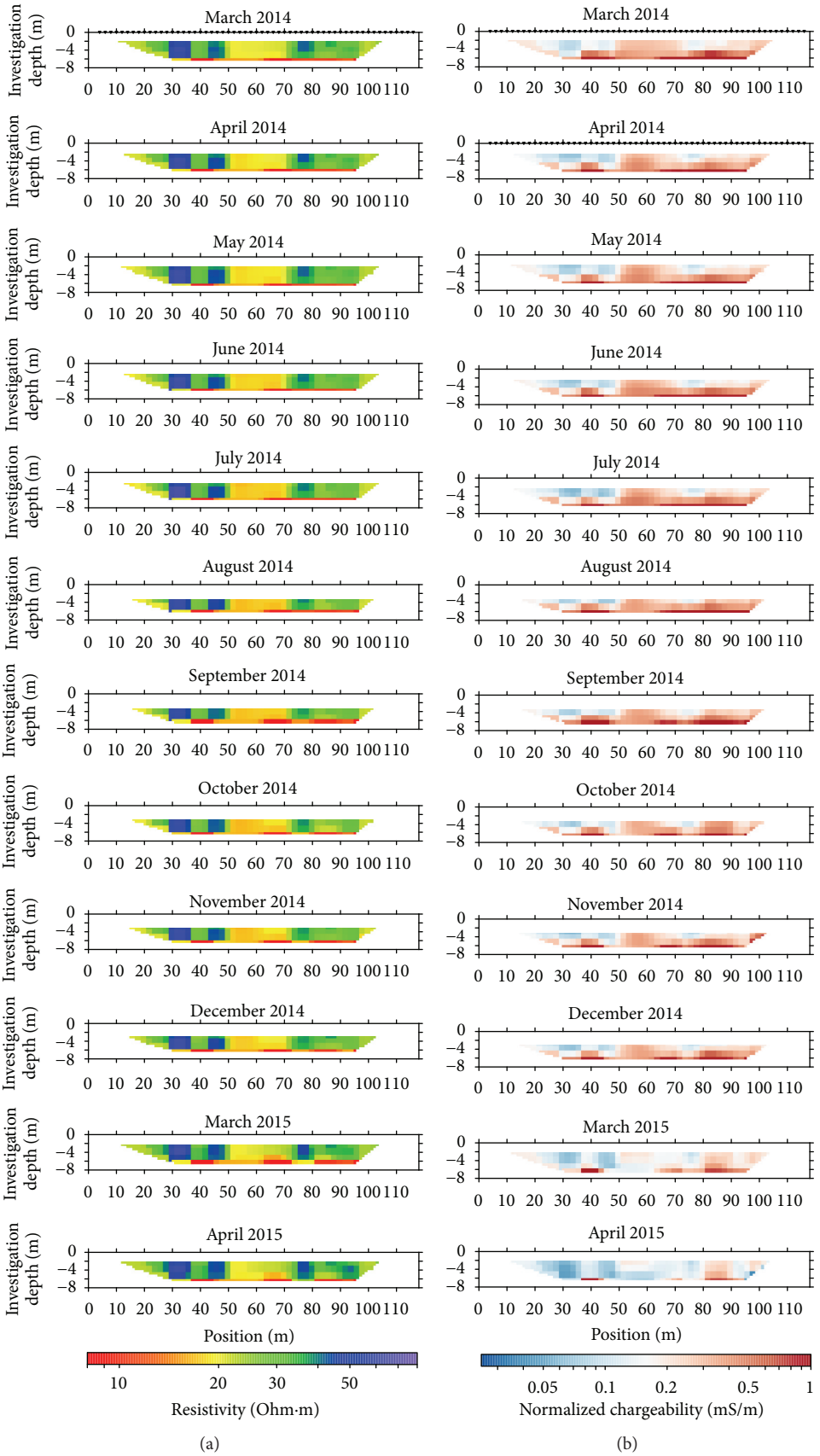

Figure 7: Resistivity (a) and normalized chargeability (b) sections, adjusted at 25°C in the saturated zone, for the permanent electrical profile, between March 2014 and April 2015. The inversion results were obtained after 5 iterations, with 0.58 and 1.82% of error for resistivity and chargeability, respectively.

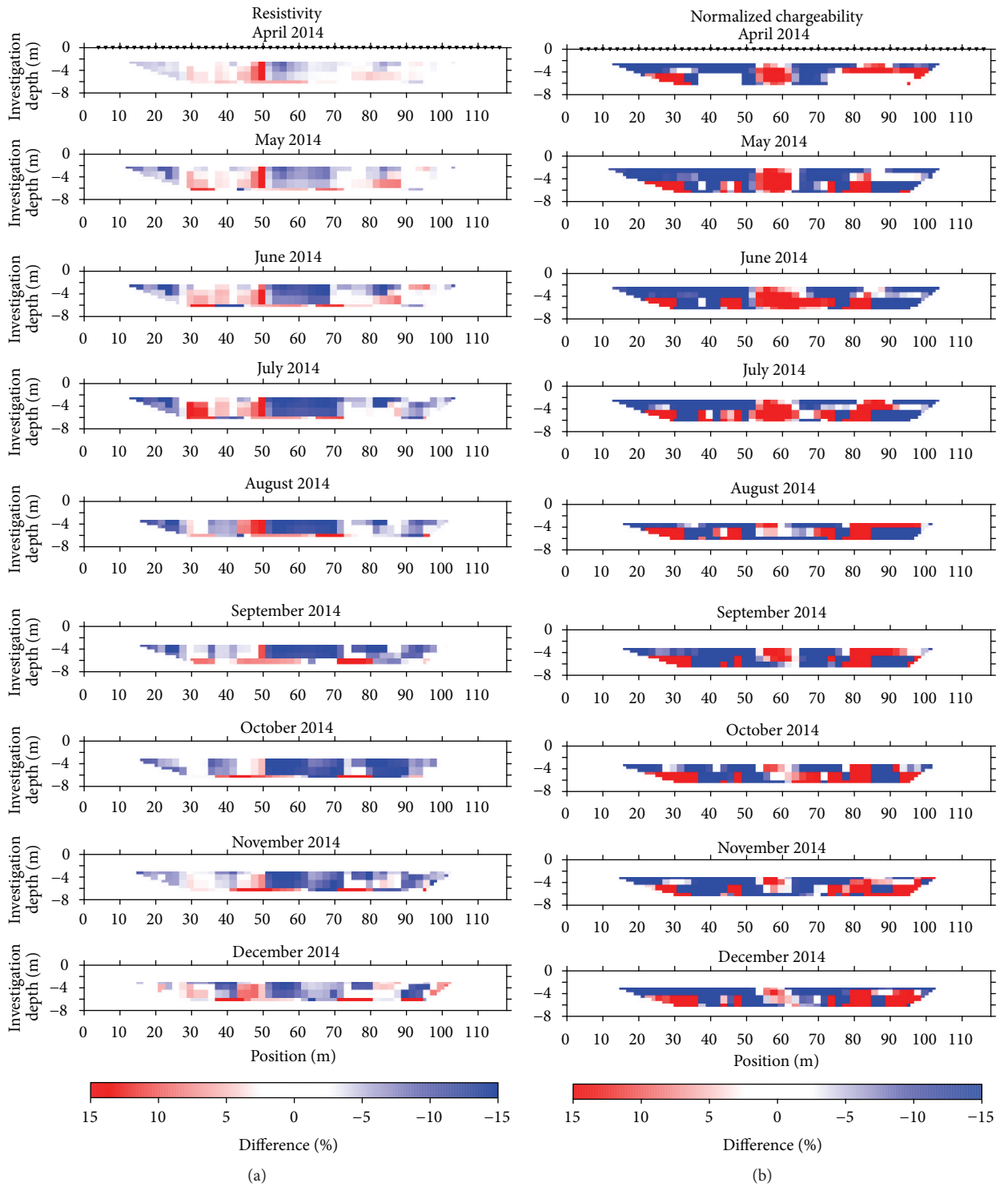

FIGURE 8: Percentage difference (P) over March 2014 of resistivity ρ (a) and normalized chargeability nm (b) sections, for the permanent electrical profile, with $P_\rho = (\rho_{ti} - \rho_{t0})/\rho_{t0} * 100$ and $P_{nm} = (nm_{ti} - nm_{t0})/nm_{t0} * 100$.

collar used to put the SPIRIT chamber, the CO_2 released at the ground surface should come from degradation of soil organic matter and mainly from hydrocarbon biodegradation. The lower emissions were recorded in February 2014. Then, they gradually increased up to August 2014, and decreased during winter 2014-2015. However, meteorological conditions affect gas emissions: CO_2 fluxes were lower when temperatures were low and ground was wet (high rainfalls) (Figure 10) [50]. In order to throw off this effect, we chose a reference measuring point, no. 7, located in the nonpolluted area, where

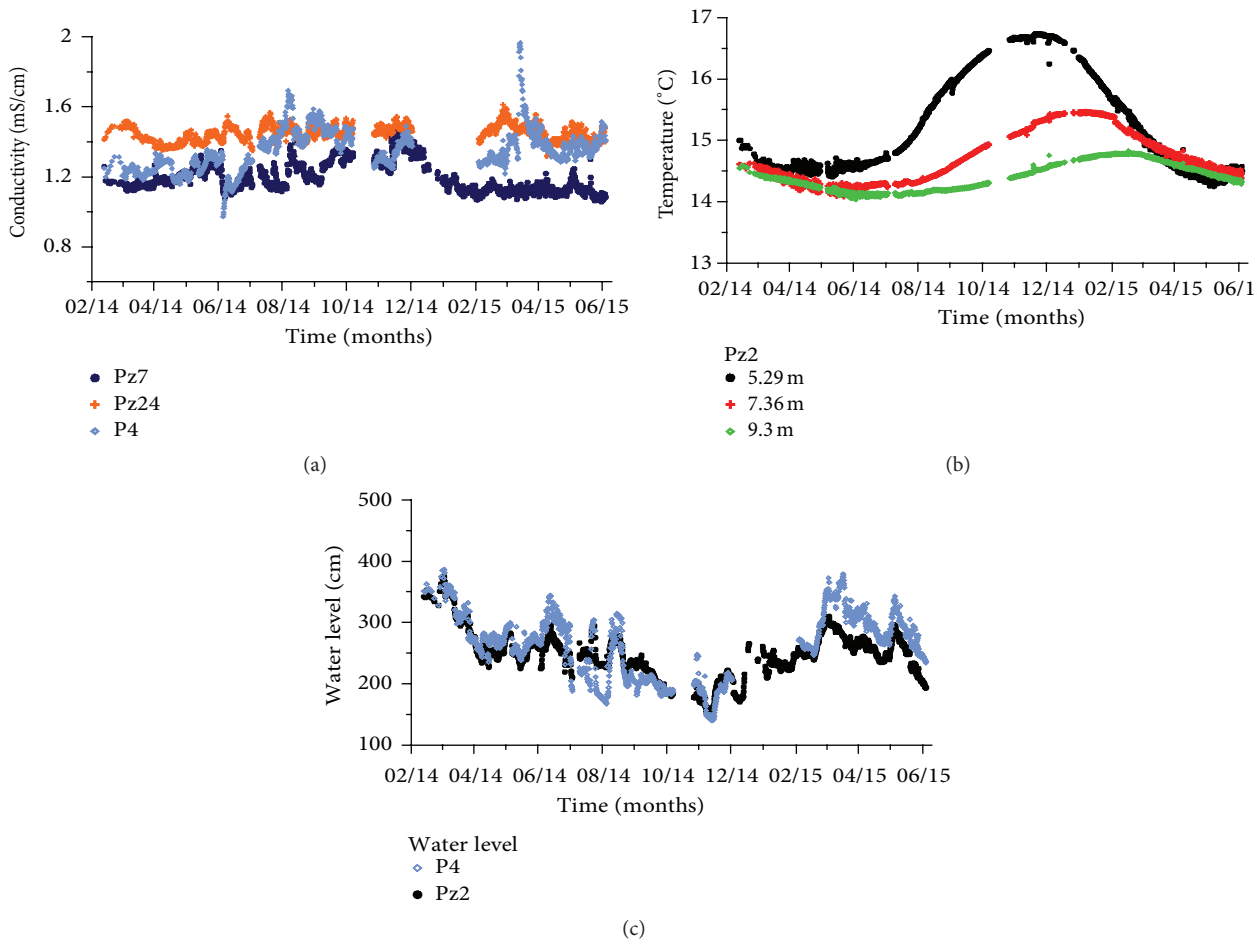

FIGURE 9: Water conductivity (a) and temperature (b) and ground water level (c) evolution over time.

changes in fluxes are supposed to be only due to temperature and moisture conditions. The difference of flux with season at this point was subtracted from the values obtained at the other measuring points to keep only the flux variations due to bacterial activity (degradation of natural organic matter and hydrocarbons) (Table 2). A seasonal variation of the CO_2 emissions is still monitored (Figure 11): there were more emissions during summer and fall, when groundwater level is low (Figure 9(c)), water temperature is warmer (Figures 9(b) and 10(b)), and ground is less moist (Figure 10(c)).

Moreover, CO_2 emissions had been measured with an isotopic signature typical of hydrocarbon biodegradation. Indeed, $\delta^{13}C(CO_2)$ were measured between −27 and −30‰ versus VPDB since February 2014 (Figure 12(a)), in accordance with the BTEX $\delta^{13}C$ signature measured in water (around −25 to −26‰ versus VPDB) (Figure 12(b)). Besides, CO_2 released at the surface originates from a more or less degraded BTEX located below the gas measuring station. Indeed, in December 2014, average evolution of $\delta^{13}C$(benzene) increased from (−28.1 ± 0.5)‰ to (−26.7 ± 1.2)‰ and $\delta^{13}C$(toluene) increased from (−27.4 ± 0.4)‰ to (−24.8 ± 1.9)‰, from upstream to downstream the pollution plume. At the same time, $\delta^{13}C(CO_2)$ increased, from upstream to downstream as well, from (−30.5 ± 0.7)‰ to (−28.3 ± 1.6)‰ in July 2014 and from (−28.1 ± 1.1)‰ to (−27.0 ± 1.2)‰ in October 2014 [49]. Although these $\delta^{13}C(CO_2)$ values were only a few per mil less than the $\delta^{13}(CO_2)$ from microbial degradation of plant material, $\delta^{13}(CO_2)$ showed a light isotopic fractionation (1 to 3‰) through the stream of the pollution plume:

(i) $\delta^{13}(CO_2)$ was lower than $\delta^{13}C$(hydrocarbon source).

(ii) The pollutant was enriched in ^{13}C when it was degraded, when residual BTEX concentrations were lower than 2000 $\mu g \cdot L^{-1}$.

(iii) The CO_2 tended to be depleted in ^{13}C, when fluxes were higher than 20 $\mu mol \cdot m^{-2} \cdot s^{-1}$.

It means that molecules with light isotopes (^{12}C) were preferred by bacterial metabolism. This is a typical isotopic fractionation due to biodegradation. This is in agreement with one example of a successful field application of isotopic assessment of biodegradation in an aviation gasoline contaminated aquifer where aerobic biodegradation of the gasoline constituents produced significantly enriched CO_2 [54]: the $\delta^{13}C(CO_2)$ values were ranging from −22.0 to −26.3‰, soil organic matter for the site ranged from −13.5 to −26.1‰, and the aviation gasoline $\delta^{13}C$ values were between

Table 2: Corrections made to CO_2 measurements from April 2014 to April 2015 (February 2014 is the baseline, uncorrected) from gas measuring point number 7.

	Apr. 2014	May 2014	June 2014	July 2014	Aug. 2014	Oct. 2014	Dec. 2014	Feb. 2015	Apr. 2015
Corrections (μmol·m^{-2}·s^{-1})	−0.6	−1.4	−3.05	−7.87	−9.9	−7.65	+1.22	+1.2	−3.27

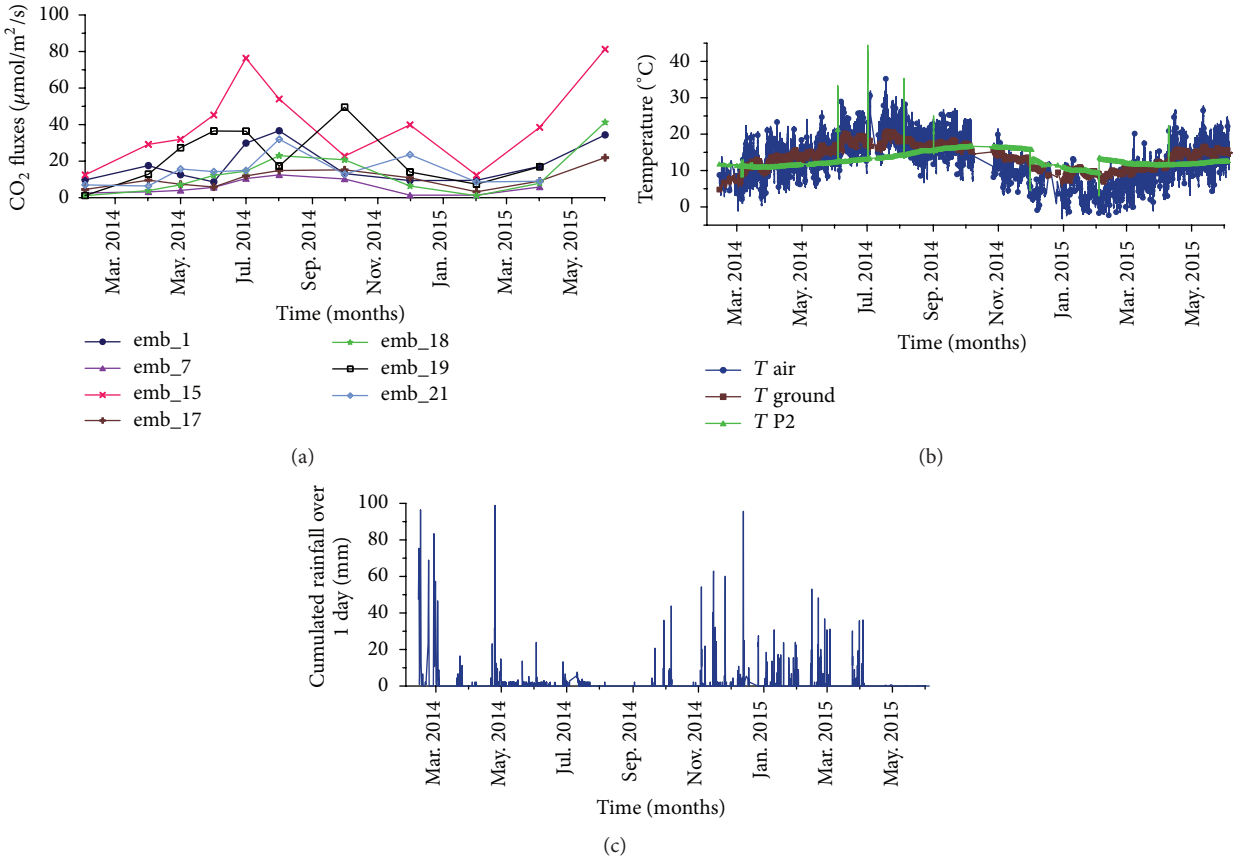

Figure 10: Measured CO_2 emissions (a); air, ground, and water temperatures (b); and rainfall (c) over time.

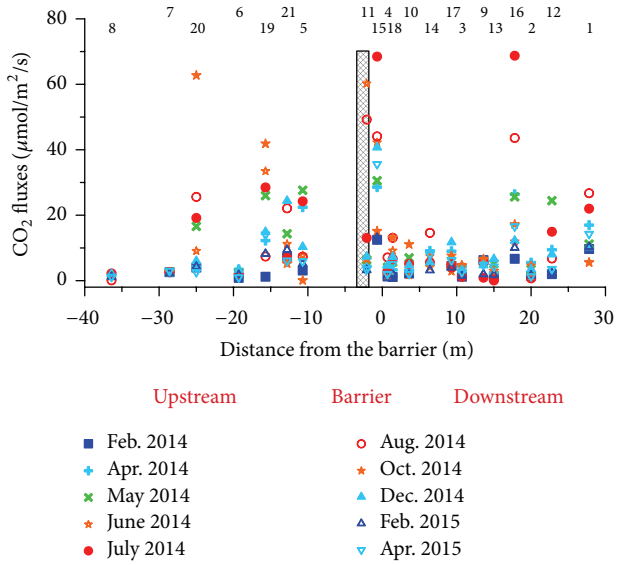

Figure 11: Measured CO_2 emissions (corrected from meteorological conditions) as a function of gas metering station location, for one year of monitoring.

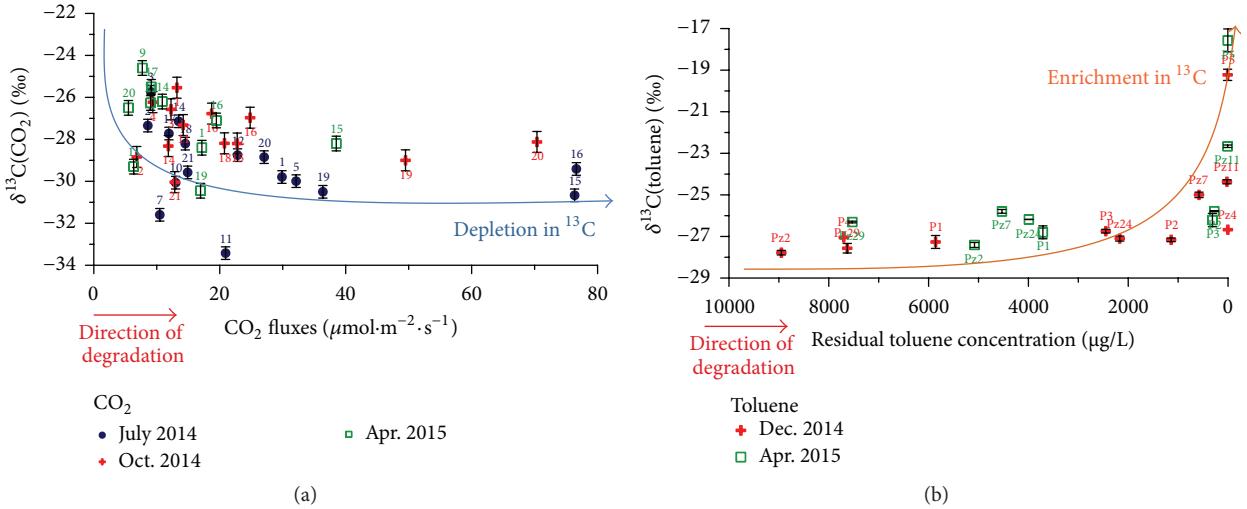

FIGURE 12: Carbon isotopic ratio versus VPDB of CO_2 (a) in function of CO_2 fluxes at the ground surface and carbon isotopic ratio versus VPDB of residual toluene (b) as a function of toluene concentrations in water.

−20.5 and −27.3‰. Conrad et al. (1999) [54] concluded that the difference of $\delta^{13}C$ was discernible. Another study from Aelion et al. (1997) [55] was carried out at a gasoline contaminated groundwater site under aerobic degradation. Although some of the $\delta^{13}C(CO_2)$ values from the contaminated site (between −35.9 and −22.0‰) overlapped with background $\delta^{13}C(CO_2)$ (between −22.9 and −23.9‰) from uncontaminated areas, on average the stable isotopic values were distinguishable between the contaminated and background sites.

4. Integration of Results and Conclusion

At the pilot site, the combination of geoelectrical measurements (ER and TDIP) with CO_2 analyses (fluxes and carbon isotopic ratios) was tested as monitoring tools to follow an enhanced biodegradation of hydrocarbons.

The results from the baseline characterisation in February-March 2014 had shown a more conductive and chargeable zone, around 3 meters in depth, which matches the polluted zone defined by geochemical borehole analyses, at the top of the water table (Figures 1, 3, 4, and 13). In this area, it can be assumed that there are numerous chargeable bacteria and production of conductive metabolites due to the pollutant degradation. This is consistent with the age of the gasoline leakage (almost twenty years ago), sufficient to allow the development of natural bacterial flora able to degrade hydrocarbons [56, 57] and to transform an electrical resistive substance in a more conductive one [12]. Moreover, CO_2 emissions were strong in this area and had an isotopic signature typical of hydrocarbon biodegradation. However, the overlap between $\delta^{13}C(CO_2)$ values from uncontaminated areas (plant root respiration and organic matter degradation) and from contaminated areas (with petroleum hydrocarbon degradation in addition) suggests that the combined measurement of $\delta^{13}C(CO_2)$ and $\delta^{13}C(BTEX)$ may be needed to confirm that the CO_2 is indeed from the contaminant degradation and not from microbial metabolism of natural plant materials. The northern zone of the site must be considered as a potential contaminated zone as well, accepting that the CO_2 emissions (measuring points 1, 12, and 16) are a sign of biodegradation and not the result of the presence of gas preferential pathways in this area (Figure 13).

The treatment for enhanced biodegradation was started in April 2014, with the activation of the reactive barrier that brought oxygen to the water table to stimulate aerobic biometabolism. The regular monitoring over one year showed that the area of biodegradation was still detected by both indirect methods (Figure 13). Moreover, a seasonal variation (after correction of effects associated with groundwater and soil temperature and soil moisture) for both electrical and gas monitoring was highlighted. Indeed, we observed highest conductivities of the ground at the end of summer and during fall, seasons when the piezometer probes measured the warmer groundwater temperatures (Figure 9(b)). The inverted resistivity sections were adjusted from temperature effect [52, 53], with a correction limited at groundwater level. In piezometer Pz2, at 5.29 m depth, the highest variation of temperature over a year is of the order of 2°C (Figure 9(b)), which corresponds to a variation of resistivity (1.4% per °C) lower than 3%. Nonetheless, a significant decrease in resistivity up to 15% was observed in the area of biodegradation at the end of the summer of 2014 and such a seasonal variation cannot be seen on water conductivity (Figure 9(a)). However, there is also a seasonal variation of the bacterial activity: when groundwaters are warmer, bacterial activity is more intensive and degrades more hydrocarbons and should produce more conductive metabolites [58–62]. Similarly, gas analyses, mainly CO_2 fluxes measurements, showed a seasonal variation. However, this should be mainly due to variation of soil respiration processes; otherwise we would have observed a seasonal variation in BTEX isotopic signatures. On the basis of this analysis, it is possible to make an assertion that seasonal variation of biodegradation processes was detected by our nonintrusive monitoring tools, especially by geoelectrical measurements.

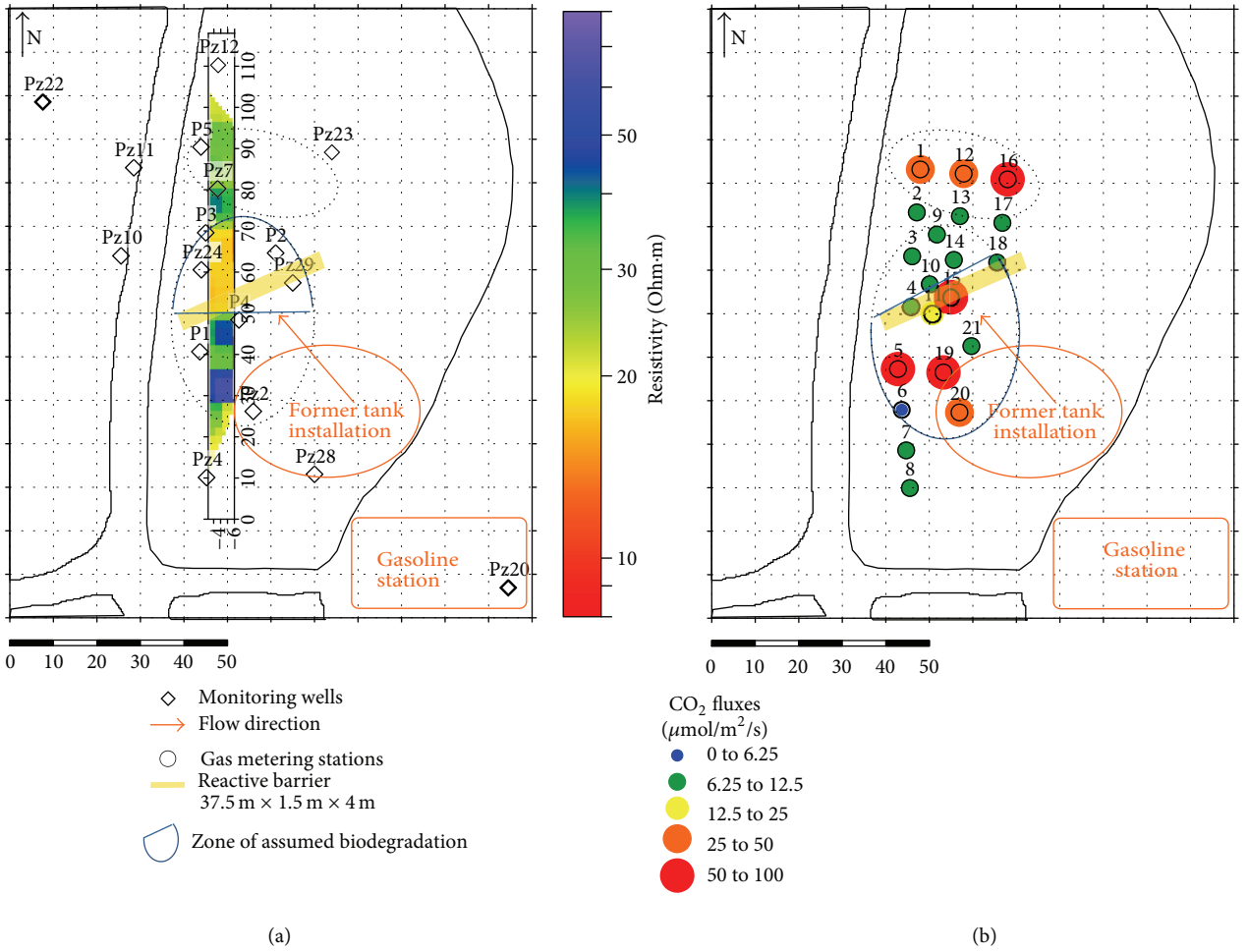

FIGURE 13: Maps of electrical resistivity measured on the permanent profile (a) and of measured CO_2 emissions (b), in July 2014. The elliptical shape highlights the area of biodegradation with production of conductive metabolites and CO_2.

However, the permeability of the ground is low and the groundwater table velocity is around 17 m/year. The oxygen from the barrier diffused slowly and its effect was not detected by both direct and indirect monitoring. The seasonal variation of bacterial activity was not yet "erased" by the continuous oxygen injection. Nonetheless, our first results over a year of monitoring show the interest of using geophysical methods and gas analyses to monitor and evaluate *in situ* remediation.

By applying the technology described here, fewer piezometers will be required for the monitoring and the understanding of bioremediation processes, leading to significant cost saving due to fewer monitoring requirements (piezometers, samples, and lab analyses) and more optimized remedial applications based on rapid identification of missed target zones.

Conflict of Interests

The authors declare that there is no conflict of interests regarding the publication of this paper.

Acknowledgments

The authors acknowledge the French Research Agency (Project BIOPHY, ANR-10-ECOT-014) and LABEX VOLTAIRE (Excellence Laboratory for Atmosphere, Resources and Environmental Interactions Study, University of Orleans, France) (ANR-10-LABX-100-01) for financial support. They also thank all the cooperation partners of the BIOPHY project: BRGM, LPC2E, Serpol, and Total. The LPC2E technical research team is gratefully acknowledged for their contribution to the development of the SPIRIT instrument. Technical support from BRGM is greatly appreciated as well. And they thank P. Gaudry, S. Williams, and G. Belot (LPC2E master's students) for their help during *in situ* measurement campaigns, as well as E. Verardo (BRGM Ph.D. student) for her contribution.

References

[1] N. Das and P. Chandran, "Microbial degradation of petroleum hydrocarbon contaminants: an overview," *Biotechnology Research International*, vol. 2011, Article ID 941810, 13 pages, 2011.

[2] F. Nadim, G. E. Hoag, S. Liu, R. J. Carley, and P. Zack, "Detection and remediation of soil and aquifer systems contaminated with petroleum products: an overview," *Journal of Petroleum Science and Engineering*, vol. 26, no. 1–4, pp. 169–178, 2000.

[3] K.-F. Chen, C.-M. Kao, C.-W. Chen, R. Y. Surampalli, and M.-S. Lee, "Control of petroleum-hydrocarbon contaminated groundwater by intrinsic and enhanced bioremediation," *Journal of Environmental Sciences*, vol. 22, no. 6, pp. 864–871, 2010.

[4] M. Farhadian, C. Vachelard, D. Duchez, and C. Larroche, "In situ bioremediation of monoaromatic pollutants in groundwater: a review," *Bioresource Technology*, vol. 99, no. 13, pp. 5296–5308, 2008.

[5] J. V. Weiss and I. M. Cozzarelli, "Biodegradation in contaminated aquifers: incorporating microbial/molecular methods," *Ground Water*, vol. 46, no. 2, pp. 305–322, 2008.

[6] M. Majone, R. Verdini, F. Aulenta et al., "In situ groundwater and sediment bioremediation: barriers and perspectives at European contaminated sites," *New Biotechnology*, vol. 32, no. 1, pp. 133–146, 2015.

[7] A. Flores Orozco, A. Kemna, C. Oberdörster et al., "Delineation of subsurface hydrocarbon contamination at a former hydrogenation plant using spectral induced polarization imaging," *Journal of Contaminant Hydrology*, vol. 136-137, pp. 131–144, 2012.

[8] J. A. Sogade, F. Scira-Scappuzzo, Y. Vichabian et al., "Induced-polarization detection and mapping of contaminant plumes," *Geophysics*, vol. 71, no. 3, pp. B75–B84, 2006.

[9] H. Vanhala, "Mapping oil-contaminated sand and till with the Spectral Induced Polarization (SIP) method," *Geophysical Prospecting*, vol. 45, no. 2, pp. 303–326, 1997.

[10] G. R. Olhoeft, "Direct detection of hydrocarbon and organic chemicals with ground penetrating radar and complex resistivity," in *Proceedings of the NWWA/API Conference on Petroleum Hydrocarbons and Organic Chemicals in Ground Water-Prevention, Detection and Restoration*, Houston, Tex, USA, November 1986.

[11] F. M. Mewafy, D. D. Werkema, E. A. Atekwana et al., "Evidence that bio-metallic mineral precipitation enhances the complex conductivity response at a hydrocarbon contaminated site," *Journal of Applied Geophysics*, vol. 98, pp. 113–123, 2013.

[12] E. A. Atekwana and E. A. Atekwana, "Geophysical signatures of microbial activity at hydrocarbon contaminated sites: a review," *Surveys in Geophysics*, vol. 31, no. 2, pp. 247–283, 2010.

[13] E. A. Atekwana and L. D. Slater, "Biogeophysics: a new frontier in Earth science research," *Reviews of Geophysics*, vol. 47, no. 4, Article ID RG4004, 2009.

[14] W. A. Sauck, "A model for the resistivity structure of LNAPL plumes and their environs in sandy sediments," *Journal of Applied Geophysics*, vol. 44, no. 2-3, pp. 151–165, 2000.

[15] V. Naudet and A. Revil, "A sandbox experiment to investigate bacteria-mediated redox processes on self-potential signals," *Geophysical Research Letters*, vol. 32, no. 11, Article ID L11405, 2005.

[16] N. Schwartz, T. Shalem, and A. Furman, "The effect of organic acid on the spectral-induced polarization response of soil," *Geophysical Journal International*, vol. 197, no. 1, pp. 269–276, 2014.

[17] R. Albrecht, J. C. Gourry, M.-O. Simonnot, and C. Leyval, "Complex conductivity response to microbial growth and biofilm formation on phenanthrene spiked medium," *Journal of Applied Geophysics*, vol. 75, no. 3, pp. 558–564, 2011.

[18] C. A. Davis, E. Atekwana, E. Atekwana, L. D. Slater, S. Rossbach, and M. R. Mormile, "Microbial growth and biofilm formation in geologic media is detected with complex conductivity measurements," *Geophysical Research Letters*, vol. 33, no. 18, Article ID L18403, 2006.

[19] A. Arato, M. Wehrer, B. Biró, and A. Godio, "Integration of geophysical, geochemical and microbiological data for a comprehensive small-scale characterizationof an aged LNAPL-contaminated site," *Environmental Science and Pollution Research*, vol. 21, no. 15, pp. 8948–8963, 2014.

[20] G. Cassiani, A. Binley, A. Kemna et al., "Noninvasive characterization of the Trecate (Italy) crude-oil contaminated site: links between contamination and geophysical signals," *Environmental Science and Pollution Research*, vol. 21, no. 15, pp. 8914–8931, 2014.

[21] R. M. Rosales, P. Martínez-Pagan, A. Faz, and J. Moreno-Cornejo, "Environmental monitoring using Electrical Resistivity Tomography (ERT) in the subsoil of three former petrol stations in SE of Spain," *Water, Air, and Soil Pollution*, vol. 223, no. 7, pp. 3757–3773, 2012.

[22] V. Che-Alota, E. A. Atekwana, E. A. Atekwana, W. A. Sauck, and D. D. Werkema Jr., "Temporal geophysical signatures from contaminant-mass remediation," *Geophysics*, vol. 74, no. 4, pp. B113–B123, 2009.

[23] K. H. Williams, A. Kemna, M. J. Wilkins et al., "Geophysical monitoring of coupled microbial and geochemical processes during stimulated subsurface bioremediation," *Environmental Science & Technology*, vol. 43, no. 17, pp. 6717–6723, 2009.

[24] K. Kaufmann, M. Christophersen, A. Buttler, H. Harms, and P. Höhener, "Microbial community response to petroleum hydrocarbon contamination in the unsaturated zone at the experimental field site Værløse, Denmark," *FEMS Microbiology Ecology*, vol. 48, no. 3, pp. 387–399, 2004.

[25] C. M. Aelion, P. Höhener, D. Hunkeler, and R. Aravena, *Environmental Isotopes in Biodegradation and Bioremediation*, CRC Press, Taylor & Francis, 2010.

[26] T. W. Boutton, "Stable carbon isotope ratios of natural materials: II. Atmospheric, terrestrial, marine, and freshwater environments," in *Carbon Isotope Techniques*, vol. 1, chapter 11, pp. 173–185, Academic Press, 1991.

[27] J. H. Troughton and K. A. Card, "Temperature effects on the carbon-isotope ratio of C3, C4 and crassulacean-acid-metabolism (CAM) plants," *Planta*, vol. 123, no. 2, pp. 185–190, 1975.

[28] C. Körner, G. D. Farquhar, and Z. Roksandic, "A global survey of carbon isotope discrimination in plants from high altitude," *Oecologia*, vol. 74, no. 4, pp. 623–632, 1988.

[29] R. U. Meckenstock, B. Morasch, C. Griebler, and H. H. Richnow, "Stable isotope fractionation analysis as a tool to monitor biodegradation in contaminated acquifers," *Journal of Contaminant Hydrology*, vol. 75, no. 3-4, pp. 215–255, 2004.

[30] S.-J. Kim, D. H. Choi, D. S. Sim, and Y.-S. Oh, "Evaluation of bioremediation effectiveness on crude oil-contaminated sand," *Chemosphere*, vol. 59, no. 6, pp. 845–852, 2005.

[31] O. Schoefs, M. Perrier, and R. Samson, "Estimation of contaminant depletion in unsaturated soils using a reduced-order biodegradation model and carbon dioxide measurement," *Applied Microbiology and Biotechnology*, vol. 64, no. 1, pp. 53–61, 2004.

[32] N. E.-D. Sharabi and R. Bartha, "Testing of some assumptions about biodegradability in soil as measured by carbon dioxide

evolution," *Applied and Environmental Microbiology*, vol. 59, no. 4, pp. 1201–1205, 1993.

[33] N. J. Sihota, O. Singurindy, and K. U. Mayer, "CO_2-Efflux measurements for evaluating source zone natural attenuation rates in a petroleum hydrocarbon contaminated aquifer," *Environmental Science and Technology*, vol. 45, no. 2, pp. 482–488, 2011.

[34] N. J. Sihota and K. U. Mayer, "Characterizing vadose zone hydrocarbon biodegradation using carbon dioxide effluxes, isotopes, and reactive transport modeling," *Vadose Zone Journal*, vol. 11, no. 4, 2012.

[35] P. K. Aggarwal, M. E. Fuller, M. M. Gurgas, J. F. Manning, and M. A. Dillon, "Use of stable oxygen and carbon isotope analyses for monitoring the pathways and rates of intrinsic and enhanced in situ biodegradation," *Environmental Science & Technology*, vol. 31, no. 2, pp. 590–596, 1997.

[36] M. E. Conrad, P. F. Daley, M. L. Fischer, B. B. Buchanan, T. Leighton, and M. Kashgarian, "Combined 14C and δ13C monitoring of in situ biodegradation of petroleum hydrocarbons," *Environmental Science and Technology*, vol. 31, no. 5, pp. 1463–1469, 1997.

[37] P. K. Aggarwal and R. E. Hinchee, "Monitoring in situ biodegradation of hydrocarbons by using stable carbon isotopes," *Environmental Science & Technology*, vol. 25, no. 6, pp. 1178–1180, 1991.

[38] K. H. Suchomel, D. K. Kreamer, and A. Long, "Production and transport of carbon dioxide in a contaminated vadose zone: a stable and radioactive carbon isotope study," *Environmental Science & Technology*, vol. 24, no. 12, pp. 1824–1831, 1990.

[39] C. Noel, J. C. Gourry, J. Deparis, I. Ignatiadis, F. Battaglia-Brunet, and C. Guimbaud, "Suitable real time monitoring of the aerobic biodegradation of toluene in contaminated sand by Spectral Induced Polarization measurements and CO_2 analyses," *Near Surface Geophysics*, In press.

[40] E. Verardo, A. Saada, V. Guerin et al., "Cas d'étude de gestion de site par atténuation naturelle: site 3—hydrocarbures pétroliers," Project ATTENA—Phase 2, Final Report, ADEME, 2013.

[41] R. Boopathy, "Factors limiting bioremediation technologies," *Bioresource Technology*, vol. 74, no. 1, pp. 63–67, 2000.

[42] R. M. Atlas, "Microbial hydrocarbon degradation—bioremediation of oil spills," *Journal of Chemical Technology & Biotechnology*, vol. 52, no. 2, pp. 149–156, 1991.

[43] L. D. Slater and D. Lesmes, "IP interpretation in environmental investigations," *Geophysics*, vol. 67, no. 1, pp. 77–88, 2002.

[44] M. H. Loke, J. E. Chambers, and R. D. Ogilvy, "Inversion of 2D spectral induced polarization imaging data," *Geophysical Prospecting*, vol. 54, no. 3, pp. 287–301, 2006.

[45] H. Craig, "Isotopic standards for carbon and oxygen and correction factors for mass-spectrometric analysis of carbon dioxide," *Geochimica et Cosmochimica Acta*, vol. 12, no. 1-2, pp. 133–149, 1957.

[46] C. Guimbaud, V. Catoire, S. Gogo et al., "A portable infrared laser spectrometer for field measurements of trace gases," *Measurement Science and Technology*, vol. 22, pp. 1–17, 2011.

[47] S. Gogo, C. Guimbaud, F. Laggoun-Défarge, V. Catoire, and C. Robert, "In situ quantification of CH4 bubbling events from a peat soil using a new infrared laser spectrometer," *Journal of Soils and Sediments*, vol. 11, no. 4, pp. 545–551, 2011.

[48] A. Grossel, B. Nicoullaud, H. Bourennane et al., "Simulating the spatial variability of nitrous oxide emission from cropped soils at the within-field scale using the NOE model," *Ecological Modelling*, vol. 288, pp. 155–165, 2014.

[49] C. Guimbaud, C. Noel, M. Chartier et al., "A quantum cascade laser infrared spectrometer for CO_2 stable isotope analysis: field implementation at a hydrocarbon contaminated site under bioremediation," *Journal of Environmental Sciences*, vol. 40, pp. 60–74, 2016.

[50] J. W. Raich and A. Tufekcioglu, "Vegetation and soil respiration: correlations and controls," *Biogeochemistry*, vol. 48, no. 1, pp. 71–90, 2000.

[51] J. W. Raich and C. S. Potter, "Global patterns of carbon dioxide emissions from soils," *Global Biogeochemical Cycles*, vol. 9, no. 1, pp. 23–36, 1995.

[52] K. Hayley, L. R. Bentley, M. Gharibi, and M. Nightingale, "Low temperature dependence of electrical resistivity: implications for near surface geophysical monitoring," *Geophysical Research Letters*, vol. 34, no. 18, 2007.

[53] M. Hayashi, "Temperature-electrical conductivity relation of water for environmental monitoring and geophysical data inversion," *Environmental Monitoring and Assessment*, vol. 96, no. 1–3, pp. 119–128, 2004.

[54] M. E. Conrad, A. S. Templeton, P. F. Daley, and L. Alvarez-Cohen, "Isotopic evidence for biological controls on migration of petroleum hydrocarbons," *Organic Geochemistry*, vol. 30, no. 8, pp. 843–859, 1999.

[55] C. M. Aelion, B. C. Kirtland, and P. A. Stone, "Radiocarbon assessment of aerobic petroleum bioremediation in the vadose zone and groundwater at an AS/SVE site," *Environmental Science & Technology*, vol. 31, no. 12, pp. 3363–3370, 1997.

[56] C.-H. Chaîneau, J.-L. Morel, and J. Oudot, "Microbial degradation in soil microcosms of fuel oil hydrocarbons from drilling cuttings," *Environmental Science & Technology*, vol. 29, no. 6, pp. 1615–1621, 1995.

[57] J. R. Van der Meer, W. M. de Vos, S. Harayama, and A. J. B. Zehnder, "Molecular mechanisms of genetic adaptation to xenobiotic compounds," *Microbiological Reviews*, vol. 56, no. 4, pp. 677–694, 1992.

[58] J. G. Leahy and R. R. Colwell, "Microbial degradation of hydrocarbons in the environment," *Microbiological Reviews*, vol. 54, no. 3, pp. 305–315, 1990.

[59] F. Garnier, *Contribution à L'évaluation Biogéochimique des Impacts Liés à L'exploitation Géothermique des Aquifères Superficiels: Expérimentations et Simulations à L'échelle D'un Pilote et D'installations Réelles*, Université d'orléans, 2012.

[60] M. Lenczewski, P. Jardine, L. McKay, and A. Layton, "Natural attenuation of trichloroethylene in fractured shale bedrock," *Journal of Contaminant Hydrology*, vol. 64, no. 3-4, pp. 151–168, 2003.

[61] B. A. Bekins, I. M. Cozzarelli, E. M. Godsy, E. Warren, H. I. Essaid, and M. E. Tuccillo, "Progression of natural attenuation processes at a crude oil spill site: II. Controls on spatial distribution of microbial populations," *Journal of Contaminant Hydrology*, vol. 53, no. 3-4, pp. 387–406, 2001.

[62] G. Lu, T. P. Clement, C. Zheng, and T. H. Wiedemeier, "Natural attenuation of BTEX compounds: model development and field-scale application," *Ground Water*, vol. 37, no. 5, pp. 707–717, 1999.

Hindawi Publishing Corporation
Applied and Environmental Soil Science
Volume 2016, Article ID 3951486, 12 pages
http://dx.doi.org/10.1155/2016/3951486

Research Article

Transport Processes in Porous Media by Self-Potential Method

Valeria Giampaolo, Daniela Calabrese, and Enzo Rizzo

Consiglio Nazionale delle Ricerche, Istituto di Metodologie per l'Analisi Ambientale, Laboratorio Hydrogeosite, Contrada Santa Loja, 85050 Tito, Italy

Correspondence should be addressed to Enzo Rizzo; enzo.rizzo@imaa.cnr.it

Received 1 October 2015; Accepted 20 December 2015

Academic Editor: Pantelis Soupios

Copyright © 2016 Valeria Giampaolo et al. This is an open access article distributed under the Creative Commons Attribution License, which permits unrestricted use, distribution, and reproduction in any medium, provided the original work is properly cited.

A controlled diffusion/infiltration column experimental activity was carried out with the aim of monitoring the leakage of a salty water plume by time-lapse self-potential (SP) measurements. In particular, three tracer tests with different NaCl concentrations (6.00, 1.00, and 0.25 g L^{-1}) were performed and all the measured SP signals showed a sharp reduction corresponding to the arrival of saline front with negative electrical potential values (−78.99 ± 3.24 mV, −54.52 ± 2.28 mV, and −24.12 ± 1.21 mV) which decrease with increasing volume of tracer introduced into the column. Then, measured self-potential values were converted into salt concentration ones by the Planck-Henderson equation and sand diffusion (D) and longitudinal dispersivity (α_L) values were estimated by modelling the transport equations in the COMSOL Multiphysics environment. Finally, the results show that measured and estimated NaCl concentrations are well correlated.

1. Introduction

One of the most difficult tasks for the hydrogeologist is to characterize solute transport mechanism in heterogeneous aquifers; in fact, flow pathways and velocity and the medium permeability are necessary information to evaluate the possible contamination effect and to design and optimize remediation strategies. Usually, subsoil heterogeneities, linked to rock texture, pore-space geometry, and mineralogy, affect solute transport processes that could display a heterogeneous behaviour and significant spatial-temporal changes of solute concentrations.

As a result of this high variability degree of the involved phenomena, typical measurements, for example, invasive soil and water sampling, are mostly unable to adequately characterize transport properties and processes.

Therefore, in the last year, environmental geophysicists have concentrated their research activity on the development of high resolution geophysical techniques for the study of flow and transport processes. In particular, several works have shown the efficacy of coupling geophysical prospecting and tracer test as a useful device to reconstruct solute transport phenomena in the subsoil [1–4]. In fact, the use of a noninvasive and indirect methodology with a high sampling density, the possibility to acquire data in an automated time-lapse manner, and the ability to modulate the measurement scale by suitable survey strategy make the geophysical methods an important tool for subsurface transport characterization. However, in order to improve the reconstruction of solute transport phenomena in heterogeneous subsoil starting from geophysical imaging techniques, it is necessary to use petrophysical relationships that link geophysical parameters to transport related ones.

The most suited geophysical methods for the transport processes monitoring are techniques sensitive to variations in the subsoil electrical properties. Traditionally, the monitoring of salt plume by geophysical techniques is performed by electrical resistivity tomography (ERT) or ground penetrating radar (GPR) [1–3]; however, also the self-potential (SP) method has been shown to be a suitable tool for monitoring solute transport processes because it is sensitive both to groundwater flow (electrokinetic potential) [5–9] and to electrochemical processes (electrochemical potential) related to gradients of the ionic species chemical potential and redox potential (Eh) in the pore water [10–23]. The most recent efforts have been those to estimate hydrological properties, starting from electrical potential values measured, using coupling equations linked by coupling coefficients

that describe the groundwater flow and the self-potential phenomena [3, 13, 14, 24–30]. One of the approaches consists in converting the measured electrical potential into solute concentration using hydrogeophysical relations [31], and then the estimated solute concentrations, combined with direct hydrologic observations, are used to condition an inversion procedure for calculating medium parameters such as hydraulic conductivity and longitudinal dispersivity. In particular, Maineult et al. [13, 14, 29] estimated NaCl plume concentration in sandbox-controlled experiments from SP measurement, while Revil and Jardani [30] assessed, using a stochastic approach, the hydraulic conductivity and dispersivity values of a fine sand using time-lapse self-potential measurements. Moreover, Ikard et al. [32] localized preferential fluid flow pathways in a porous medium by measuring time-lapse electrical potential values during a salt tracer injection in a sandbox experiment. In order to replicate the time-lapse self-potential distribution measured, they performed a synthetic case study and, with a finite element model by COMSOL Multiphysics, they determined the porosity and hydraulic conductivity of the medium.

In this work, the self-potential method was applied to trace in real time the front of a leaking salt plume during three pulse input tracer tests at different salt concentration and estimated the diffusion and the dispersivity parameters of the porous material applying a hydrogeophysical inversion approach. A laboratory experiment was performed at the Hydrogeosite Laboratory of IMAA-CNR of Marsico Nuovo (Italy). The main objective of this study was to analyse in time-lapse the contamination phenomenon by self-potential measurements in the presence of simulated constant water flow and evaluate the transport processes occurring in a homogeneous porous medium in saturated conditions. In detail, a sand column was set up performing a controlled diffusion/infiltration experiment in order to monitor the leakage of a salty water plume by time-lapse self-potential measurements. Finally, a finite element inversion model was implemented with COMSOL Multiphysics software, in order to build a numerical model and to have a comparison between experimental measurements and the modelled one. Moreover, inversion approach refines and improves the interpretation of experimental studies by providing system transport parameters assessment.

2. Theoretical Background

The self-potential (SP) method is a passive geoelectrical technique consisting in measuring the electrical potential differences (V) long profiles and/or maps, between two nonpolarisable electrodes driven into the ground, at the surface of the earth, or in boreholes. These voltage differences are linked to electric fields generated by natural sources distributed in the subsoil, produced by various phenomena (hydraulic, chemical, and thermal).

The instrumentation typically used in SP measurement surveys consists of a multimeter, two nonpolarisable electrodes, and electric cables (Figure 1). Currently, there are multichannel systems for SP measurement not only for a better spatial coverage along profiles or maps, but also for a continuous observation during time of the evolution of the related phenomena [34].

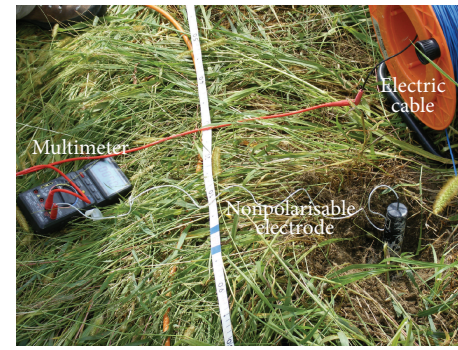

Figure 1: Instrumentation for SP measurement [33].

In the last years, the objective of SP interpretation became to solve coupled problems characterized by a system of linear equations, in order to obtain information about where and how the natural electrical current sources generate SP signal measured at surface and how big these sources are.

From Poisson's continuity equation, the general equation for SP signals can be written as follows:

$$\nabla \cdot (\sigma \nabla \varphi) = \nabla \cdot J_s, \tag{1}$$

where σ is the bulk electrical conductivity, φ is the self-potential, J_s is the external current density (electrical current source), and the total electric current density is divergence-free [17]. The self-potential source mechanisms were firstly theorized in the framework of Onsager's equations for coupled flows [5, 35, 36]:

$$\begin{aligned} J_s &= \sum_i j_i, \\ J_i &= -\sum_k L_{ik} \nabla x_k, \end{aligned} \tag{2}$$

where ∇x_k are external forces (hydraulic, chemical, and thermal gradients) and L_{ik} are the phenomenological coefficients (coupling coefficients). The self-potential data are therefore a function of the medium electrical resistivity, of the remote thermal, chemical, and hydraulic gradient, and of the coupling coefficient distribution.

Neglecting the thermal contribution, the self-potential source term can be described as the superposition of two components: the so-called electrokinetic and electrochemical potentials.

2.1. Electrokinetic Potential. The electrokinetic potential (or streaming potential) is induced by the motion of electrolytic fluids through porous media. It is generated, in particular, by the flow of the water circulating in the subsoil that, during its path in the interconnected pores, carries with

it electrical charges present at the mineral/water interface, where it generates a triple electric layer [37–39].

The fluid, under a pressure gradient, flows and carries with it a part of the cations, causing a separation of electric charges at the mineral/water interface. Consequently, an electric field, induced along it, develops, whose potential difference is called ζ potential.

In particular, in saturated and isothermal conditions, the current density (J_s) is linked to the pressure (∇P) and the electric potential (∇V) gradients by the coupling equation:

$$J_s = -L_{22}\nabla V - L_{21}\nabla P. \tag{3}$$

The first term represents Ohm's law, where the coupling coefficient L_{22} is the bulk electrical conductivity σ_r (S m^{-1}), while L_{21} represents the electrokinetic coupling coefficient that is usually experimentally obtained by applying a hydraulic gradient and measuring the resulting electric potential (ΔV):

$$C_{\text{sat}} = -\frac{L_{21}}{\sigma_r} = \frac{\Delta P}{\Delta V} = \frac{\zeta \varepsilon_f}{\mu_f \sigma_f}, \tag{4}$$

where μ_f is the electrolyte dynamic viscosity (kg m^{-1} s^{-1}), ε_f is the electrolyte dielectric constant (F m^{-1}), σ_f is the electrolyte electrical conductivity (S m^{-1}), and $\Delta P = \rho_w g \Delta h$ is the pressure gradient (Pa) with ρ_w, g, and Δh corresponding to fluid density (kg m^{-3}), gravity acceleration coefficient (m s^{-2}), and hydraulic head (m), respectively.

Considering the modern approach that tries to interpret SP solving coupled problems characterized by a system of linear equations, J_s generated by the water flux in the subsoil can be described by [40]:

$$J_s = Q_v u, \tag{5}$$

where Q_v (C m^{-3}) is the effective charge per unit pore volume that can be dragged by the flow of the pore water and u is the Darcy velocity (m s^{-1}). Equation (5) is valid also under unsaturated conditions, and, in saturated condition, Revil and Leroy [40] related Q_v to the coupling coefficient C_{sat} (VPa^{-1}) through

$$Q_v = -\frac{C_{\text{sat}} \sigma_f \mu_f}{\rho_f g K_0}, \tag{6}$$

where K_0 is the hydraulic conductivity (m s^{-1}). Laboratory measurements suggest that C_{sat} is mainly dependent by the pore water electrical conductivity σ_f [41]; moreover, Jardani et al. [42] showed that Q_v increases with decreasing hydraulic conductivity.

2.2. Electrochemical Potential. The electrochemical potential was used primarily in the mining exploration because the greatest anomalies of self-potential are generated in correspondence with bodies of pyrite, graphite, or other metallic-conductor minerals [43].

Electrochemical sources can be produced by several phenomena. The common ones are the diffusion of ions dissolved in water and the presence of a redox potential. In the last case, the current source J_s can be generated by the contaminant biodegradation through microbially mediated redox reactions and can be described by the following equation [23]:

$$J_s = -\sigma_e \nabla E_H, \tag{7}$$

where σ_e is the electrical conductivity of an electronically conducting body and E_H is the redox potential. This phenomenon is equivalent to the corrosion of two metals in a short-circuited energy-producing cell described by Bockris and Reddy [44]. For this reason, this kind of self-potential source has been defined as "biogeobattery" [23, 45–47].

The absence of strong SP anomalies may be due to the lack of an electron conductor (σ_e in (7)). In this case, the SP signals are explained as diffusion potential [21].

The diffusion potential is another common electrochemical source mechanism caused by the presence of a gradient of the ionic species chemical potential in groundwater. It is described by the following equation:

$$J_s = -k_b T \sum_{i=1}^{n} \frac{t_i^{\pm} \sigma_w}{q_i} \nabla \ln \{C_i\}, \tag{8}$$

where k_b is the Boltzmann constant, T is the absolute temperature (K), $t_i^{\pm}$ is the Hittorf transport number of a species i dissolved in water, q_i is the charge of the species i, and C_i is the concentration of ions (g L^{-1}).

The diffusion potential is also called junction potential when an electrical double layer of positive and negative charges is created at the junction of two solutions at different concentration. The more concentrated solution will tend to spread into the less concentrated one, developing a potential difference at the point of connection, due to the ionic transfer. The electrical potential anomaly generated depends on the relative speeds of the ions.

Assume the case of a saturated porous medium where a very small amount of NaCl solution behaving as a tracer is injected. Ideally, it is possible to neglect the variation of the electrokinetic potential due to the introduction of the NaCl solution, while the junction potential (φ) can be calculated by integrating (8). Therefore, according to Revil [31], Maineult et al. [13, 14], and Martinez-Pagan et al. [3], the measured electrical potential differences ($\Delta\varphi$, V) inside a moving saline front depend on (Planck-Henderson equation)

$$\Delta\varphi = -n\frac{K_b T}{e}\left(2t^+ - 1\right)\frac{\nabla C}{C} = n\alpha^* \frac{\nabla C}{C}, \tag{9}$$

where n is the porosity, e is the elementary charge of the electron ($e = 1.602 \times 10^{-19}$ C), C (g L^{-1}) represent the solution concentration, and α^* is called junction coupling coefficient that, for a NaCl tracer, is around 5.15×10^{-3} V [30].

As suggested by Bolève et al. [48] and Crespy et al. [49], (8) and (9) are valid in porous media only for small Dukhin numbers (i.e., the ratio between the surface conductivity of the grains and the pore water electrical conductivity).

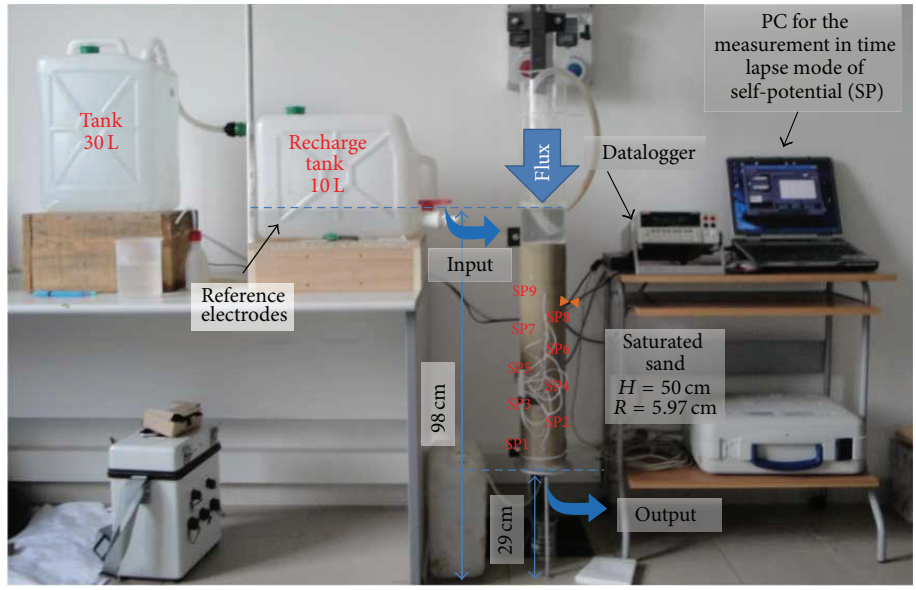

Figure 2: Experimental column facility installed at the Hydrogeosite Laboratory of CNR-IMAA (Marsico Nuovo, Italy).

The junction potential term can be obtained by integrating (9):

$$\varphi = -\frac{\varphi_0}{\ln(n\alpha^* + 1)} \ln\left(\frac{C_0 + n\alpha^* C}{C_0(1 + n\alpha^*)}\right). \quad (10)$$

Therefore, (10) allows us to estimate, starting from electrical potential measurements, the salt solution breakthrough curve at each point, where the junction potential is measured during the experiment:

$$C = -\frac{C_0}{n\alpha^*}\left[(n\alpha^* + 1)^{(\varphi-\varphi_0)/\varphi_0} - 1\right]. \quad (11)$$

Considering one-dimensional flow and transport, the analytical solution of the breakthrough curve is [50] as follows:

$$\frac{C(x,t)}{C_0} = \frac{1}{2}\operatorname{erfc}\left[\frac{x - (u/n_c)t}{2\sqrt{Dt/n_c}}\right] + \exp\left(\frac{ux}{D}\right)\operatorname{erfc}\left[\frac{x + (u/n_c)t}{2\sqrt{Dt/n_c}}\right], \quad (12)$$

where u is Darcy's velocity ($\mathrm{m\,s^{-1}}$), n_c is the kinematic porosity (dimensionless), and D is the dispersion ($\mathrm{m^2\,s^{-1}}$). In conclusion, (12) allows us to estimate the medium diffusion (D) and dispersivity values (α_L).

3. Materials and Methods

3.1. Sand Column Experimental Setup. The aim of this experiment was to use SP method for locating the front of a leaking salt plume during a tracer test experiment and estimating the dispersivity parameters of a porous material. The experimental setup is shown in Figure 2. The experiment was performed in a 1 m high Plexiglas column with a radius of about 6 cm. The column is open at the top and close at the bottom where a little hole was done to allow the water outflow. The water level in the column can be controlled by a hydraulic circuit consisting of two tanks connected to the column. This system is also used to keep the recharge rate constant.

The column was partially filled with well-sorted silica sand, saturated by tap water, for a total height of 0.50 m. This sand has been already used in previous hydrogeophysical experiments at the laboratory [51–53] and is characterized by mostly spherical grains, with a diameter ranging from 0.063 to 0.125, a porosity $n = 0.49$, a tortuosity $\tau = 0.79$, and a hydraulic conductivity of $5.26 \times 10^{-6}\,\mathrm{m\,s^{-1}}$. Moreover, the sand is characterized by an electrical resistivity value of 50 Ωm (in tap water saturated conditions) and a formation factor F of about 2.62.

The first step was to fix nine flat nonpolarising Ag-AgCl electrodes of 1 mm diameter (FIAB) along one column side with a spacing of 5 cm. These electrodes used for medical applications (electrocardiogram) have very high performance in terms of noise and voltages offset. Moreover, a reference electrode was put in the first recharge tank, in direct contact with fresh water, and always kept outside the salt plume.

In order to monitor SP signal during the infiltration experiment, all the electrodes were connected to a multichannel voltmeter (2700/EDMM, Keithley Instruments Inc.) and a PC, to collect and visualise the electrical potential differences between column electrodes and the reference one in real time. For the entire experiment, the sand into column was kept saturated; in particular, a hydraulic head of about 0.70 m was set in order to establish a one-dimensional steady-state flow in the sand ($Q = 0.35\,\mathrm{L\,h^{-1}}$). In this way, about 2 litres of

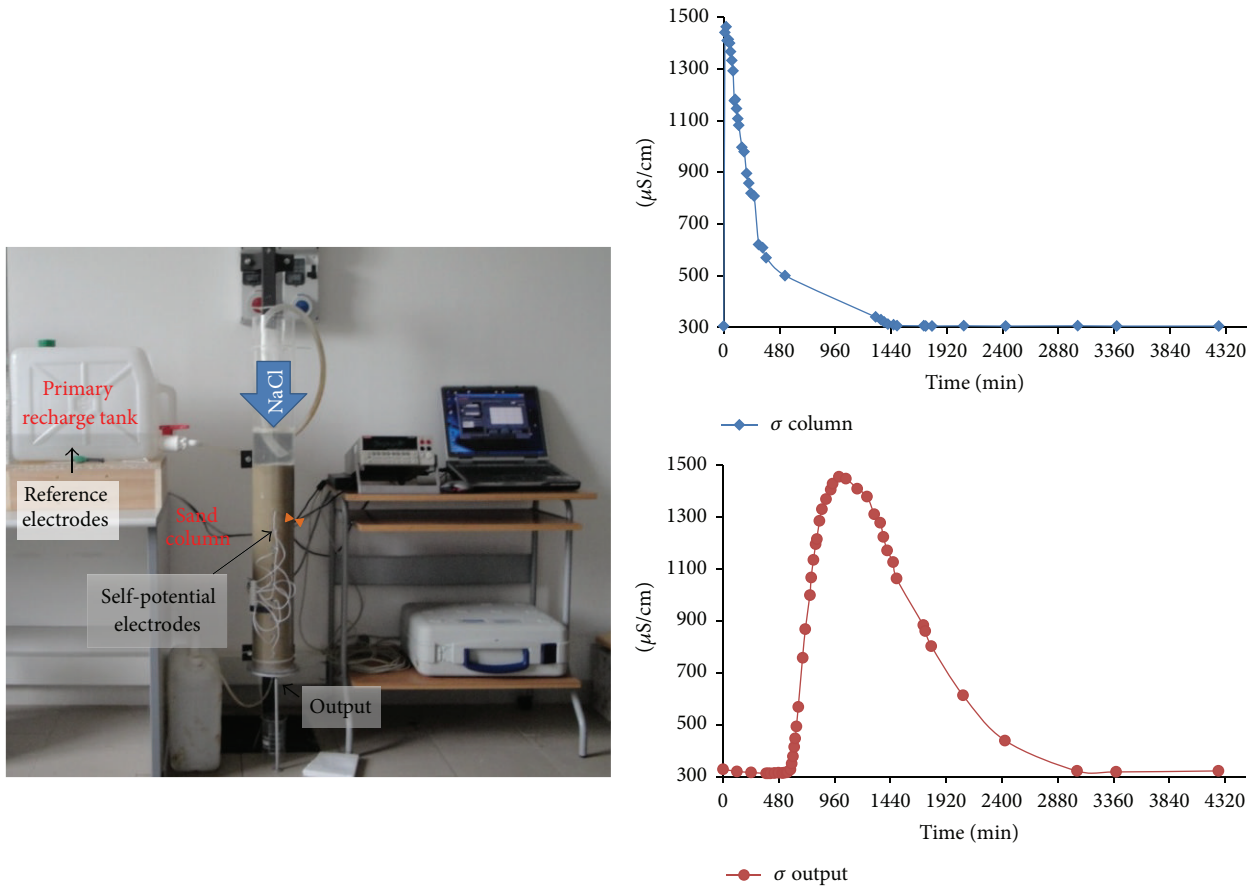

Figure 3: Tracer test experiments: the salt solution was injected at the top of the sand. Water electrical conductivity, monitored both in the column and at the output, shows the tracer behaviour during the test.

water remained above the sand body. After the steady-state flow was created, the voltage difference for each electrode was measured every 10 minutes for one day in order to set up a background baseline and noise level for the used geophysical method (characterization experimental phase).

3.2. Tracer Test Monitoring by SP. One day after steady-state flow was created, a salt solution of tap water and NaCl was injected at the top of the sand; in this way, the salt water began to migrate in the column by advection and diffusion. Three experimental phases were performed with a diminishing amount of salt concentration by injecting small volumes of salt solution into the system in order to make steady-state flow disturbances negligible. During the three experiments, the SP signals and the solution concentration were monitored every 1 and 15 minutes, respectively. The water electrical conductivity was measured both in the column and in a small box at the column end (output box) where the spreading solutions were collected (Figure 3).

The experiments lasted about 40 hours which was a time long enough to observe the return of normal conditions of water electrical conductivity in the output box.

The first experimental phase consisted in the monitoring by self-potential measurements of the saline front movement after the injection of 6.00 g L^{-1} NaCl solution at the top of the column. When this salt solution was injected up to the sand body, the water was mixed to the tap water in order to ensure a homogeneous input concentration. These actions required less than 15 seconds; therefore, we can approximate the solution injection as a pulse. Few minutes after the injection, the electrical conductivity of water suddenly increased from 312 to 1455 μS cm^{-1} (normalized at 20°C) and then quickly reduced its values as the effect of the migration of salt solution and the inflow of tap water from the recharge tanks.

The second experimental phase consisted in the monitoring by SP of the saline front movement after the injection of 1.00 g L^{-1} NaCl solution. In this case, when this salt solution was injected, the electrical conductivity of water increased from 295 to 458 μS cm^{-1} (normalized at 20°C).

Finally, the third experimental phase consisted in monitoring by SP the saline front movement after the injection of 0.25 g L^{-1} NaCl solution. In this last experimental phase, after the salt solution injection, the electrical conductivity of water recorded a small variation from 308 to 343 μS cm^{-1} (normalized at 20°C). Converting water electrical conductivity into solution concentration, it was possible to monitor the input salt concentrations evolution at the top of the column during the three experiments (Figure 4).

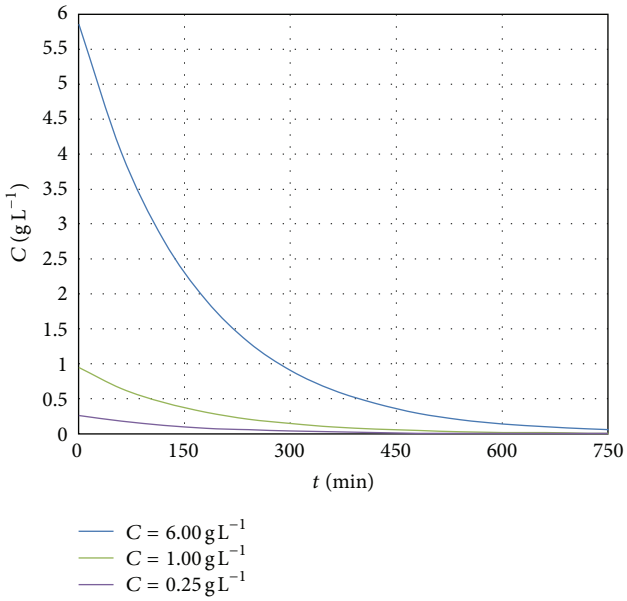

Figure 4: Input salt concentration measured at the top of the column during the experiment.

4. Results and Discussion

Figure 5 shows the SP values, acquired during the tracer test, at different salt solution concentration, while Figure 6 shows the comparison between SP values measured at different salt solution concentration (blue = 6.00 g L^{-1}, green = 1.00 g L^{-1}, and violet = 0.25 g L^{-1}), at three different positions of the column. SP data have been corrected taking into account SP signals measured during the characterization experimental phase.

In particular, analysing SP measured values, it is possible to observe that (1) all electrodes measured a sharp reduction of the SP signal, in correspondence with the saline front passage; (2) this phenomenon is more rapid with the diminishing concentration of injected solution; and (3) the absolute values of SP anomaly increase with increasing amount of NaCl solution added to the system, where the greater negative measured SP anomalies were about −78.99 ± 3.24 mV for the salt concentration of 6.00 g L^{-1}, −54.52 ± 2.28 mV for the salt concentration of 1.00 g L^{-1}, and −24.12 ± 1.21 for the salt concentration of 0.25 g L^{-1}. During the last experimental phase, the electrode SP8 measured very low SP values (−5 mV) with a great noise level; therefore, it is not considered in the following discussions.

Moreover, analysing the response of SP electrodes, it is possible to see that, in all experimental phases, the SP3 electrode reacts to the salt passage with some delay; therefore, also in this case SP3 was not considered.

The salt front took about 21 min to reach the first electrodes (SP9). The average travel time of the salt front at each electrode resulted to be 39.22, 32.33, and 29.67 min with an error of ±1.27 min, for salt concentrations of 6.00, 1.00, and 0.25 g L^{-1}, respectively.

Table 1: Hydrogeophysical input parameter for the simulation.

Parameters	Values
Hydraulic permeability K	$5.26e-6$ (m s^{-1})
Porosity θ	0.49 (dimensionless)
Dispersivity	$1e-3$ (m)
Diffusion coefficient	1–9 (m^2 s^{-1})
Tortuosity factor	0.79 (dimensionless)

For a one-dimensional flow configuration, the salt front average velocity at each electrode can be calculated, for the different salt concentration, knowing the average travel time. The average flow velocities were estimated to be 1.3, 1.5, and 1.7 mm min^{-1} with an error of ±0.2 mm min^{-1}, for the 6.00, 1.00, and 0.25 g L^{-1} concentrations, respectively.

4.1. SP Modelling. In order to estimate sand dispersivity parameters and determine the flow pathway of the salt solution and its concentration changes inside the column, a hydrogeophysical inversion approach has been used. In particular, self-potential measurements were transformed in salt concentration values using (11) and then concentration values were optimized to obtain transport parameters (see (12)). Figure 7 shows concentration curves obtained from SP data at different time instants and heights in the column.

Both the forward finite element model and the inversion were performed with COMSOL Multiphysics 4.3b, a multiphysics software tool for the solution of partial differential equations (PDEs), which is based on the finite element method. Physical properties used in the starting forward model are assumed to be constant throughout the entire solution domain and are summarized in Table 1.

The sand column is fully saturated and a water flux was created. The system physical conditions allowed us to use the module *Fluid Flow* → *Porous Media and Saturated Flow* → *Darcy's Law* → *Stationary conditions* to estimate Darcy's velocity field that was characterized by $u = v_x = 0$, $v = v_y = 0$, and $w = v_z \neq 0$.

Because the salt solution travels through the column according to the advection-dispersion equation, the *Fluid Flow* module wascoupled to the module *Chemical Species Transport* → *Solute transport* → *Time depending conditions*. Moreover, in order to perform the optimization of transport parameters the *Optimization* module has been further added to the simulation. The entire 3D domain was discretized in 1247 domain tetrahedral elements.

In the case of a pulse tracer injection from the top, the boundary condition at the top of the column ($x = 0.5$ m) is that, (1) for $t_0 = 0$ s, the concentration C is null ($C_0 = 0$), and the hydraulic head is $H = 0.70$ m, while (2) at the time t_i, H remains constant due to the low concentrations of solute introduced.

Moreover, considering the salt solution small amount injected, it is possible to neglect the effect of salt concentration upon dynamic viscosity and mass density of the pore water.

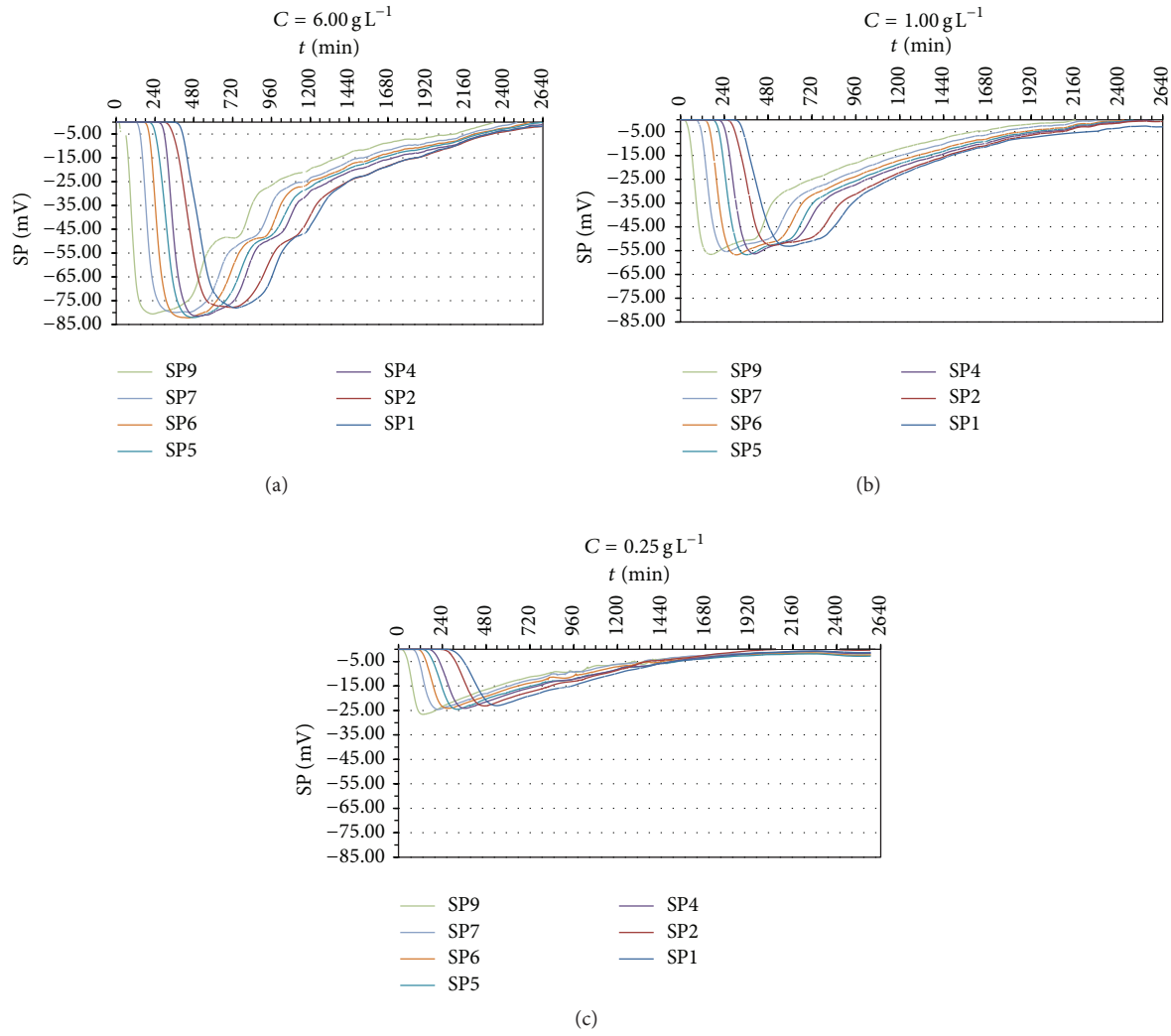

FIGURE 5: SP data measured during the tracer test with a salt concentration of (a) 6.00 g L^{-1}, (b) 1.00 g L^{-1}, and (c) 0.25 g L^{-1}.

On the contrary, the boundary condition at the bottom of the column (x = 0 m) is atmosphere/gauge for the *Fluid Flow* module and outflow for the *Solute transport* one. Finally, the sides boundaries are characterized by *no flow* and *no flux* conditions.

The input parameters for the *Optimization* module are constituted by salt breakthrough curves inside the column during all the experiments estimated starting from measured SP measurements (Figure 7). On the contrary, the terms D and α_L (diffusion and dispersion) represent the parameters to optimize because they mostly influence the variation of the saline concentrations in the investigated medium. The dispersion tensor is constituted by the linear terms α_x = alpha$L$; α_y = alpha$L$/10; and α_z = alpha$L$/10. In particular, the nonlinear last square Nelder-Mead optimization method was chosen.

Figure 8 shows the results of the inversion obtained by COMSOL Multiphysics of the saline trace test in the column (input salt concentration of 6.00 g L^{-1}), where the solution concentration inside the sand body reaches the maximum values just after the injection and then decreases during time. The values of D and α_L, determined for all three experiments, are shown in Table 2. The diffusion and longitudinal dispersivity values estimated are comparable with fine sands typical ones measured in laboratory [13, 30].

For each experiment, Figure 9 shows a comparison between the NaCl concentrations calculated by (11), starting from the electrical potential differences measured by SP electrodes, and those modelled by the COMSOL Multiphysics inverse procedure. These results confirm the validity of the model, showing a good agreement between the modelled and observed NaCl concentrations.

5. Conclusions

At the Hydrogeosite Laboratory of CNR-IMAA, a controlled diffusion/infiltration sand column experimental activity was

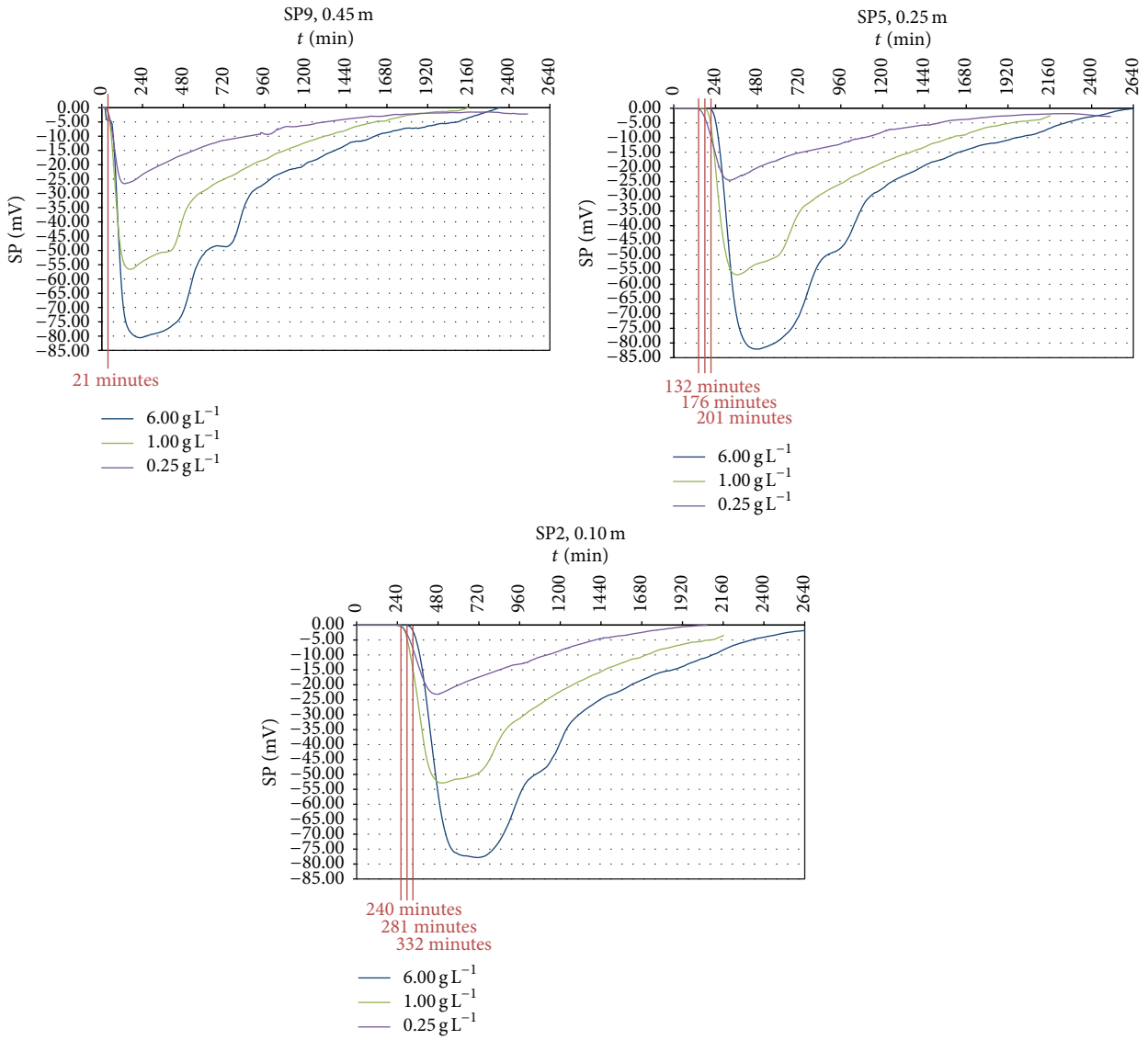

Figure 6: Comparison between SP values measured at different salt solution concentration (blue = 6.00 g L^{-1}, green = 1.00 g L^{-1}, and violet = 0.25 g L^{-1}), at three different positions of the column. The red lines indicate the arrival time of the saline front at the electrodes.

Table 2: Values of diffusion and longitudinal dispersivity calculated using self-potential signals registered at each electrode along the column using a hydrogeophysical inversion approach.

Tracer test	D (m^2 s^{-1})	α_L (m)	R^2
6.00 (kg m^{-3})	$1e-8.95$	0.00186	0.986
0.95 (kg m^{-3})	$1e-8.95$	0.00128	0.985
0.26 (kg m^{-3})	$1e-9.03$	0.00114	0.984

carried out with the aim of monitoring the leakage of a plume of salty water using time-lapse self-potential measurements.

In particular, three pulse input tracer tests were monitored by SP and the diffusion and the dispersivity parameters of the porous material were estimated applying a hydrogeophysical inversion approach.

The salt plume movement inside the column generated clear negative self-potential anomalies; in fact, all electrodes showed a sharp reduction in the measured SP signal, in correspondence with the saline front passage. In particular, this phenomenon is more rapid with the diminishing concentration of injected solution, while the absolute values of SP anomaly increase with increasing NaCl solution added to the system.

These measured self-potential anomalies were produced by the combination of the streaming potential, due to the pore water flow, and the diffusion potential linked to the ions chemical potential gradients in groundwater. Moreover, due to the low concentrations of solute introduced into the system, we assumed that the electrokinetic effect linked to the injection of the NaCl solution was negligible.

Self-potential measurements have been used to obtain diffusion (D, m^2 s^{-1}) and longitudinal dispersivity (α_L, m)

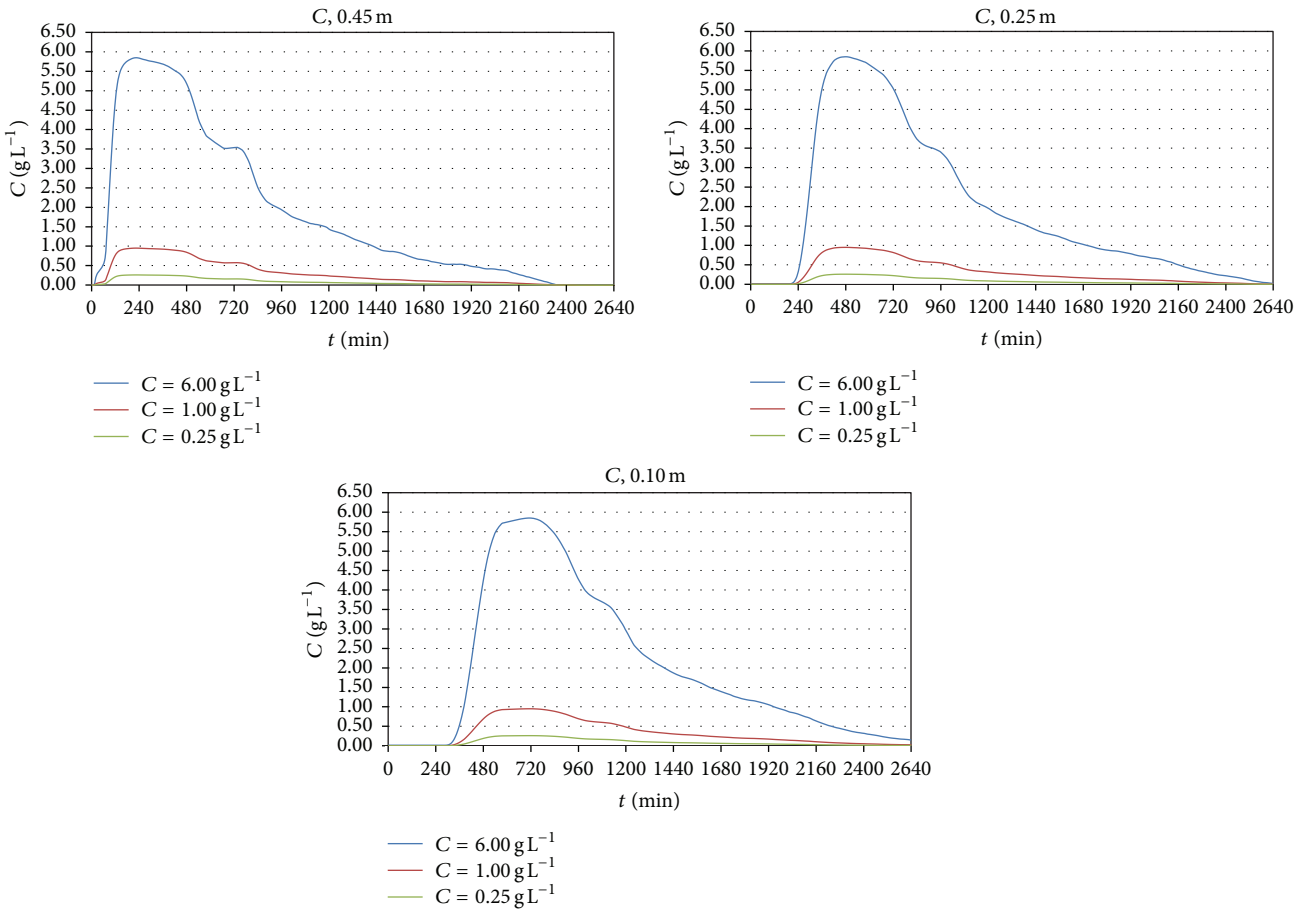

Figure 7: Salt concentration obtained by the measured SP signals at three different positions of the column.

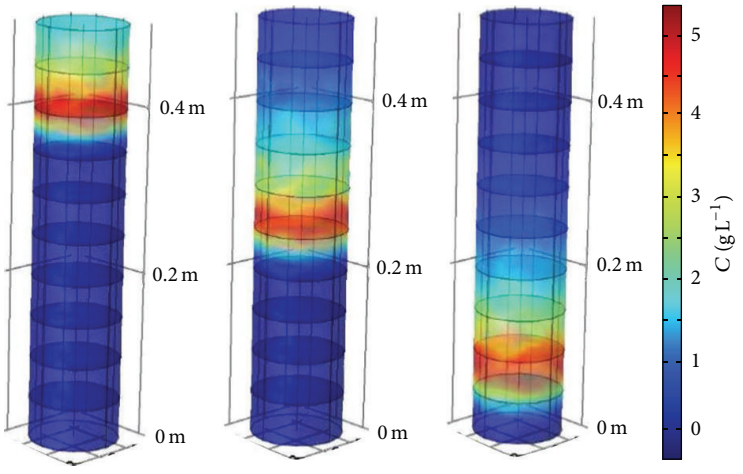

Figure 8: Simulation of a saline trace test in the column water flow by COMSOL Multiphysics.

firstly converting electrical potential values (mV) into concentration values (g L^{-1}) by the Planck-Henderson equation and then calculating the transport parameters by the equations implemented in the COMSOL Multiphysics environment.

This paper shows the capability of self-potential as a cheap tool to detect contaminants at very low concentrations. Moreover, the use of the SP data allows us to define and optimize the physical parameters of the model that simulates the distribution of the contaminant in the simulated aquifer.

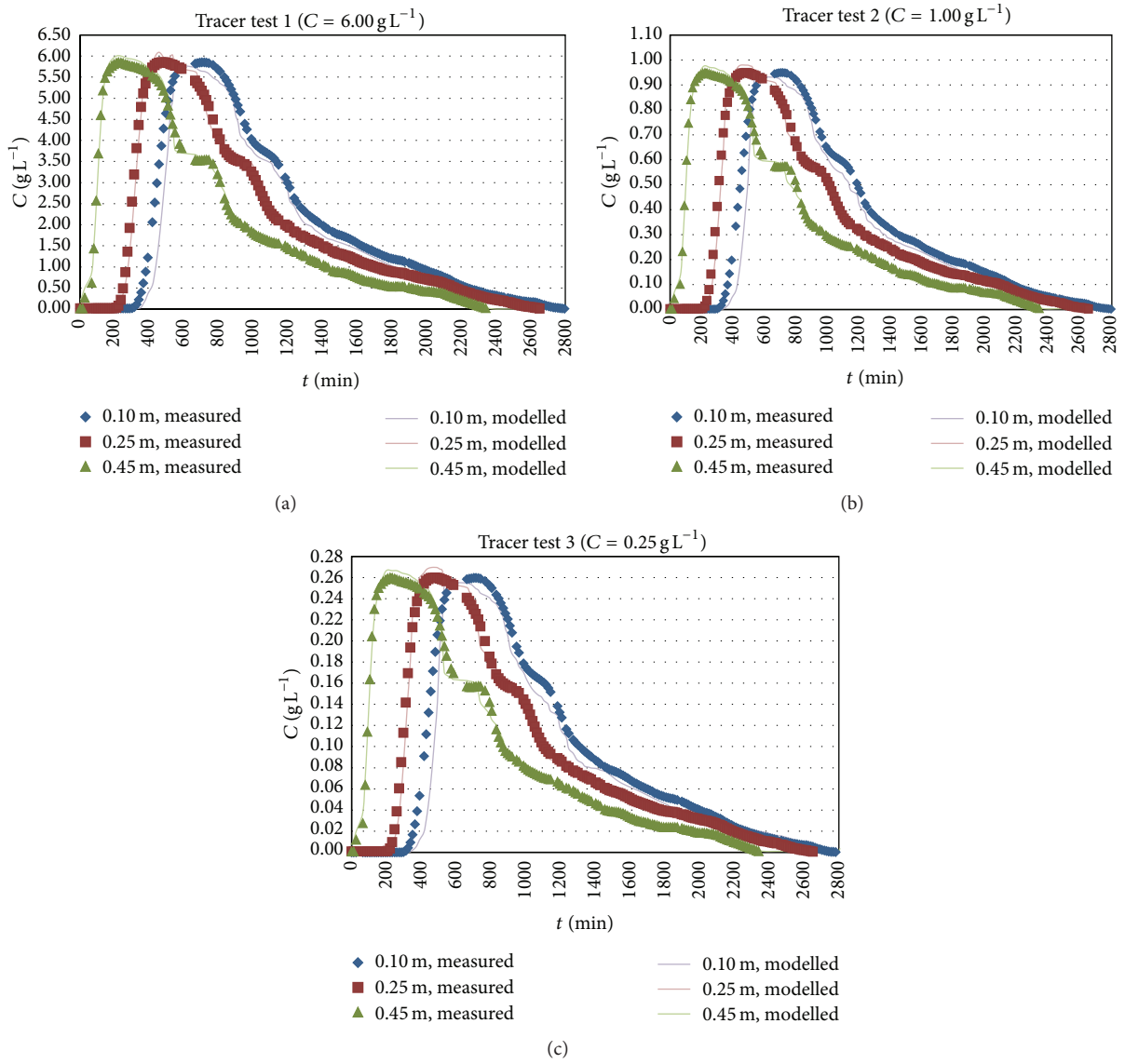

Figure 9: Comparison between breakthrough curves obtained from self-potential signals (dots) and those calculated by inversion (lines) for the tracer test with a salt concentration of (a) 6.00 g L^{-1}, (b) 1.00 g L^{-1}, and (c) 0.25 g L^{-1}.

More field work of this nature is necessary to validate the usefulness of self-potential in real heterogeneous conditions with limited hydrological data.

Conflict of Interests

The authors declare that there is no conflict of interests regarding the publication of this paper.

Acknowledgment

This research has been performed in the frame of the Ticamosc Project "Tecnologie Idrogeofisiche per la Caratterizzazione ed il Monitoraggio di Siti Contaminati" funded by a PO FSE Basilicata 2007–2013: "Promozione della Ricerca e dell'Innovazione e Sviluppo di Relazioni con il Sistema Produttivo Regionale" DD no. 796/2013, Azione no. 19/AP/05/2013/REG.

References

[1] L. Slater, A. Binley, R. Versteeg, G. Cassiani, R. Birken, and S. Sandberg, "A 3D ERT study of solute transport in a large experimental tank," *Journal of Applied Geophysics*, vol. 49, no. 4, pp. 211–229, 2002.

[2] A. Binley, G. Cassiani, R. Middleton, and P. Winship, "Vadose zone flow model parameterisation using cross-borehole radar and resistivity imaging," *Journal of Hydrology*, vol. 267, no. 3-4, pp. 147–159, 2002.

[3] P. Martínez-Pagán, A. Jardani, A. Revil, and A. Haas, "Self-potential monitoring of a salt plume," *Geophysics*, vol. 75, no. 4, pp. 17–25, 2010.

[4] A. Bolève, F. Janod, A. Revil, A. Lafon, and J.-J. Fry, "Localization and quantification of leakages in dams using time-lapse self-potential measurements associated with salt tracer injection," *Journal of Hydrology*, vol. 403, no. 3-4, pp. 242–252, 2011.

[5] W. R. Sill, "Self-potential modeling from primary flows," *Geophysics*, vol. 48, no. 1, pp. 76–86, 1983.

[6] Y. Bernabé, "Streaming potential in heterogeneous networks," *Journal of Geophysical Research: Solid Earth*, vol. 103, no. 9, pp. 20827–20841, 1998.

[7] A. Revil, P. A. Pezard, and P. W. J. Glover, "Streaming potential in porous media: 1. Theory of the zeta potential," *Journal of Geophysical Research: Solid Earth*, vol. 104, no. 9, pp. 20021–20031, 1999.

[8] A. Revil, H. Schwaeger, L. M. Cathles III, and P. D. Manhardt, "Streaming potential in porous media. 2. Theory and application to geothermal systems," *Journal of Geophysical Research: Solid Earth*, vol. 104, no. 9, Article ID 1999JB900090, pp. 20033–20048, 1999.

[9] E. Rizzo, B. Suski, A. Revil, S. Straface, and S. Troisi, "Self-potential signals associated with pumping tests experiments," *Journal of Geophysical Research B: Solid Earth*, vol. 109, no. 10, Article ID B10203, 2004.

[10] E. A. Atekwana, E. Atekwana, F. D. Legall, and R. V. Krishnamurthy, "Field evidence for geophysical detection of subsurface zones of enhanced microbial activity," *Geophysical Research Letters*, vol. 31, no. 23, pp. 1–5, 2004.

[11] E. A. Atekwana, E. A. Atekwana, D. D. Werkema et al., "Evidence for microbial enhanced electrical conductivity in hydrocarbon-contaminated sediments," *Geophysical Research Letters*, vol. 31, no. 23, Article ID L23501, 2004.

[12] V. Naudet and A. Revil, "A sandbox experiment to investigate bacteria-mediated redox processes on self-potential signals," *Geophysical Research Letters*, vol. 32, no. 11, Article ID L11405, 4 pages, 2005.

[13] A. Maineult, Y. Bernabé, and P. Ackerer, "Detection of advected concentration and pH fronts from self-potential measurements," *Journal of Geophysical Research: Solid Earth*, vol. 110, no. 11, Article ID B11205, 2005.

[14] A. Maineult, L. Jouniaux, and Y. Bernabé, "Influence of the mineralogical composition on the self-potential response to advection of KCl concentration fronts through sand," *Geophysical Research Letters*, vol. 33, no. 24, Article ID L24311, 2006.

[15] A. Revil and N. Linde, "Chemico-electromechanical coupling in microporous media," *Journal of Colloid and Interface Science*, vol. 302, no. 2, pp. 682–694, 2006.

[16] T. Arora, N. Linde, A. Revil, and J. Castermant, "Non-intrusive characterization of the redox potential of landfill leachate plumes from self-potential data," *Journal of Contaminant Hydrology*, vol. 92, no. 3-4, pp. 274–292, 2007.

[17] B. J. Minsley, J. Sogade, and F. D. Morgan, "Three-dimensional self-potential inversion for subsurface DNAPL contaminant detection at the Savannah River Site, South Carolina," *Water Resources Research*, vol. 43, no. 4, Article ID W04429, 2007.

[18] B. J. Minsley, J. Sogade, and F. D. Morgan, "Three-dimensional source inversion of self-potential data," *Journal of Geophysical Research: Solid Earth*, vol. 112, no. 2, Article ID B02202, 2007.

[19] C. A. Mendonça, "Forward and inverse self-potential modeling in mineral exploration," *Geophysics*, vol. 73, no. 1, pp. F33–F43, 2008.

[20] L. Jouniaux, A. Maineult, V. Naudet, M. Pessel, and P. Sailhac, "Review of self-potential methods in hydrogeophysics," *Comptes Rendus Geoscience*, vol. 341, no. 10-11, pp. 928–936, 2009.

[21] A. Revil, F. Trolard, G. Bourrié, J. Castermant, A. Jardani, and C. A. Mendonça, "Ionic contribution to the self-potential signals associated with a redox front," *Journal of Contaminant Hydrology*, vol. 109, no. 1–4, pp. 27–39, 2009.

[22] E. A. Atekwana and E. A. Atekwana, "Geophysical signatures of microbial activity at hydrocarbon contaminated sites: a review," *Surveys in Geophysics*, vol. 31, no. 2, pp. 247–283, 2010.

[23] A. Revil, C. A. Mendonça, E. A. Atekwana, B. Kulessa, S. S. Hubbard, and K. J. Bohlen, "Understanding biogeobatteries: where geophysics meets microbiology," *Journal of Geophysical Research*, vol. 115, Article ID G00G02, 2010.

[24] A. A. Ogilvy, M. A. Ayed, and V. A. Bogoslovsky, "Geophysical studies of water leakages from reservoirs," *Geophysical Prospecting*, vol. 17, no. 1, pp. 36–62, 1969.

[25] F. Perrier, M. Trique, B. Lorne, J.-P. Avouac, S. Hautot, and P. Tarits, "Electric potential variations associated with yearly lake level variations," *Geophysical Research Letters*, vol. 25, no. 10, pp. 1955–1958, 1998.

[26] M. Trique, F. Perrier, T. Froidefond, J. Avouac, and S. Hautot, "Fluid flow near reservoir lakes inferred from the spatial and temporal analysis of the electric potential," *Journal of Geophysical Research B: Solid Earth*, vol. 107, no. 10, p. 2239, 2002.

[27] A. Revil, D. Hermitte, M. Voltz et al., "Self-potential signals associated with variations of the hydraulic head during an infiltration experiment," *Geophysical Research Letters*, vol. 29, no. 7, pp. 101–104, 2002.

[28] K. Titov, Y. Ilyin, P. Konosavski, and A. Levitski, "Electrokinetic spontaneous polarization in porous media: petrophysics and numerical modelling," *Journal of Hydrology*, vol. 267, no. 3-4, pp. 207–216, 2002.

[29] A. Maineult, Y. Bernabé, and P. Ackerer, "Electrical response of flow, diffusion, and advection in a laboratory sand box," *Vadose Zone Journal*, vol. 3, no. 4, pp. 1180–1192, 2004.

[30] A. Revil and A. Jardani, "Stochastic inversion of permeability and dispersivities from time lapse self-potential measurements: a controlled sandbox study," *Geophysical Research Letters*, vol. 37, no. 11, Article ID L11404, 2010.

[31] A. Revil, "Ionic diffusivity, electrical conductivity, membrane and thermoelectric potentials in colloids and granular porous media: a unified model," *Journal of Colloid and Interface Science*, vol. 212, no. 2, pp. 503–522, 1999.

[32] S. J. Ikard, A. Revil, A. Jardani, W. F. Woodruff, M. Parekh, and M. Mooney, "Saline pulse test monitoring with the self-potential method to nonintrusively determine the velocity of the pore water in leaking areas of earth dams and embankments," *Water Resources Research*, vol. 48, no. 4, 2012.

[33] V. Giampaolo, E. Rizzo, K. Titov et al., "Self-potential monitoring of a crude oil-contaminated site (Trecate, Italy)," *Environmental Science and Pollution Research*, vol. 21, no. 15, pp. 8932–8947, 2014.

[34] V. Lapenna, K. Binieris, E. Rizzo et al., "New prototype for 4D self-potential tomography in near-surface geophysical exploration," in *Subsurface Sensing Technologies and Applications II*, C. Nyguyen, Ed., vol. 4129 of *Proceedings of SPIE*, pp. 447–456, San Diego, Calif, USA, July 2000.

[35] L. Onsager, "Reciprocal relations in irreversible processes. I.," *Physical Review Letters*, vol. 37, no. 4, pp. 405–426, 1931.

[36] B. Nourbehecht, *Irreversible thermodynamic effects in inhomogeneous media and their applications in certain geoelectric problems [Ph.D. thesis]*, Massachusetts Institute of Technology, Cambridge, Mass, USA, 1963.

[37] D. G. Grahame, "The electrical double layer and the theory of electrocapillarity," *Chemical Reviews*, vol. 41, no. 3, pp. 441–501, 1947.

[38] J. A. Davis, R. O. James, and J. O. Leckie, "Surface ionization and complexation at the oxide/water interface," *Journal of Colloid and Interface Science*, vol. 63, no. 3, pp. 480–499, 1978.

[39] A. Revil, V. Naudet, J. Nouzaret, and M. Pessel, "Principles of electrography applied to self-potential electrokinetic sources and hydrogeological applications," *Water Resources Research*, vol. 39, no. 5, pp. SBH31–SBH315, 2003.

[40] A. Revil and P. Leroy, "Constitutive equations for ionic transport in porous shales," *Journal of Geophysical Research B: Solid Earth*, vol. 109, no. 3, Article ID B03208, 2004.

[41] B. Suski, A. Revil, K. Titov et al., "Monitoring of an infiltration experiment using the self-potential method," *Water Resources Research*, vol. 42, no. 8, Article ID W08418, 2006.

[42] A. Jardani, A. Revil, A. Bolève, J. P. Dupont, W. Barrash, and B. Malama, "Tomography of groundwater flow from self-potential (SP) data," *Geophysical Research Letters*, vol. 34, Article ID L24403, 2007.

[43] M. Sato and H. M. Mooney, "The electrochemical mechanism of sulphide self-potentials," *Geophysics*, vol. 25, no. 1, pp. 226–249, 1960.

[44] J. Bockris and A. K. N. Reddy, *Modern Electrochemistry*, Plenum Press, New York, NY, USA, 2000.

[45] J. Bigalke and E. W. Grabner, "The Geobattery model: a contribution to large scale electrochemistry," *Electrochimica Acta*, vol. 42, no. 23-24, pp. 3443–3452, 1997.

[46] F. Timm and P. Möller, "The relation between electric and redox potential: evidence from laboratory and field measurements," *Journal of Geochemical Exploration*, vol. 72, no. 2, pp. 115–128, 2001.

[47] V. Naudet, A. Revil, E. Rizzo, J.-Y. Bottero, and P. Bégassat, "Groundwater redox conditions and conductivity in a contaminant plume from geoelectrical investigations," *Hydrology and Earth System Sciences*, vol. 8, no. 1, pp. 8–22, 2004.

[48] A. Bolève, A. Crespy, A. Revil, F. Janod, and J. L. Mattiuzzo, "Streaming potentials of granular media: influence of the Dukhin and Reynolds numbers," *Journal of Geophysical Research: Solid Earth*, vol. 112, no. 8, Article ID B08204, 2007.

[49] A. Crespy, A. Bolève, and A. Revil, "Influence of the Dukhin and Reynolds numbers on the apparent zeta potential of granular porous media," *Journal of Colloid and Interface Science*, vol. 305, no. 1, pp. 188–194, 2007.

[50] J. Bear, *Hydraulics of Groundwater*, McGraw-Hill, New York, NY, USA, 1979.

[51] S. Straface, E. Rizzo, and F. Chidichimo, "Estimation of hydraulic conductivity and water table map in a large-scale laboratory model by means of the self-potential method," *Journal of Geophysical Research: Solid Earth*, vol. 115, no. 6, Article ID B06105, pp. 1–18, 2010.

[52] S. Straface, E. Rizzo, V. Giampaolo, and F. Chidichimo, "Estimation of hydraulic conductivity in a large scale laboratory model by means of the self-potential method," *International Water Technology Journal*, vol. 1, no. 1, pp. 24–36, 2011.

[53] F. Chidichimo, M. De Biase, E. Rizzo, S. Masi, and S. Straface, "Hydrodynamic parameters estimation from self-potential data in a controlled full scale site," *Journal of Hydrology*, vol. 522, pp. 572–581, 2015.

Hindawi Publishing Corporation
Applied and Environmental Soil Science
Volume 2015, Article ID 435741, 10 pages
http://dx.doi.org/10.1155/2015/435741

Research Article

Determination of Tetracycline and Fluoroquinolone Antibiotics at Trace Levels in Sludge and Soil

Marie-Virginie Salvia, Maëva Fieu, and Emmanuelle Vulliet

Université de Lyon, Institut des Sciences Analytiques, UMR5280 CNRS, Equipe TRACES, Université Lyon 1, ENS-Lyon, 5 rue de la Doua, 69100 Villeurbanne, France

Correspondence should be addressed to Emmanuelle Vulliet; emmanuelle.vulliet@isa-lyon.fr

Received 13 September 2015; Revised 7 November 2015; Accepted 29 November 2015

Academic Editor: Dimitrios Ntarlagiannis

Copyright © 2015 Marie-Virginie Salvia et al. This is an open access article distributed under the Creative Commons Attribution License, which permits unrestricted use, distribution, and reproduction in any medium, provided the original work is properly cited.

This work describes the development of a sensitive analytical method to determine simultaneously traces of tetracycline and fluoroquinolone antibiotics in sludge and soil, based on PLE extraction, followed by SPE purification and finally an analysis by LC-MS/MS. Recoveries were greater than 87% in the case of fluoroquinolones and between 25.4 and 41.7% for tetracyclines. Low relative standard deviations (<15%) were obtained in both matrices. The limits of quantification were comprised between 1.1 and 4.6 ng/g and between 5 and 20 ng/g in soil and sludge, respectively. The method was then successfully applied to the analysis of the target antibiotics in sludge as well as soil that received spreading. The substances most frequently found and with the highest levels were fluoroquinolones with concentrations exceeding 1,000 ng/g in several samples of sludge and up to 16 ng/g in soil.

1. Introduction

The presence of many organic substances in all compartments of the environment, from our domestic life as well as from agricultural and industrial activities, is now a proven fact [1–4]. Among the compounds that represent a source of concern to the scientific community are veterinary and human antibiotics. Many prescriptions are given to treat bacterial infections in human or animals and antibiotics are also used for growth promotion [5–7]. After their administration, antibiotics are partially metabolized by the body [5, 8] and subsequently excreted and pass through treatment plants where they can appear recalcitrant to treatments [9–11]. These compounds are then present in the effluent or sewage sludge and also in the manure applied to agricultural land. The dissemination of antibiotics into the environment can have adverse effects over time. Indeed, they can induce pathogen resistance [12–14] and be harmful to ecosystems and human health.

According to a report from ANMV (French National Agency of Veterinary Medicine), the total sales volume in France amounted to 782 tons of veterinary antibiotics in 2012 [15]. This is the lowest tonnage recorded since tracking began. However, given the differences of activity of antibiotics and their varied doses, tonnages sold do not accurately reflect the use of antibiotics. Indeed, recent antibiotics are generally more active and require the administration of a lower amount. In human medicine, the quantitative consumption level has increased continuously since 2010, according to ANSM (French National Agency for Medicines Safety and Health Products). Thus, it reaches 32.3 numbers of defined daily doses per 1,000 inhabitants per day.

Two families of antibiotics are especially noteworthy: tetracyclines and fluoroquinolones. Tetracyclines represent almost half the sales of antibiotics for veterinary purpose in France [15]. These molecules have the characteristic of having four linearly annelated six-membered rings with a characteristic arrangement of double bonds (Table 1). They are substituted with more or less hydrophilic groups (hydroxyl, amide, or ketone) which form chelates with the cations (Ca^{2+}, Mg^{2+}) naturally present in the environment [16, 17]. Consequently tetracyclines will tend to complex with di- or trivalent cations present in the soil and thus to be strongly adsorbed on this matrix and therefore not leached. In addition, these molecules have an amphoteric character. Indeed, they have three ionizable sites and can exist in cationic, anionic, or zwitterionic forms. The adsorption

Table 1: Physicochemical properties of selected substances.

Compound	Formula	Log K_{ow}	Water solubility (mg/L)	pK_a
Ciprofloxacine	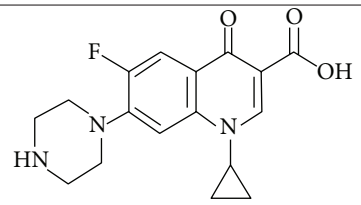	0.28	30000 (20°C)	pK_{a1} = 5.90 pK_{a2} = 8.89
Danofloxacin	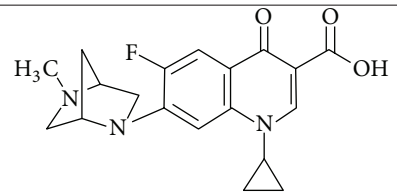	−0.3	172000 (25°C)	pK_{a1} = 6.07 pK_{a2} = 8.56
Difloxacin	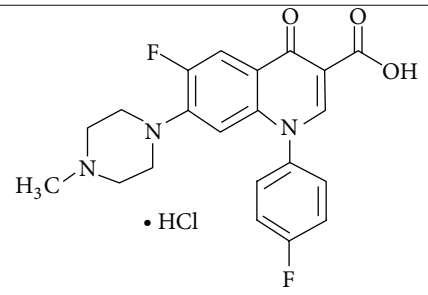	0.89	1330 (25°C)	pK_{a1} = 4.33 pK_{a2} = 9.05
Enrofloxacin	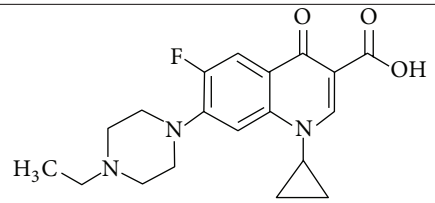	0.70	3400 (25°C)	pK_{a1} = 6.27 pK_{a2} = 8.30
Marbofloxacin	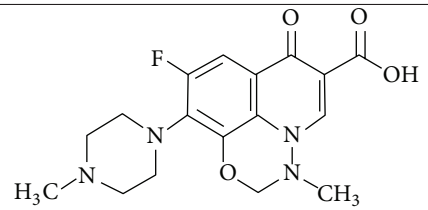	−0.83	7520 (25°C)	pK_{a1} = 5.77 pK_{a2} = 8.22
Norfloxacin	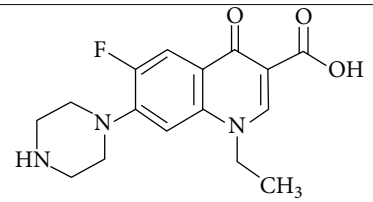	−1.03	178000 (25°C)	pK_{a1} = 6.23 pK_{a2} = 8.55
Ofloxacin	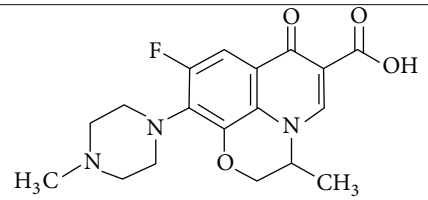	−0.39	28300 (25°C)	pK_{a1} = 5.97 pK_{a2} = 8.28

Table 1: Continued.

Compound	Formula	Log K_{ow}	Water solubility (mg/L)	pK_a
Orbifloxacin	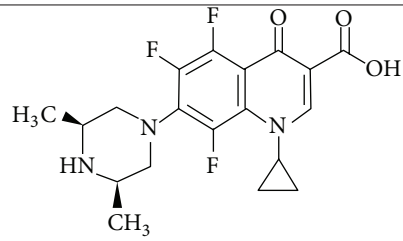	−0.78	909 (25°C)	pK_{a1} = 5.95 pK_{a2} = 9.01
Chlortetracycline	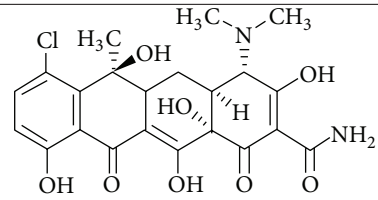	−0.62	630 (25°C)	pK_{a1} = 3.30 pK_{a2} = 7.44 pK_{a3} = 9.27
Doxycycline	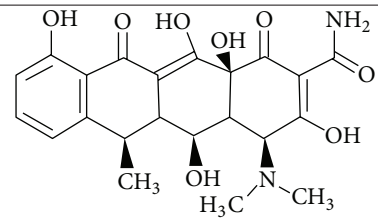	−0.02	630 (25°C)	pK_{a1} = 3.50 pK_{a2} = 7.70 pK_{a3} = 9.50
Oxytetracycline	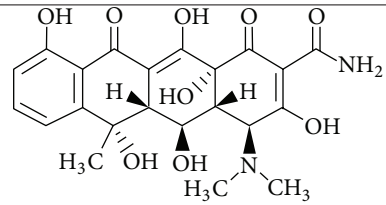	−0.90	313 (25°C)	pK_{a1} = 3.27 pK_{a2} = 7.32 pK_{a3} = 9.11
Tetracycline	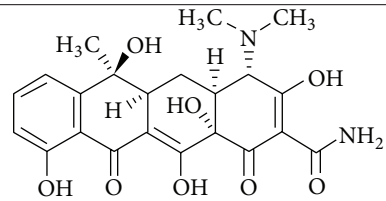	−1.30	231 (25°C)	pK_{a1} = 3.30 pK_{a2} = 7.68 pK_{a3} = 9.30

of tetracyclines on the soil strongly depends on the pH; the cation exchange interaction is also known to be a very important adsorption process [18]. These substances present low log K_{ow} (octanol-water partition coefficient) values as shown in Table 1. Log K_{ow} is currently used to characterize or evaluate the presence of organic micro pollutants in the various phases of the environment. It is a measure of the equilibrium concentration of a compound between octanol and water that indicates the potential for partitioning into soil organic matter.

The volume of sales of fluoroquinolones for veterinary use is lower than tetracyclines (0.6% of total sales). However, total sales of fluoroquinolones tend to increase gradually. It went from 3.3 to 4.9 tonnes between 1999 and 2012 [15]. Of the 14 years of monitoring, the level of exposure of animals to fluoroquinolones has increased by a factor of 2 [15]. Moreover, they are often used in human. Fluoroquinolones have been categorized as being of the highest priority for risk management among antimicrobials in a report of the WHO Advisory Group on Integrated Surveillance of Antimicrobial Resistance [19]. This document emphasizes that fluoroquinolones are the sole or one of the few alternatives to treat serious disease such as severe *Salmonella* and *E. coli* infections. But these antibiotics are known to select for fluoroquinolone-resistant *Salmonella* and *E. coli* in animals.

Quinolones have a bicycle structure with nitrogen at position 1, a carboxylic acid function in position 3, and a carbonyl in position 4 (Table 1). Fluoroquinolones contain, in addition, fluorine in position 7. The presence of fluorine as well as a carboxylic acid functional group imparts a polar character (log K_{ow} between −1.03 and 0.89). As tetracyclines, these substances tend to form stable complexes with di- and trivalent cations (Ca^{2+}, Mg^{2+}, and Al^{3+}). Interactions are also being established between the ion, the oxygen of the ketone in position 4, and the carboxylic acid function (position 3) [20]. Fluoroquinolones will therefore tend to adsorb on

solid matrices. In addition, these compounds have mostly two ionizable functions, the carboxyl group and the nitrogen atom in the ring. Different shapes, cationic, anionic, and zwitterionic, will be present in the medium according to the pH, which will affect their mobility or transfer in soil.

Several methods have already been published to analyze fluoroquinolone and/or tetracycline antibiotics in soil or sludge. Assuredly, the most difficult and time-consuming task for the determination of these substances in solid environmental matrices is the sample preparation, which often combines one or more extraction and purification procedures. Pressurised liquid extraction (PLE) [21–23], ultrasonic-assisted extraction [22, 24, 25], or techniques based on the use of microwaves [22, 24, 26] have been described. An additional purification step is necessary to eliminate residual interfering substances that affect the quality and robustness of the analysis. Solid phase extraction (SPE) appears as the most suitable technic [21, 23–25] since it is fast and efficient and the range of phase available is very wide. Moreover, it requires a low quantity of solvent and presents limited risk of sample contamination.

Few procedures have been dedicated to the quantification of both tetracyclines and fluoroquinolones and, above all, there is lack of method allowing the evaluation of the transfer of these compounds from sludge to soil. Therefore, detection and quantification with few steps and in a reasonable time of these antibiotics are a necessity to evaluate their occurrence and levels in sludge and soil or to estimate the potential of transfer of these compounds from sludge through the environment.

In this paper, we describe the development of a sensitive method capable of determining simultaneously traces of tetracycline and fluoroquinolone antibiotics in sludge and soil. This method is based on PLE extraction, followed by SPE purification and finally an analysis by LC-MS/MS. The method is then successfully applied to the analysis of the target antibiotics in both sludge and soil that received spreading. Our approach was a bit different from what is usual since we have developed the method of extraction from 13 substances to better understand the role of each of the optimization settings. However, once optimal conditions are identified, we have validated and applied the method on real samples only for five substances most likely to be found in the environment.

2. Experimental

2.1. Chemicals and Materials. High purity (>98%) analytical standards were used. Tetracycline, oxytetracycline, chlortetracycline, doxycycline, minocycline, norfloxacin, danofloxacin, enrofloxacin, ofloxacin, ciprofloxacin, marbofloxacin, orbifloxacin, and difloxacin were purchased from Sigma-Aldrich (Saint-Quentin Fallavier, France).

Stock solutions of each standard were prepared at concentrations of 200 mg/L in methanol and were stored at −23°C in amber glass. Working solutions were prepared by the appropriate mixture and dilution of the stock solutions.

Methanol (MeOH), acetonitrile (ACN) (LC-MS grade), dimethylsulfoxide (DMSO), and acetone (HPLC grade) were purchased from Sigma-Aldrich. Pure water was obtained from a MilliQ device from Millipore (Saint-Quentin-en-Yvelines, France). Formic acid (98%, LC-MS grade) and citric acid monohydrate were purchased from Sigma-Aldrich while sodium hydroxide was obtained from Prolabo (Paris, France).

2.2. Solid Samples. For the development and validation of the method, clay-loam soil that was never treated with manure or sludge was used. The soil sample was passed through 3 mm sieve to remove coarse particles. It was subsequently ground in a mortar and passed through 0.63 mm sieve to obtain a homogeneous sample. For the application to real samples, soils were collected in amber glass bottles, at a depth of 10 cm, and then were stored at −23°C before the pretreatment and analysis.

For the development and validation of the method in sludge, digested sludge was used. It was frozen in a previously burnt aluminium tray and then freeze-dried for 48 h. It was finally ground in a mortar and sieved to 0.25 mm. For the application to real samples, sludge measurements were carried out in glass bottles by authorized personnel of each treatment plant, according to the norm NF EN ISO 5667-15 (Oct. 2009) dealing with the conservation and treatment of sludge.

2.3. Extraction and Clean-Up. PLE experiments were performed with the system ASE 350 from Thermo Scientific (Villebon-sur-Yvette, France). 11-mL PLE cell was filled with 5 g of soil or 0.5 g of sludge and completed with diatomaceous earth from Sartorius (Germany).

The extraction procedures were performed at the temperature of 80°C, the pressure of 120 bar, 10 min of static time, and 2 cycles. The composition of the solvent was MeOH, ACN, and 0.2 M citric acid (pH = 4.5) in the proportions 40/40/20. At the end of the two cycles, the extract was supplemented to 500 mL with MilliQ water.

After PLE, the clean-up was performed by SPE using the Thermo Scientific Dionex AutoTrace 280 Instrument with StrataX cartridges (200 mg/3 mL) from Phenomenex (Le Pecq, France). The cartridge was previously conditioned with 5 mL MeOH and then 5 mL H_2O. The volume of 500 mL of reconstituted PLE extract was loaded in the cartridge at the flow rate of 5 mL/min. The cartridge was subsequently washed with 5 mL H_2O and then dried for 15 min under a stream of nitrogen and finally eluted with 6 mL MeOH at the flow rate of 2 mL/min. Then, 100 μL of DMSO was added to the extract before the evaporation of MeOH under a gentle stream of nitrogen at the temperature of 40°C. Finally, 375 μL H_2O and 25 μL ACN were added prior to LC-MS/MS analysis.

2.4. Analysis by Liquid Chromatography-Tandem Mass Spectrometry. The liquid chromatographic separation was performed on an Agilent Series 1100 HPLC system from Agilent Technologies (Les Ulis, France) equipped with a binary pump, a degasser, and a column oven. The separation was performed with a Poroshell 120 EC-C18 (100 × 2.1 mm, 2.7 μm) column from Agilent Technologies preceded by column prefilter KrudKatcher from Phenomenex. The mobile phase was composed of 0.1% formic acid in MilliQ water (A) and 0.1% formic acid in MeOH (B) with the following

Table 2: Precursor and product ions, collision energy (CE), and declustering potential (DP).

Compounds	Precursor ion → product ion (CE (eV))	DP (V)
Tetracycline	445 → 410 (25) and 445 → 154 (35)	36
Oxytetracycline	461 → 426 (25) and 461 → 443 (19)	36
Chlortetracycline	479 → 444 (27) and 479 → 462 (23)	36
Minocycline	479 → 441 (27) and 479 → 352 (23)	36
Doxycycline	445 → 428 (23) and 445 → 154 (41)	41
Ciprofloxacin	332 → 288 (23) and 332 → 231 (49)	51
Enrofloxacin	360 → 316 (25) and 360 → 245 (35)	51
Ofloxacin	362 → 261 (35) and 362 → 318 (23)	51
Norfloxacin	320 → 276 (27) and 320 → 231 (51)	61
Danofloxacin	358 → 340 (27) and 358 → 82 (67)	26
Marbofloxacin	363 → 72 (37) and 363 → 320 (23)	21
Orbifloxacin	396 → 295 (33) and 396 → 352 (23)	31
Difloxacin	400 → 356 (25) and 400 → 299 (35)	41

gradient: 85% (A) for 4 min and from 85% to 0% (A) in 2 min. At the end of the analysis, the column was rinsed by 100% (B) for 5 min. The flow rate was 0.4 mL/min, the oven temperature was 60°C, and the injection volume was 20 μL.

The LC system was coupled to a triple-stage 3200 QTRAP (ABSciex, Les Ulis, France) with an electrospray ion source used in positive mode. The MS/MS settings and the parameters of the source were optimized by manual infusion and by the flow injection of each standard at 10 mg/L. The source parameters were as follows: 5500 V source voltage, 600°C source temperature, nebulisation gas at 45 psi, and desolvation gas at 55 psi (nitrogen). The MS/MS conditions are summarised in Table 2. The analytes were identified both by their chromatographic characteristics and by their specific multiple reaction monitoring (MRM) fragmentation patterns. Data processing was performed with Analyst software (version 1.5.1).

3. Results and Discussion

3.1. Development of the PLE. During the development of the method based on PLE, several parameters had to be optimized such as the temperature, the pressure, the static time, and the number of cycles, as well as the nature of the extraction solvent. The solvent is the parameter that most affects the extraction efficiency. Therefore, the temperature, the pressure, the static time, and the number of cycles were chosen based on literature data and we optimized the extraction solvent.

Some previous studies have been dedicated to the extraction of tetracyclines and fluoroquinolones from soil by PLE. Relatively low temperatures, comprised between room temperature and 100°C, were used to extract tetracyclines, substances sensitive to thermal degradation [27–29]. In addition, the use of an elevated temperature can lead to another limitation: the coextraction of compounds of the matrix that may interfere with the target analytes [29]. Regarding fluoroquinolones, a temperature of 100°C was generally used [8, 30]. We therefore set a temperature of 80°C. A pressure between 100 and 150 bar is often used for these two families of antibiotics [8, 27, 28, 30]. We therefore set the pressure at 120 bar. A 10-minute static time was generally reported [8, 27, 28, 30]; therefore we chose this time. Finally, 2 or 3 cycles were often mentioned in the literature to extract tetracyclines or fluoroquinolones. We chose to run 2 cycles [27, 28].

With these conditions, we attributed great importance to the choice of solvent to optimize the extraction of both tetracyclines and fluoroquinolones. These tests were carried out from 1 g of soil spiked at 500 ng/g with each substance. The sample was then left for 8 hours at room temperature before the extraction, to allow the solvent to evaporate.

The extracts obtained were relatively loaded with organic matter making their direct injection into the LC-MS/MS system difficult. Therefore, purification by SPE was performed using the polymeric StrataX cartridges. In order to evaluate only the recoveries from the PLE during the optimization, we compared the responses of the solids spiked before the extraction and after the PLE extraction but before the purification step.

As preliminary tests, we evaluated the effectiveness of acetone, MeOH, or mixtures acetone/MeOH (50/50), MeOH/H_2O (80/20), and ACN/H_2O (70/30). The extracts obtained were evaporated and dissolved in 1 mL of 95/5 H_2O/MeOH and then injected into LC-MS/MS. The results showed that only mixtures of organic solvent with water allowed the extraction of a minimum of fluoroquinolones.

We therefore continued the optimization with mixtures of more complex solvents, including an aqueous portion. We first chose to evaluate solvents based on citric acid. Indeed, it was demonstrated that fluoroquinolones and tetracyclines easily form strong complexes with di- and trivalent cations contained between the layers of clay or with the hydroxyl groups at the solid particle surface [8, 27]. In addition, cation exchange, hydrophobic reactions, or hydrogen bond formation could also take place [27], making the extraction of these antibiotics difficult. To reduce these interactions, a complexing agent could be added in the extraction solvent. Citric acid could represent a good choice. Moreover, acidic pH could favor electrostatic repulsion between target substances and soil surface, both protonated.

Preliminary experiments dealing with the choice of the solvent described above put in evidence the notion that fluoroquinolones were better extracted with ACN/H_2O (70/30). On the other hand, tetracyclines appeared to be more extracted from the solid matrix with MeOH/H_2O (80/20). We therefore assessed various compositions of solvents containing acetonitrile, methanol, and citric acid. Jacobsen et al. investigated the amount of citric acid to the tetracyclines extraction from soil [27]; they demonstrated that a concentration of 0.2 M in the aqueous portion of the solvent mixture allowed reaching the most interesting recoveries. We therefore chose to introduce 0.2 M citric acid in the aqueous fraction of each of the mixtures and the equivalent of 0.1 M to 50/50 methanol/acetonitrile. Sodium hydroxide was added to adjust the pH values of 3 or 4.5. The recoveries obtained with the various compositions of solvent (MeOH/ACN/0.2 M citric acid) and pH values are presented in Figures 1(a) and 1(b) for tetracyclines and fluoroquinolones, respectively.

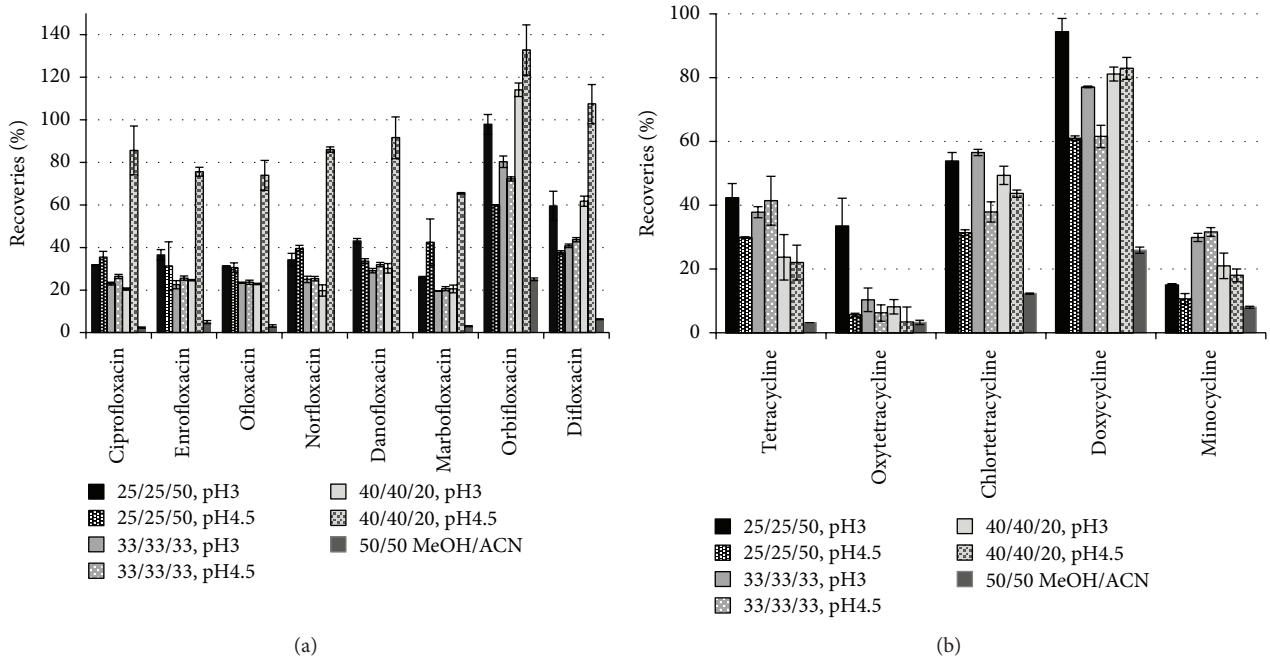

Figure 1: Recoveries obtained for (a) fluoroquinolones and (b) tetracyclines, with various compositions of PLE solvent (MeOH/ACN/0.2 M citric acid) and pH values.

These figures show that the 50/50 mixture of MeOH/ACN containing citric acid very little extracted the target substances. A minimum volume of water was required for extraction of tetracyclines and fluoroquinolones. Moreover, we note that fluoroquinolones were better extracted with the composition 40/40/20 MeOH/ACN/citric acid adjusted to pH = 4.5 (recoveries between 65 and 133%). On the other hand, the extraction of tetracyclines appeared to be less affected by the composition of the solvent and the pH, except in the case of oxytetracycline for which the extraction was favored with the 25/25/50 MeOH/ACN/citric acid composition and the pH = 3. Under these conditions, the choice of the extraction solvent for both families was 40/40/20 MeOH/ACN/citric acid adjusted to pH = 4.5.

3.2. Optimization of the Injection Conditions. In a previous study dealing with the development of a method dedicated to the analyses of pharmaceutical compounds and hormones in sludge by LC-ToF-MS [31], we put in evidence the positive role of DMSO in the response of the target compounds. We showed that DMSO was playing a double role. Firstly, it prevented the complete evaporation of the extract, thereby facilitating the dissolution of the residue in the injection solvent. And secondly, it allowed a significant increase of the ionization of certain substances in the electrospray source in the presence of acidified water.

Therefore, we evaluated the influence of the presence of DMSO on the signal of tetracyclines and fluoroquinolones. Two sets of experiments were conducted: the first one to assess whether DMSO played a role and what was the best proportion in the mixture of solvents and the second one to evaluate the optimal final volume of solvents. For these optimizations, soil was previously spiked at 80 ng/g with each of the target substances and was submitted to the PLE extraction and then the SPE purification as described above. Various volumes of DMSO were added to the extract and MeOH was evaporated under nitrogen. A volume of 50 μL ACN was added and the solvent was made up with water to 1 mL. The response obtained by LC-MS/MS for these various proportions of DMSO is presented in Figure 2. The results indicate that DMSO played a positive role in the response obtained in the case of fluoroquinolones but had no

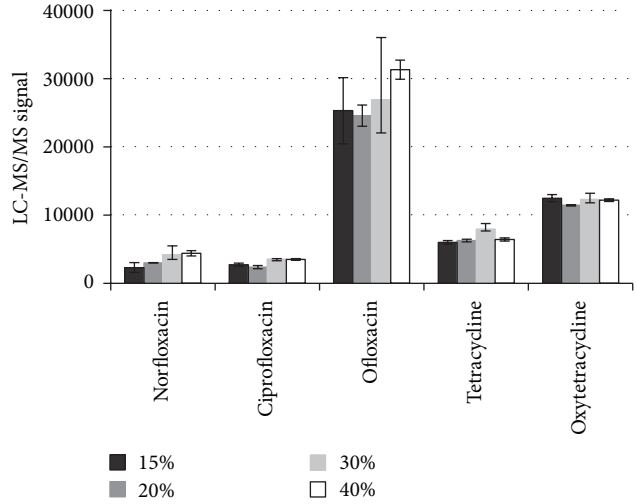

Figure 2: Signal response of some tetracyclines and fluoroquinolones as a function of the percentage of DMSO in 1 mL of extract.

Table 3: Validation parameters: linearity, limits of detection and quantification (MDL and MQL), recoveries (R), and precision (relative standard deviation, RSD) in soil and sludge.

Compounds	Linearity (r^2)		MDL (ng/g)		MQL (ng/g)		R (%)		Intraday precision RSD (%)		Interday precision RSD (%)	
	Soil 1–200 ng/g	Sludge 5–2500 ng/g	Soil	Sludge	Soil	Sludge	Soil	Sludge	Soil	Sludge	Soil	Sludge
Norfloxacin	0.9956	0.9906	0.7	3.8	1.1	12.7	96.6	91.4	1.2	15.0		16.5
Ciprofloxacin	0.9869	0.9911	1.4	6	4.6	20.0	92.6	87.1	1.2	13.1		8.0
Ofloxacin	0.9947	0.9941	0.4	1.5	1.3	5.0	96.9	89.8	7.0	11.0		2.8
Tetracycline	0.9948	0.9917	0.3	2.4	1.9	6.2	38.9	41.7	14.7	1.9		6.7
Oxytetracycline	0.9970	0.9968	0.7	6	2.3	20.0	25.4	33.5	4.7	5.4		15.1

significant effect on the tetracyclines. The best response was generally obtained for a volume of 300 μL. However, the measure was less reproducible with this content than with 200 μL DMSO. Therefore, the following proportions were selected: 20% DMSO, 5% ACN, and 75% H_2O. Second, several total volumes of solvent from 400 μL to 1000 μL were tested with these proportions of DMSO, ACN, and H_2O. The best signal intensities were obtained for a volume of 500 μL. To the best of our knowledge, the influence of DMSO on the MS response of tetracyclines or fluoroquinolones was not evidenced.

Finally, the injection volume was also optimized. The volume could be increased up to 20 μL while maintaining good sharpness of the peaks.

3.3. Performance of the Methods. The validation procedure of the method was carried out using spiked soil or sludge. As it was not possible to find sludge that was free of the target analytes, the sludge samples were previously analyzed and the LC-MS/MS signals corresponding to the target compounds were subtracted. With regard to the soil, analysis of unspiked soil showed that it was free of targeted substances.

The methods were evaluated in terms of linearity, recoveries, and intra- and interday repeatability as well as the limits of detection and quantification.

The linearity was evaluated by assessing the signal response of each compound from spiked samples over a concentration range from 1 to 200 ng/g in soil and from 5 to 2500 ng/g in sludge. The model was evaluated in triplicate on three days. Table 3 indicates that the methods were linear over the specified concentration ranges, in both matrices. The determination coefficients (R^2) were higher than 0.99, except in the case of ciprofloxacin in soil (0.9869).

To evaluate recoveries, the signal obtained for solid samples spiked before the sample preparation ($S_{\text{spiked before}}$) was compared with the signal obtained for solid extract spiked after the sample preparation with MeOH solution containing the target substances at the same concentration ($S_{\text{spiked after}}$), where S_{blank} corresponds to the signal of a nonspiked extract of the sample, according to

$$\text{recovery}\,(\%) = \left(\frac{S_{\text{spiked before}} - S_{\text{blank}}}{S_{\text{spiked after}}}\right) \times 100. \quad (1)$$

Recoveries were different for tetracyclines and fluoroquinolones (Table 3). Indeed, they were greater than 87% in the case of fluoroquinolones but only between 25.4 and 41.7% for tetracyclines. These lower values confirmed the strong interactions that exist between tetracyclines and environmental solid matrices. The difficult extraction of tetracyclines was previously reported by Carvalho et al. [24] that compared the efficiency of vortex agitation, ultrasonic extraction, and microwave assisted extraction but did not obtain recoveries higher than 59% and 42% for tetracycline and oxytetracycline, respectively, in sediment. Similarly, previous methods involving SPE for the extraction did not exceed 27% for the recovery of tetracycline from sludge [21] or 54% for tetracycline and oxytetracycline [23]. Recently, Huang et al. [25] developed a method that allowed recoveries superior to 81% for tetracycline. However, this efficient method was quite complex and time and solvent consuming since it involved extraction overnight by a solvent, then three successive ultrasonic-assisted extraction procedures aided by mechanical shaking, and finally clean-up by solid phase extraction.

Precision was appraised through intra- and interday analyses. It was performed at 80 ng/g and 250 ng/g, in soil and sludge, respectively. It consisted in three replicates conducted on the same day or three different days, respectively, and was expressed as the relative standard deviation (RSD, %). Good intraday precision results were obtained, with RSD values inferior to 15% for all the compounds in both matrices (Table 3).

The limits of detection and quantification of the method (MDL and MQL, resp.) were finally determined. They were defined as the analyte concentration that produced a peak signal of three and ten times the background noise, respectively. The method appeared to be sensitive since MQL values were all inferior to 5 ng/g in soil and inferior to 20 ng/g in sludge (Table 3). These limits were broadly the same order of magnitude as the methods proposed in the literature for the quantification of fluoroquinolones [22, 25, 32]. Only Lillenberg et al. [21] developed a method for their analysis to levels below 2 ng/g in sludge. On the other hand, the limit of quantification of tetracyclines did not fall below 80 ng/g. For the analysis of tetracyclines, the MQL of the developed method are generally lower than or equivalent to those reported in the literature [21–25, 33].

For quantification in sludge or soil, one of the drawbacks is the presence of residual interfering compounds in the

Table 4: Levels (ng/g dry matter) of target tetracyclines and fluoroquinolones measured in sludge and soil that received the corresponding sludge.

Sludge	Sludge 1	Sludge 2	Sludge 3	Sludge 4	Sludge 5	Sludge 6	Sludge 7	Sludge 8	Sludge 9	Sludge 10	Sludge 11	Sludge 12
Norfloxacin	nd	2,055 (157)	nd	937 (41)	132 (8)	74 (3)	nd	130 (5)	84 (7)	1,004 (42)	362 (17)	562 (21)
Ciprofloxacin	nd	3,148 (94)	63 ± (2)	2,786 (115)	251 (11)	55 (2)	nd	356 (15)	123 (5)	379 (16)	576 (28)	755 (33)
Ofloxacin	nd	8,492 (212)	66 ± (3)	2,577 (93)	398 (14)	93 (30)	208 (67)	824 (29)	156 (54)	1,189 (42)	641 (25)	1,152 (39)
Tetracycline	nd	124 (3)	nd	nd	nd	nd	nd	nd	nd	61 (2)	nd	135 (2)
Oxytetracycline	nd	nd	nd	nd	nd	nd	nd	nd	nd	nd	nd	nd
Soil	Soil 1	Soil 2	Soil 3	Soil 4	Soil 5	Soil 6	Soil 7	Soil 8	Soil 9	nd	Soil 11	Soil 12
Norfloxacin	nd	16.5 (0.3)	nd	9.7 (0.2)	nd	nd	nd	nd	nd	3.6 (0.1)	nd	nd
Ciprofloxacin	nd	nd	nd	nd	nd	nd	nd	nd	nd	nd	nd	nd
Ofloxacin	nd	nd	<MQL	nd	<MQL	<MQL	<MQL	1.8 (0.2)	<MQL	1.31 (0.1)	<MQL	<MQL
Tetracycline	nd	nd	nd	nd	nd	nd	nd	nd	nd	nd	nd	6.9 (1.1)
Oxytetracycline	nd	nd	nd	nd	nd	nd	nd	nd	nd	nd	nd	nd

nd: not detected
The analyses were performed in duplicate. The standard deviation appears in parentheses.

extract that causes the suppression or enhancement of the signal in the mass spectrometer. Several strategies can be involved in such complex matrices, in order to compensate these so-called matrix effects. Each of the strategies presents advantages, but also disadvantages. Isotopic-labelled internal standards are often used to compensate the matrix effects. However, it can be difficult to find such substances affordable in the case of tetracyclines. Moreover, because of the difference between the MRM transitions of the target compounds and their respective internal standard, the compensation may not be correct [34]. The matrix-matched calibration can be used if a matrix similar to the matrix to be analyzed and free of the target compounds is available. Finally, the standard addition method is probably the most rigorous since it fits all samples and their different compositions but is also the most time-consuming approach. In the absence of samples free of the contaminants of interest (or blank samples), sludge samples were quantified by addition standards. In case the contents in the sludge exceeded the calibration range, the extracts were diluted accordingly. The soil used in the development and validation of the method was also used to build the calibration by matrix matching.

3.4. Application to Real Samples. The developed method was applied to 12 sludge samples from various sewage treatment plants in France. The results (Table 4) indicated that fluoroquinolone antibiotics were present in all the samples except one, with concentrations up to 8,492 ng/g (dry weight). The substance most frequently found and with the highest levels was ofloxacin, whose average concentration was about 1,400 ng/g. Tetracycline was also quantified in 3 sludge samples with levels comprised between 31 and 135 ng/g.

The sludge from these stations is regularly applied to agricultural soils. The soils that had been amended with these sewage sludge samples were also analyzed. Samples were collected about two months after sludge spreading. The results (Table 4) indicate the presence of fluoroquinolones at low levels in the soil, in all samples except one. Ofloxacin was present in most samples, but its concentration rarely exceeded the limit of quantification (maximum value: 1.8 ng/g). The frequency of detection of norfloxacin was lower than that of ofloxacin, but the levels were slightly higher (between 3.6 and 16.5 ng/g). These results suggest transfer of ofloxacin and norfloxacin from sludge to soil. Tetracycline was present in a single sample. Ciprofloxacin, which was quantified in most sludge samples, was not detected in soils. It should be noted, however, that the MDL of ciprofloxacin was slightly higher than the MDL of ofloxacin and norfloxacin. The absence of detectable ciprofloxacin did not exclude its presence at very low level in soil.

4. Conclusions

A method for the determination of tetracyclines and fluoroquinolones was developed, adapted to both soil and sludge matrices. This method involved extraction by PLE followed by SPE clean-up. The analysis of sludge and soil that received spreading from this sludge indicated relatively high levels of the target compounds in sludge (sometimes exceeding 1000 ng/g in the case of fluoroquinolones) and suggested transfer of certain substances between sludge and soil. The method would therefore be useful to get more information regarding this phenomenon, which is critical to assess the risks associated with the presence of tetracyclines and fluoroquinolones in biosolids.

Conflict of Interests

The authors declare that there is no conflict of interests regarding the publication of this paper.

References

[1] L. Dsikowitzky and J. Schwarzbauer, "Industrial organic contaminants: identification, toxicity and fate in the environment," *Environmental Chemistry Letters*, vol. 12, no. 3, pp. 371–386, 2014.

[2] J. J. Harwood, "Molecular markers for identifying municipal, domestic and agricultural sources of organic matter in natural waters," *Chemosphere*, vol. 95, pp. 3–8, 2014.

[3] M. E. Karpuzcu, D. Fairbairn, W. A. Arnold et al., "Identifying sources of emerging organic contaminants in a mixed use watershed using principal components analysis," *Environmental Sciences: Processes and Impacts*, vol. 16, no. 10, pp. 2390–2399, 2014.

[4] J. Pastor and A. J. Hernández, "Heavy metals, salts and organic residues in old solid urban waste landfills and surface waters in their discharge areas: determinants for restoring their impact," *Journal of Environmental Management*, vol. 95, pp. S42–S49, 2012.

[5] K. Kumar, S. C. Gupta, Y. Chander, and A. K. Singh, "Antibiotic use in agriculture and its impact on the terrestrial environment," *Advances in Agronomy*, vol. 87, pp. 1–54, 2005.

[6] K.-R. Kim, G. Owens, S.-I. Kwon, K.-H. So, D.-B. Lee, and Y. S. Ok, "Occurrence and environmental fate of veterinary antibiotics in the terrestrial environment," *Water, Air, and Soil Pollution*, vol. 214, no. 1–4, pp. 163–174, 2011.

[7] A. K. Sarmah, M. T. Meyer, and A. B. A. Boxall, "A global perspective on the use, sales, exposure pathways, occurrence, fate and effects of veterinary antibiotics (VAs) in the environment," *Chemosphere*, vol. 65, no. 5, pp. 725–759, 2006.

[8] P. Sukul, M. Lamshöft, S. Kusari, S. Zühlke, and M. Spiteller, "Metabolism and excretion kinetics of 14C-labeled and non-labeled difloxacin in pigs after oral administration, and antimicrobial activity of manure containing difloxacin and its metabolites," *Environmental Research*, vol. 109, no. 3, pp. 225–231, 2009.

[9] W. Xu, G. Zhang, X. Li et al., "Occurrence and elimination of antibiotics at four sewage treatment plants in the Pearl River Delta (PRD), South China," *Water Research*, vol. 41, no. 19, pp. 4526–4534, 2007.

[10] J. Du, Y. Fan, and X. Qian, "Occurrence and behavior of pharmaceuticals in sewage treatment plants in eastern China," *Frontiers of Environmental Science & Engineering*, vol. 9, no. 4, pp. 725–730, 2015.

[11] W. Qi, H. Singer, M. Berg et al., "Elimination of polar micropollutants and anthropogenic markers by wastewater treatment in Beijing, China," *Chemosphere*, vol. 119, pp. 1054–1061, 2015.

[12] A. E. Van Den Bogaard and E. E. Stobberingh, "Epidemiology of resistance to antibiotics: links between animals and humans," *International Journal of Antimicrobial Agents*, vol. 14, no. 4, pp. 327–335, 2000.

[13] R. I. Aminov and R. I. Mackie, "Evolution and ecology of antibiotic resistance genes," *FEMS Microbiology Letters*, vol. 271, no. 2, pp. 147–161, 2007.

[14] H. Storteboom, M. Arabi, J. G. Davis, B. Crimi, and A. Pruden, "Identification of antibiotic-resistance-gene molecular signatures suitable as tracers of pristine River, urban, and agricultural sources," *Environmental Science and Technology*, vol. 44, no. 6, pp. 1947–1953, 2010.

[15] A. Chevance and G. Moulin, *Suivi des Ventes de Médicaments Vétérinaires Contenant des Antibiotiques en France en 2010 (Volumes et Estimation de la Consummation d'Antibiotiques chez les Animaux)*, Agence Nationale du Médicament Vétérinaire (ANSES), 2011.

[16] Y. J. Wang, D. A. Jia, R. J. Sun, H. W. Zhu, and D. M. Zhou, "Adsorption and cosorption of tetracycline and copper(II) on montmorillonite as affected by solution pH," *Environmental Science & Technology*, vol. 42, no. 9, pp. 3254–3259, 2008.

[17] P.-H. Chang, Z. Li, J.-S. Jean et al., "Desorption of tetracycline from montmorillonite by aluminum, calcium, and sodium: an indication of intercalation stability," *International Journal of Environmental Science and Technology*, vol. 11, no. 3, pp. 633–644, 2014.

[18] S. A. Sassman and L. S. Lee, "Sorption of three tetracyclines by several soils: assessing the role of pH and cation exchange," *Environmental Science and Technology*, vol. 39, no. 19, pp. 7452–7459, 2005.

[19] WHO, *Criticall Important Antimicrobials for Human Medicine*, 3rd revision, 2011.

[20] Y. Picó and V. Andreu, "Fluoroquinolones in soil-risks and challenges," *Analytical and Bioanalytical Chemistry*, vol. 387, no. 4, pp. 1287–1299, 2007.

[21] M. Lillenberg, S. Yurchenko, K. Kipper et al., "Simultaneous determination of fluoroquinolones, sulfonamides and tetracyclines in sewage sludge by pressurized liquid extraction and liquid chromatography electrospray ionization-mass spectrometry," *Journal of Chromatography A*, vol. 1216, no. 32, pp. 5949–5954, 2009.

[22] N. Dorival-García, A. Zafra-Gómez, F. J. Camino-Sánchez, A. Navalón, and J. L. Vílchez, "Analysis of quinolone antibiotic derivatives in sewage sludge samples by liquid chromatography-tandem mass spectrometry: comparison of the efficiency of three extraction techniques," *Talanta*, vol. 106, pp. 104–118, 2013.

[23] Y. Ding, W. Zhang, C. Gu, I. Xagoraraki, and H. Li, "Determination of pharmaceuticals in biosolids using accelerated solvent extraction and liquid chromatography/tandem mass spectrometry," *Journal of Chromatography A*, vol. 1218, no. 1, pp. 10–16, 2011.

[24] P. N. Carvalho, A. Pirra, M. C. P. Basto, and C. M. R. Almeida, "Multi-family methodologies for the analysis of veterinary pharmaceutical compounds in sediment and sludge samples: comparison among extraction techniques," *Analytical Methods*, vol. 5, no. 22, pp. 6503–6510, 2013.

[25] Y. Huang, M. Cheng, W. Li et al., "Simultaneous extraction of four classes of antibiotics in soil, manure and sewage sludge and analysis by liquid chromatography-tandem mass spectrometry with the isotope-labelled internal standard method," *Analytical Methods*, vol. 5, no. 15, pp. 3721–3731, 2013.

[26] Z. Jiao, Z. N. Guo, S. L. Zhang, and H. W. Chen, "Microwave-assisted micro-solid-phase extraction for analysis of tetracycline antibiotics in environmental samples," *International Journal of Environmental Analytical Chemistry*, vol. 95, no. 1, pp. 82–91, 2015.

[27] A. M. Jacobsen, B. Halling-Sørensen, F. Ingerslev, and S. H. Hansen, "Simultaneous extraction of tetracycline, macrolide and sulfonamide antibiotics from agricultural soils using pressurised liquid extraction, followed by solid-phase extraction and liquid chromatography-tandem mass spectrometry," *Journal of Chromatography A*, vol. 1038, no. 1-2, pp. 157–170, 2004.

[28] M. S. Díaz-Cruz and D. Barceló, "Recent advances in LC-MS residue analysis of veterinary medicines in the terrestrial environment," *TrAC—Trends in Analytical Chemistry*, vol. 26, no. 6, pp. 637–646, 2007.

[29] S. O'Connor and D. S. Aga, "Analysis of tetracycline antibiotics in soil: advances in extraction, clean-up, and quantification," *TrAC Trends in Analytical Chemistry*, vol. 26, no. 6, pp. 456–465, 2007.

[30] E. M. Golet, A. Strehler, A. C. Alder, and W. Giger, "Determination of fluoroquinolone antibacterial agents in sewage sludge and sludge-treated soil using accelerated solvent extraction

followed by solid-phase extraction," *Analytical Chemistry*, vol. 74, no. 21, pp. 5455–5462, 2002.

[31] W. Peysson and E. Vulliet, "Determination of 136 pharmaceuticals and hormones in sewage sludge using quick, easy, cheap, effective, rugged and safe extraction followed by analysis with liquid chromatography-time-of-flight-mass spectrometry," *Journal of Chromatography A*, vol. 1290, pp. 46–61, 2013.

[32] A. Speltini, M. Sturini, F. Maraschi, A. Profumo, and A. Albini, "Analytical methods for the determination of fluoroquinolones in solid environmental matrices," *TrAC Trends in Analytical Chemistry*, vol. 30, no. 8, pp. 1337–1350, 2011.

[33] A. Pamreddy, M. Hidalgo, J. Havel, and V. Salvadó, "Determination of antibiotics (tetracyclines and sulfonamides) in biosolids by pressurized liquid extraction and liquid chromatography–tandem mass spectrometry," *Journal of Chromatography A*, vol. 1298, pp. 68–75, 2013.

[34] C. vom Eyser, K. Palmu, R. Otterpohl, T. C. Schmidt, and J. Tuerk, "Determination of pharmaceuticals in sewage sludge and biochar from hydrothermal carbonization using different quantification approaches and matrix effect studies," *Analytical and Bioanalytical Chemistry*, vol. 407, no. 3, pp. 821–830, 2015.

Hindawi Publishing Corporation
Applied and Environmental Soil Science
Volume 2015, Article ID 253729, 8 pages
http://dx.doi.org/10.1155/2015/253729

Research Article

Aggregate Indices Method in Soil Quality Evaluation Using the Relative Soil Quality Index

Ho Ngoc Pham,[1] Hai Xuan Nguyen,[1] Anh Ngoc Nguyen,[2] and Diep Ngoc Tran[1]

[1]*Research Centre for Environmental Monitoring and Modeling (CEMM), VNU University of Science, 334 Nguyen Trai Street, Thanh Xuan District, Hanoi 120000, Vietnam*
[2]*Faculty of Geography, Hanoi National University of Education, 136 Xuan Thuy Street, Cau Giay District, Hanoi 122000, Vietnam*

Correspondence should be addressed to Ho Ngoc Pham; hopn2008@yahoo.com.vn

Received 21 September 2015; Revised 25 October 2015; Accepted 2 November 2015

Academic Editor: Victor Kavvadias

Copyright © 2015 Ho Ngoc Pham et al. This is an open access article distributed under the Creative Commons Attribution License, which permits unrestricted use, distribution, and reproduction in any medium, provided the original work is properly cited.

This paper presents a new approach to assess the soil quality by aggregate indices using the Relative Soil Quality Index (RSQI) proposed by Ho Ngoc Pham. RSQI is integrated from the individual indices into a simple formula for overall assessment of the soil quality. RSQI is different from other approaches. Particularly, the individual indices and the weighting factors of Pham are calculated from the analytical laboratory data and the environmental standards, respectively, and not self-regulated as in methods of some other authors. In this paper, the authors applied the RSQI to assess the Soil Environmental Quality of rice intensive cultivation areas through a case study in Haiduong province in 2013. The RSQI is calculated for sampling points in 12 districts and simulated the Soil Environmental Quality on GIS map. The results show that the Soil Environmental Quality of rice intensive cultivation areas in Haiduong is predominantly divided into three levels: good, moderate, and poor. According to the report of General Statistics Office for Haiduong province, rice intensive cultivation areas in 2013 achieved a relatively high average rice yield of 5.90 tonnes per hectare; it means actual soil properties are in line with results of the research.

1. Introduction

The assessment of soil degradation in the world is primarily based on single criteria to build the assessment thresholds for each group of total content of bioelements, content of available forms of bioelements, heavy metals, and so forth, in which each parameter in the group of total content of bioelements and the group of content of available forms of bioelements is categorized into three levels: high, medium, and low or rich, moderate, and poor, respectively, to serve for the degradation assessment of agricultural land and forestry. The environmental quality index (EQI) approach to assess air, water, and soil was first mentioned in the work of Ott [1], and afterwards, the application of EQI to assess the soil quality (SQ) is continuously developed and widely used [2–7].

The soil degradation assessment in Vietnam has interested many scientists. Vietnamese scientists have made in-depth studies on the thresholds and the assessing scale for the group of total content of bioelements, content of available forms of bioelements and heavy metals, and so forth. In which, typical studies are of Nguyen [8], Le [9], Tran [10], Nguyen [11], Le and Tran [12], and the National Technical Standards on the soil environment for the heavy metals group [13]. However, the approach to assess soil degradation by aggregate indices in Vietnam is still new. Such approach was first mentioned in the dissertation of Nguyen in order to create an environmental land map at the provincial scale [14]. The author applied the Total Soil Quality Index (TSQI) proposed by Pham [15] to determine the Soil Environmental Quality for agricultural land (rice cultivated areas). Nevertheless, calculating the weighting factors of each group is complicated. Therefore, Pham developed the TSQI into the Relative Soil Quality Index (RSQI) which simplifies the calculation of the weighting factors of total content of bioelements, content of available forms of bioelements, pH_{KCl}, and heavy metals group in reality [16]. Because of the paper's scope, the authors

only apply RSQI into aggregate assessment of the SQ of rice intensive areas in Haiduong province.

2. Materials and Method

2.1. Materials. (i) The research used the soil sample analysis data for 12 districts with rice intensive cultivation areas in Haiduong province [17].

(ii) Research materials of Vietnamese authors [8–12] and Vietnam's environmental regulations [13] were used to convert the categorized scale of individual index into the individual assessing scale of SQ which served for the calculation of the SQ assessment by aggregate indices, using RSQI.

2.2. Method

2.2.1. Formula of Relative Soil Quality Index (RSQI). RSQI is a new approach to assess the SQ by aggregate indices. It is based on the synthesis or integration of individual index q_i of n surveyed parameters in order to form a formula which simplifies the SQ assessment at each monitoring point. RSQI proposed by Pham is determined by the following formula [16]:

$$\text{RSQI} = 100\left(1 - \frac{P_k}{P_n}\right), \tag{1}$$

where

$$P_k = \sum_{i=1}^{k} W_i\left(q_i - 1\right), \tag{2}$$

$$P_m = \sum_{i=1}^{m_1} W_i q_i + \sum_{i=1}^{m_2} W_i\left(1 - q_i\right), \tag{3}$$

$$P_n = P_m + P_k, \tag{4}$$

$$n = m + k = m_1 + m_2 + k, \tag{5}$$

where P_n is the common sum (sum of separate sums P_k and P_m); P_m includes m of numbers of q_i with values ≤1; P_k includes k of numbers of q_i with values >1; n is the number of monitored parameters.

Noting. Formula (1) clearly shows that RSQI depends on the relative ratio P_k/P_n. The higher the value of the ratio is, the smaller the value of RSQI will be. Thus, the SQ is poorer.

(i) Calculating Individual Index q_i (Subindex) of Each Parameter i. To calculate RSQI in formula (1), we first need to calculate individual index as the following:

(a) The groups below in Vietnam's environmental regulation (to the heavy metals group) are

$$q_i = \frac{C_i}{C_i^*}. \tag{6}$$

There are three cases:

$$\begin{aligned}&\text{Case 1: If } C_i < C_i^* \text{ so } q_i < 1\\ &\left(\text{Soil with good quality—nondegraded soil}\right),\\ &\text{Case 2: If } C_i = C_i^* \text{ so } q_i = 1\\ &\left(\text{Soil with moderate quality—soil starting to degrade}\right),\\ &\text{Case 3: If } C_i > C_i^* \text{ so } q_i > 1\\ &\left(\text{Soil with poor quality—degraded soil}\right).\end{aligned} \tag{7}$$

(b) The groups in the interval $[a, b]$ in Vietnam's environmental regulation (group of total content of bioelements, group of content of available forms of bioelements):

$$\begin{aligned}&\text{Case 1: If } C_i < a \text{ so } q_i = \frac{a}{C_i} > 1\\ &\left(\text{Soil with poor quality—degraded soil}\right),\end{aligned} \tag{8}$$

$$\begin{aligned}&\text{Case 2: If } a \le C_i \le b \text{ so } q_i = \frac{C_i}{C_i^*} = 1\\ &\left(\text{Soil with moderate quality—soil starting to degrade}\right),\end{aligned} \tag{9}$$

$$\begin{aligned}&\text{Case 3: If } C_i > b \text{ so } q_i = \frac{b}{C_i} < 1\\ &\left(\text{Soil with good quality—nondegraded soil}\right).\end{aligned} \tag{10}$$

(ii) Calculating the Separate Sums P_k, P_m, and the Common Sum P_n Using Formulas (2) to (4). From (1) to (10),

C_i is the actual monitoring value of parameter i,

C_i^*, a, and b are the permitted limit values of parameter i,

m_1 is the number of parameters with $q_i = 1$ (as $C_i = C_i^*$),

m_2 is the number of parameters with $q_i < 1$,

k is the number of parameters with $q_i > 1$.

2.2.2. Calculating the Temporary Weighting Factors W_i' and the Final Weighting Factors W_i. W_i is the final weighting factors of the parameter i; W_i accounts for the importance which presents the relation between each parameter i; and j is the number of parameters of each examination group. The final weighting factor W_i is determined through the temporary weighting factor W_i' as follows.

(a) Groups Below in Environmental Regulation (Heavy Metals Group). W_i' is calculated by formula:

$$W_i' = \frac{(1/j)\sum_1^j C_i^*}{C_i^*} = \frac{\sum_1^j C_i^*}{j \times C_i^*}, \tag{11}$$

where C_i^* is allowance limited value of parameter i and j is the number of parameters selected by the group for examination.

(b) Groups in the Interval $[a, b]$ *in Environmental Regulations (Group of the Total Content of Bioelements, Group of the Content of Available Forms of Bioelements).* Consider parameter groups in the intervals: $[a_1, b_1], [a_2, b_2], [a_3, b_3], \ldots, [a_j, b_j]$.

The formula to calculate W_i' of parameter i for each group is as below:

$$W_i' = \frac{\sum_{i=1}^{j} (b_i - a_i)}{j \times (b_i - a_i)}, \tag{12}$$

where the environmental regulation value of parameter i in the interval $[a_i, b_i]$ is $(b_i - a_i)$ and j is the number of parameters of each group.

Example. There are 2 parameters ($j = 2$) given in $[a_1, b_1]$, $[a_2, b_2]$. The environmental regulation values of $[a_1, b_1]$ and $[a_2, b_2]$ are $(b_1 - a_1)$ and $(b_2 - a_2)$, respectively. According to (12), we calculate

$$W_1' = \frac{(b_1 - a_1) + (b_2 - a_2)}{2 \times (b_1 - a_1)};$$
$$W_2' = \frac{(b_1 - a_1) + (b_2 - a_2)}{2 \times (b_2 - a_2)}. \tag{13}$$

(c) Calculate the Final Weighting Factor of Parameter i (W_i). The final weighting factor of each parameter i of each group is identified by the following formula:

$$W_i = \frac{W_i'}{\sum_1^j W_i'} \tag{14}$$

$$\text{Obviously, } \sum_1^j W_i = 1, \tag{15}$$

where j is the number of parameters selected by the group for examination.

2.2.3. Hierarchy for Assessing SQ of RSQI Index [16]. See Table 1.

2.2.4. Converting Hierarchy for Assessing Criterion to Hierarchy for Assessing SQ. To apply (7)–(10) formulas, first, levels and hierarchy for assessing criterion need to be converted to levels and hierarchy for assessing soil quality (SQ) for each individual criterion.

The conversion Tables 2, 3, and 4 are based on the application of Vietnam research materials about criterion for assessing soil groups.

3. Results and Discussion

3.1. Results

3.1.1. Hierarchy for Assessing SQ of RSQI. The hierarchical scale for aggregate assessing soil quality of RSQI corresponding to $n = 10$ parameters in Table 1 is shown in Table 5.

3.1.2. Calculating the Temporary Weighting Factors W_i' *and the Final Weighting Factors* W_i. (i) Calculating the Temporary Weighting Factors W_i' is as follows:

The group of heavy metals (formula (11)):

$$W_{\text{Cd}}' = \frac{2 + 50 + 70}{3 \times 2} = 20.33;$$
$$W_{\text{Cu}}' = \frac{2 + 50 + 70}{3 \times 50} = 0.81; \tag{16}$$
$$W_{\text{Pb}}' = \frac{2 + 50 + 70}{3 \times 70} = 0.58.$$

The group of the total content of bioelements (formula (12)):

$$W_{\text{OM}}' = \frac{(2.5 - 1.25) + (0.2 - 0.1) + (0.1 - 0.06) + (2 - 1)}{4 \times (2.5 - 1.25)}$$
$$= \frac{2.39}{5} = 0.48;$$
$$W_{\text{N}_t}' = \frac{2.39}{4 \times (0.2 - 0.1)} = 5.98; \tag{17}$$
$$W_{\text{P}_2\text{O}_{5t}}' = \frac{2.39}{4 \times (0.1 - 0.06)} = 14.94;$$
$$W_{\text{K}_2\text{O}_t}' = \frac{2.39}{4 \times (2 - 1)} = 0.60.$$

The group of the content of available forms of bioelements (formula (12)):

$$W_{\text{N}_{\text{av}}}' = \frac{(8 - 2) + (4.6 - 3.6) + (15 - 10)}{3 \times (8 - 2)} = \frac{12}{18}$$
$$= 0.67;$$
$$W_{\text{P}_2\text{O}_{5\text{av}}}' = \frac{12}{3 \times (4.6 - 3.6)} = 4; \tag{18}$$
$$W_{\text{K}_2\text{O}_{\text{av}}}' = \frac{12}{3 \times (15 - 10)} = 0.8.$$

(ii) Calculating the Final Weighting Factors W_i (formula (14)) is as follows:

$$W_{\text{Cd}} = \frac{20.33}{20.33 + 0.81 + 0.58} = \frac{20.33}{21.72} = 0.93;$$
$$W_{\text{Cu}} = \frac{0.81}{21.72} = 0.04; \tag{19}$$
$$W_{\text{Pb}} = \frac{0.58}{21.72} = 0.03.$$

The final weighting factors of other parameters of total content of bioelements group and content of available forms of bioelements group are calculated, respectively, and results are shown in Table 6.

Table 1: Hierarchy for assessing SQ of RSQI = I index.

$I-n$ is even	$I-n$ is odd	SQ	Colour
$50\frac{2n-1}{n} < I \le 100$	$50\frac{2n-1}{n} < I \le 100$	Good/excellent ($I = 100$) (no degradation)	Green
$100\frac{n-1}{n} < I \le 50\frac{2n-1}{n}$	$100\frac{n-1}{n} < I \le 50\frac{2n-1}{n}$	Moderate (start degradation)	Yellow
$50 < I \le 100\frac{n-1}{n}$	$50\frac{n-1}{n} < I \le 100\frac{n-1}{n}$	Poor (degradation)	Orange
$\frac{100}{n} < I \le 50$	$\frac{100}{n} < I \le 50\frac{n-1}{n}$	Very poor (strong degradation)	Red
$0 \le I \le \frac{100}{n}$	$0 \le I \le \frac{100}{n}$	Hazardous (very strong degradation)	Brown

Note.
(i) When $n = 2$, the levels poor, very poor, and hazardous are overlapped; therefore the hierarchy will consist of only 3 levels; when $n = 3$, the levels very poor and hazardous are overlapped; therefore the hierarchy will consist of 4 levels.
(ii) When $W_i = 1$ in (2) and (3) formulas, RSQI does not have weighting factors.
(iii) Suggestions are the following:
(a) Good/excellent SQ does not need treatment.
(b) Moderate SQ needs to be monitored.
(c) Poor SQ needs to be properly fertilized.
(d) Very poor: hazardous SQ needs appropriate technological treatment for parameters significantly greater than acceptable standard.

Table 2: Converting hierarchy for assessing criterion to hierarchy for assessing SQ for the group of total content of bioelements.

Parameter	Criterion (%)	Hierarchy	Reference	Hierarchy for SQ $\in [a, b]$ (%)	SQ
SOM	>2.5	High	Nguyen [8]	>2.5	Good
	1.25–2.5	Medium		1.25–2.5	Moderate
	<1.25	Low		<1.25	Poor
Total N	>0.2	Rich	Nguyen [11]	>0.2	Good
	0.1–0.2	Moderate		0.1–0.2	Moderate
	<0.1	Poor		<0.1	Poor
Total P	>0.1	Rich	Le [9]	>0.1	Good
	0.06–0.1	Moderate		0.06–0.1	Moderate
	<0.06	Poor		<0.06	Poor
Total K	>2	Rich	Tran [10]	>2	Good
	1-2	Moderate		1-2	Moderate
	<1	Poor		<1	Poor

3.1.3. Calculating q_i, P_{m1}, P_{m2}, P_k, P_n, and RSQI. Based on the research materials mentioned in Section 2.1, this research calculated individual parameter q_i using formulas (7)–(10), calculated P_k and P_n using formulas (2)–(4), and calculated the RSQI index using formula (1) for soil samples.

Because of the large sample size of the rice intensive cultivation areas surveyed in Haiduong including relatively high, medium, and low plains, we present how to calculate individual index q_i, the separate sums P_{m1}, P_{m2}, and P_k, and the common sum P_n ($n = 10$ parameters) in order to determine the RSQI of a particular soil sample S1 (Table 7). Thus, only result of other samples is shown in Table 8:

$$\begin{aligned}
P_{m_1} &= \sum_{i=1}^{3} W_i q_i = 0.02 \times 1 + 0.27 \times 1 + 0.12 \times 1 \\
&= 0.41; \\
P_{m_2} &= \sum_{i=1}^{5} W_i \left(1 - q_i\right) \\
&= 0.93 \times (1 - 0.01) + 0.04 \times (1 - 0.19) + 0.03 \\
&\quad \times (1 - 0.26) + 0.68 \times (1 - 0.6) + 0.73 \\
&\quad \times (1 - 0.3) = 1.76; \\
P_m &= P_{m_1} + P_{m_2} = 0.41 + 1.76 = 2.17; \\
P_k &= \sum_{i=1}^{2} W_i \left(q_i - 1\right) \\
&= 0.03 \times (1.64 - 1) + 0.15 \times (2.5 - 1) = 0.24; \\
P_n &= P_m + P_k = 2.17 + 0.24 = 2.41; \\
\text{RSQI} &= 100 \times \left(1 - \frac{P_k}{P_n}\right) = 100 \times \left(1 - \frac{0.24}{2.41}\right) \\
&= 90.04\text{—Moderate } \left(\text{according to Table 5}\right).
\end{aligned} \tag{20}$$

Table 3: Converting hierarchy for assessing criterion to hierarchy for assessing SQ for the group of content of available forms of bioelements.

Parameter	Criterion ($mg{\cdot}kg^{-1}$)	Hierarchy	Reference	Hierarchy for SQ $\in [a, b]$ ($mg{\cdot}kg^{-1}$)	SQ
N bioavailable	>80	Rich	Le and Tran [12]	>80	Good
	20–80	Moderate		20–80	Moderate
	<20	Poor		<20	Poor
P bioavailable	>46	Rich	Nguyen [11]	>46	Good
	36–46	Moderate		36–46	Moderate
	<36	Poor		<36	Poor
K bioavailable	>150	Rich	Tran [10]	>150	Good
	100–150	Moderate		100–150	Moderate
	<100	Poor		<100	Poor

Table 4: Converting hierarchy for assessing criterion to hierarchy for assessing SQ for heavy metals ($mg{\cdot}kg^{-1}$, top soil).

Parameter	Land for agricultural purpose, reference (QCVN 03:2008/BTNMT) [9]	Hierarchy for SQ	SQ
(1) Cadmium (Cd)	2	<2	Good
		=2	Moderate
		>2	Poor
(2) Copper (Cu)	50	<50	Good
		=50	Moderate
		>50	Poor
(3) Lead (Pb)	70	<70	Good
		=70	Moderate
		>70	Poor

Table 5: Hierarchy for assessing SQ of RSQI = I with $n = 10$ parameters (Cd, Cu, Pb, SOM, N_t, P_t, K_t, N_{av}, P_{av}, and K_{av}).

RSQI	SQ	Colour
96–100	Good/excellent ($I = 100$) (no degradation)	Green
91–95	Moderate (start degradation)	Yellow
51–90	Poor (degradation)	Orange
11–50	Very poor (strong degradation)	Red
0–10	Hazardous (very strong degradation)	Brown

3.1.4. Creating the Soil Environmental Quality Map. From the Table 8, GIS technology with the spatial interpolation is applied to develop a simulated map of the SEQ assessment at the research area (Figure 1).

3.2. Discussion. (i) From Table 8, the SQ of rice intensive cultivation areas in Haiduong is good (nondegraded soil), moderate (soil starting degradation), and poor (degraded).

(ii) From the SQ map (Figure 1), incorporation with digital land use map (Haiduong DoNRE, 2013 [18]) will calculate the area of rice intensive cultivation for 12 districts in hectare that consists of 3 groups: good (nondegraded), moderate (starting degradation), and poor (degradation) Soil Environmental Quality. Particularly, the nondegraded area of the province is 25,106.85 ha (36.29%), the area which starts to degrade is 28,821.69 ha (41.66%), and the degraded area is 15,254.33 ha (22.05%). To districts in the provinces with the moderate and poor soil quality, the soil with moderate and poor quality needs to be monitored and fertilized properly.

(iii) According to the General Statistics Office (2013) [19], rice intensive cultivation areas in Haiduong province 2013 reached a relatively high average yield of 5.90 tonnes/ha. Because the RSQI approach shows results of the soil with good quality (nondegraded), the soil with moderate quality (start degraded), and the soil with poor quality (degraded), in which the degraded soil area accounts for only 22.05%, the soil quality of rice intensive cultivation areas is considered fairly good. Therefore, results of the research are in line with the relatively high yield in reality.

4. Conclusion

The research used the soil sample analysis data for twelve districts in Haiduong province to calculate individual indices for 10 parameters. The selected basic parameters are Cd, Cu, and Pb; P_t, SOM, N_t, and K_t; N_{av}, P_{av}, and K_{av}. The separate sum P_m is integrated from parameters group with $q_i \leq 1$ whereas the separate sum P_k is integrated from parameters group with $q_i > 1$. The common sum P_n equals P_m plus P_k. Using these sums, we calculated the RSQI values for 36 soil samples (16 samples in relatively high plains; 7 samples in medium plains; and 13 samples in low plains).

The results of calculations show that the soil sample with good quality ($q_i < 1$) accounts for $14/36 = 38.88\%$; the proportions of soil sample with medium quality ($q_i = 1$) and poor quality ($q_i > 1$) are equal; both of them account for $11/36 = 30.56\%$.

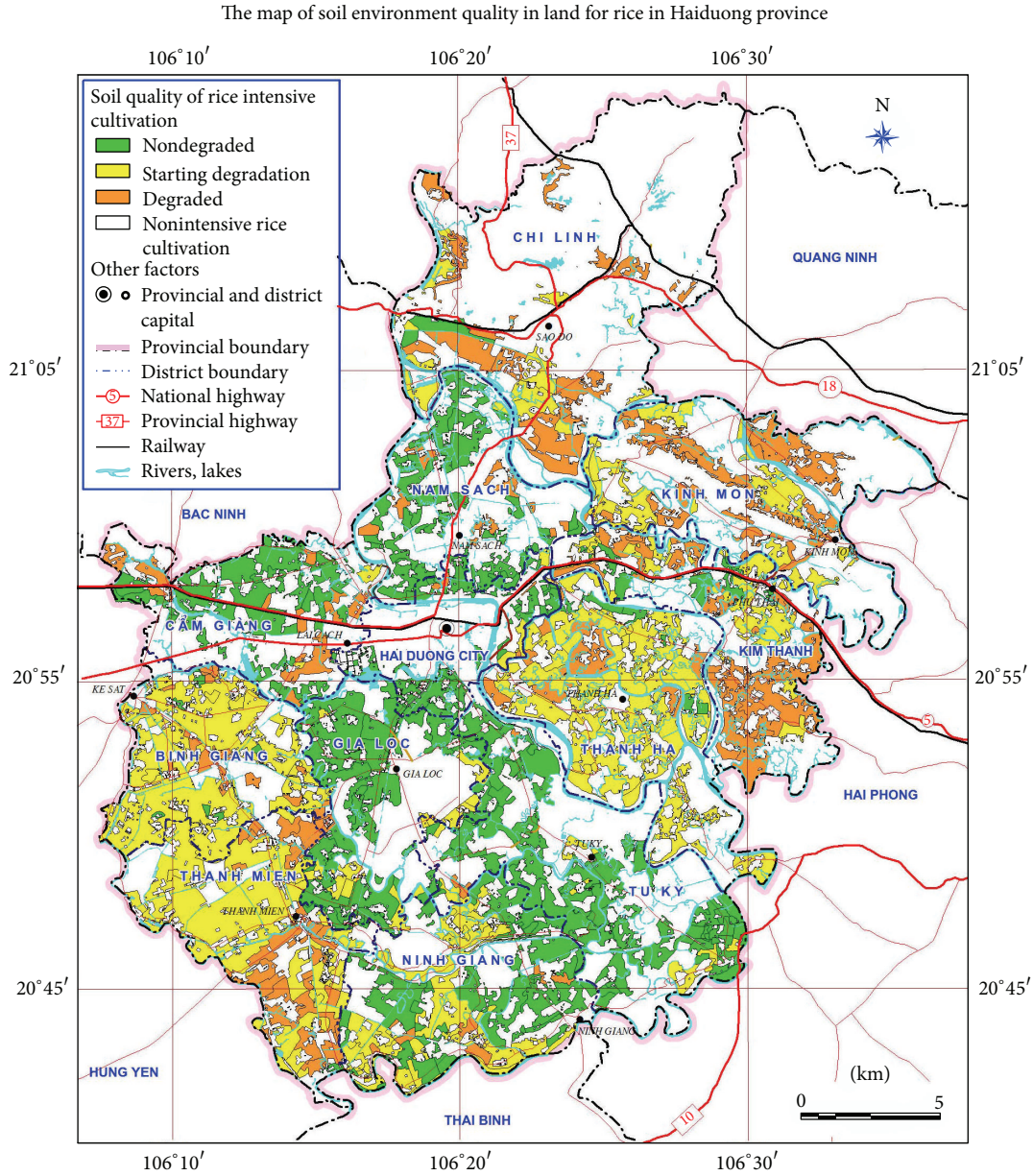

FIGURE 1: The SEQ map of rice intensive cultivation areas in Haiduong province in 2013 developed from the aggregate SQ assessment approach by using RSQI. (The map is scaled from a map with the scale of 1 : 100,000.)

TABLE 6: The temporary weighting factors W_i' and the final weighting factors W_i of 10 surveyed parameters.

Parameters	Heavy metals			Total content of bioelements				Content of available forms of bioelements		
	Cd	Cu	Pb	P_t	SOM	N_t	K_t	N_{av}	P_{av}	K_{av}
i	1	2	3	4	5	6	7	8	9	10
W_i'	20.33	0.81	0.58	14.94	0.48	5.98	0.60	0.67	4	0.80
W_i	0.93	0.04	0.03	0.68	0.02	0.27	0.03	0.12	0.73	0.15
$\sum W_i$		1				1			1	

Table 7: Calculating RSQI for a particular soil sample S1 with C_i, monitoring values.

Parameters	Heavy metals			Total content of bioelements				Content of available forms of bioelements		
	Cd	Cu	Pb	P_t	SOM	N_t	K_t	N_{av}	P_{av}	K_{av}
i	1	2	3	4	5	6	7	8	9	10
S1-C_i	0.01	9.55	18.58	0.17	1.64	0.18	0.61	61.60	155.60	40
q_i	0.01	0.19	0.26	0.60	1	1	1.64	1	0.30	2.50
W_i	0.93	0.04	0.03	0.68	0.02	0.27	0.03	0.12	0.73	0.15

Table 8: Results of calculation of RSQI based on monitoring data.

Soil samples	P_m	P_k	P_n	RSQI	SQ
(a) Relatively high plains					
S1	2.17	0.24	2.41	90.04	Moderate (starting degradation)
S3	1.93	0	1.93	100	Excellent (nondegraded)
S5	2.02	0.03	2.05	98.54	Good (nondegraded)
S7	2.03	0.12	2.15	94.42	Moderate (starting degradation)
S9	1.73	0.08	1.81	95.58	Good (nondegraded)
S11	2.30	0.16	2.46	93.50	Moderate (starting degradation)
S13	2.24	0.17	2.41	92.95	Moderate (starting degradation)
S15	2.01	0.23	2.24	89.73	Poor (degradation)
S17	1.94	0.15	2.09	92.82	Moderate (starting degradation)
S19	2.11	0.21	2.32	90.95	Moderate (starting degradation)
S21	1.95	0.22	2.17	89.86	Poor (degradation)
S23	2.05	0.20	2.25	91.11	Moderate (starting degradation)
S25	2.40	0.15	2.55	94.12	Moderate (starting degradation)
S27	2.21	0.09	2.30	96.09	Good (nondegraded)
S29	2.26	0.07	2.33	96.99	Good (nondegraded)
S31	2	0.66	2.66	75.19	Poor (degradation)
(b) Medium plains					
S57	1.82	0.22	2.04	89.22	Poor (degradation)
S59	1.72	0.08	1.80	95.56	Good (nondegraded)
S61	2.09	0.07	2.16	96.76	Good (nondegraded)
S63	2.04	0.45	2.49	81.93	Poor (degradation)
S65	2.03	0.40	2.43	83.54	Poor (degradation)
S67	2.32	0	2.32	100	Excellent (nondegraded)
S69	2.42	0	2.42	100	Excellent (nondegraded)
(c) Low plains					
S73	2.26	0.27	2.53	89.33	Poor (degradation)
S75	2.22	0.37	2.59	85.71	Poor (degradation)
S77	2.25	0.07	2.32	96.98	Good (nondegraded)
S79	1.64	0.03	1.67	98.20	Good (nondegraded)
S81	1.30	0.01	1.31	99.24	Good (nondegraded)
S83	2.04	0.37	2.41	84.65	Poor (degradation)
S85	2.33	0.16	2.49	93.57	Moderate (starting degradation)
S87	2.08	0.35	2.43	85.60	Poor (degradation)
S89	1.70	0.28	1.98	85.86	Poor (degradation)
S91	1.91	0.09	2.00	95.50	Good (nondegraded)
S93	1.93	0.14	2.07	93.24	Moderate (starting degradation)
S95	2.24	0.21	2.45	91.43	Moderate (starting degradation)
S97	2.12	0.11	2.23	95.07	Good (nondegraded)

Based on the hierarchical scale of soil quality of RSQI, the soil quality of rice intensive cultivation areas in Haiduong is predominantly divided into three levels: good (nondegraded soil), moderate (soil starting degradation), and poor (degraded soil), corresponding to 3 levels which were assessed by individual index.

The RSQI values are simulated on digital land use map by GIS technology. Each area has the same level described by the same colour on the map. Based on this map, calculating the area of each level (good, moderate, and poor) in hectare, the nondegraded area of the province is 25,106.85 ha (36.29%), the area which starts to degrade is 28,821.69 ha (41.66%), and the degraded area is 15,254.33 ha (22.05%). The map which is developed from the aggregate SQ assessment approach by using RSQI provides local managers an overview of the level of soil degradation before promptly taking appropriate measures to prevent or reduce pollution.

In summary, our results are consistent with the reality. Therefore, the calculation method using individual indices q_i and the aggregate index RSQI has a scientific basis and high accuracy; the method could be applied in warning service and environmental management at the provincial scale.

Disclosure

The content of this paper is one of the results of theses at level VNU, code QMT.12.01.

Conflict of Interests

The authors declare that there is no conflict of interests regarding the publication of this paper.

Acknowledgments

The authors hereby express sincere thanks to the Ministry of Natural Resources and Environment and Vietnam National University for funding the subject.

References

[1] W. R. Ott, *Environmental Indices—Theory and Practice*, Ann Arbor Science Publishers, New York, NY, USA, 1978.

[2] M. C. Amacher, K. P. O'Neil, and C. H. Perry, "Soil vital signs: a new Soil Quality Index (SQI) for assessing forest soil health," Research Paper RMRS-RP-65WWW, U.S. Department of Agriculture, Forest Service, Rocky Mountain Research Station, Fort Collins, Colo, USA, 2007.

[3] J. W. Doran and T. B. Parkin, "Quantitative indicators of soil quality: a minimum data set," in *Methods for Assessing Soil Quality*, J. W. Doran and A. J. Jones, Eds., Soil Science Society of America Special Publication no. 49, pp. 25–37, Soil Science Society of America, Madison, Wis, USA, 1996.

[4] T. Nakajima, R. Lal, and S. Jiang, "Soil quality index of a crosby silt loam in central Ohio," *Soil and Tillage Research B*, vol. 146, pp. 323–328, 2015.

[5] S. Kalu, M. Koirala, U. R. Khadka, and K. C. Anup, "Soil quality assessment for different land use in the Panchase area of Western Nepal," *International Journal of Environmental Protection*, vol. 5, no. 1, pp. 38–43, 2015.

[6] A. Morugán-Coronado, V. Arcenegui, F. García-Orenes, J. Mataix-Solera, and J. Mataix-Beneyto, "Application of soil quality indices to assess the status of agricultural soils irrigated with treated wastewaters," *Solid Earth*, vol. 4, no. 1, pp. 119–127, 2013.

[7] T. Paz-Kagan, M. Shachak, E. Zaady, and A. Karnieli, "A spectral soil quality index (SSQI) for characterizing soil function in areas of changed land use," *Geoderma*, vol. 230-231, pp. 171–184, 2014.

[8] M. Nguyen, *Practice of Soil Science*, Agriculture Publisher, Hanoi, Vietnam, 1979 (Vietnamese).

[9] C. V. Le, *Agrochemistry*, Science and Technology Publishing House, Hanoi, Vietnam, 2005 (Vietnamese).

[10] C. V. Tran, *Soil Science*, Hanoi University of Agriculture I, Hanoi, Vietnam, 2000 (Vietnamese).

[11] H. N. Nguyen, *Soils and Fertilizers*, Hanoi Publishing House, Hanoi, Vietnam, 2005 (Vietnamese).

[12] D. Le and H. K. Tran, *Soil and Soil Protection*, Hanoi Publishing House, Hanoi, Vietnam, 2005 (Vietnamese).

[13] "National technical regulation on the allowable limits of heavy metals in the soils," QCVN 03: 2008/BTNMT, 2008 (Vietnamese).

[14] A. N. Nguyen, *Scientific basis of provincial environmental mapping land serving for land management and environmental protection (sampling of Haiduong province) [Dissertation of Geography]*, 2014 (Vietnamese).

[15] H. N. Pham, "Weighted and standardized total environmental quality index (TEQI) approach in assessing environmental components (air, soil and water)," *VNU Journal of Science, Earth Sciences*, vol. 27, no. 3, pp. 127–134, 2011.

[16] H. N. Pham, "Relative Soil Quality Index (RSQI) of VNU theme: 'Building a set of aggregate index of environmental quality for each element: air, water and soil, service monitoring and environmental management'," code: QMT.12.01, 2012-2014, 2014 (Vietnamese).

[17] H. N. Pham, *Thematic Reports on Investigating and Surveying of the Soil Environmental Parameters of 12 Districts of Haiduong Province in 2013*, Research Centre for Environmental Monitoring and Modeling (CEMM), VNU University of Science, 2013 (Vietnamese).

[18] Department of Natural Resources and Environment of Haiduong province, The land use map, 2013 (Vietnamese).

[19] GSO Vietnam, 2015 (Vietnamese), http://www.gso.gov.vn/.